

MemoSnake

Design and analysis of a snake-like system with mechanical shape control

Sander d'Hont

MSc Thesis
Department of BioMechanical Engineering
Delft University of Technology
Delft, The Netherlands
November 2019



MemoSnake

Design and analysis of a snake-like system with mechanical shape control

by

Sander d'Hont

to obtain the degree of Master of Science
at the Delft University of Technology,
to be defended publicly on November 12, 2019 at 10:00 AM.

Student number: 4209893
Project duration: September, 2018 – November, 2019
Thesis committee: Prof. dr. ir. P. Breedveld, TU Delft (BME), chairman
Prof. dr. ir. V. van der Wijk, TU Delft (PME)
MSc. C. Culmone, TU Delft (BME), daily supervisor
Dr. ir. A. Sakes, TU Delft (BME), daily supervisor

An electronic version of this thesis is available at <http://repository.tudelft.nl/>.

Abstract

Introduction: When navigating through tight and delicate environments, steerable tools are highly desired. Follow-the-leader locomotion, as in the biological snake, is a solution that is obtained with shape memory control. The often used electric equipment to control the shape makes the current state-of-the-art of snake-like robots too complex. This thesis focused on a snake-like system using mechanical shape control to generate forward motion, to analyze the motion and comment on the expected behavior.

Method: A 3D Simulink model was created with friction between the snake-like system and the surroundings as an important relation. A pre-defined sinus wave was passed through the snake-like system to analyze the motion. A low-cost, 3D printed, prototype was developed to validate the friction relation of the model. The prototype contains a belt feature with pre-defined path as shape control system and a snake-like system with four wheeled segments. Different configurations were assessed in the model by changing the wheel axis length, sinus amplitude and sinus frequency.

Results: The prototype validated the realistic friction parameters in the model. Given the results of the model, the snake-like system creates forward motion by pushing against the surroundings when a sinus wave is pushed through the system. The wave parameters have a significant influence on displacement. When the configuration of the snake-like system creates more friction with the surroundings, the system is able to push itself further forward and generates more forward displacement.

Conclusion: It is demonstrated that forward motion is possible when a snake-like system is connected to a mechanical shape control system. Now, the next step is to investigate random paths, to enable adaptable mechanical shape control being applied.

Preface

You see my Master Thesis “MemoSnake: Design and analysis of a snake-like system with mechanical shape control” in front of you, the result of my graduation project. This thesis is written to complete the graduation requirements of the “Medical Instruments and Medical Safety” specialisation of the master program “BioMedical Engineering” within the BioMechanical Engineering department of Delft University of Technology. The thesis lasted from September 2018 till November 2019.

I can proudly say that this thesis is the result of dedicated working. A few people helped and inspired me throughout the project. First of all, I would like to thank my daily supervisor Costanza Culmone for the regular meetings and the constructive feedback. The enthusiasm and patience of Costanza helped me to overcome even the most difficult moments of this project. Furthermore, I would like to thank professor Paul Breedveld for presenting such a challenging project and the meetings which kept me on the right track. I learned a lot from these inspiring discussions. Moreover, I would like to thank Aimée Sakes, for the valuable meetings and feedback in the early phase of the project, and Juan Cuellar Lopez, for the assistance with 3D printing of the prototype.

Furthermore, I want to thank my fellow students for providing a new view on the subject in difficult situations. Lastly, I would like to express my appreciation to my girl friend, family, and friends, for listening to me when I had the need to and providing support in challenging phases of the project. The support and encouragements were the key in successfully completing my graduation project.

*Sander d’Hont
Delft, November 2019*

Contents

1	Introduction	1
1.1	Navigation Challenges	1
1.2	Snake Locomotion	1
1.3	Goal of this Study	2
2	State-of-the-Art of Shape Control	3
2.1	Categorization	3
2.2	Pre-defined Shape Control	5
2.2.1	Electric Control Systems	5
2.2.2	Mechanical Control Systems	5
2.3	Adjustable Shape Control	6
2.3.1	Electric Control Systems	6
2.3.2	Mechanical Control Mechanisms	7
2.4	Void Evaluation	7
3	Background Projects	9
3.1	Mechanical Shape Control	9
3.2	Pre-defined Shape Control	9
3.2.1	MemoFlex I	9
3.2.2	MemoFlex II	10
3.3	Adjustable Shape Control	10
3.3.1	PuzzleBox	10
3.3.2	MemoSlide	11
3.4	Design Perspective	13
4	3D Simulink Model	15
4.1	MemoSlide Simplification	15
4.2	Simulink Model Explanation	16
4.2.1	Parts of the Model	16
4.2.2	Relations and Parameters	17
4.2.3	Subsystems in the Code	17
4.3	Basic Analysis	19
5	Design and Prototyping	21
5.1	Design Goal & Requirements	21
5.2	Design Ideas in Categories	22
5.3	Preliminary Concept Design	24
5.4	Final Prototype Design	26
5.5	Prototype Manufacturing	29
5.6	Evaluation and Validation	30
5.6.1	Evaluation Method	30
5.6.2	Results and Assessment	30
6	Parameter Assessment	33
6.1	Parameter Selection	33
6.2	Wheel Axis Length	33
6.2.1	Assessment Range	33
6.2.2	Extreme Configurations	34
6.3	Sinus Amplitude	34
6.3.1	Assessment Range	34
6.3.2	Extreme Configurations	34
6.4	Sinus Frequency	34
6.4.1	Assessment Range	34
6.4.2	Extreme Configurations	35

6.5	Simulation Results	36
6.5.1	Wheel Axis Length Results	36
6.5.2	Sinus Amplitude Results	37
6.5.3	Sinus Frequency Results	39
7	Discussion	41
7.1	Model and Validation	41
7.2	Parameter Assessment	41
7.3	Limitations in the Project	42
7.4	Personal Learning Process	42
8	Conclusion	45
	Bibliography	47
A	3D Simulink Simulation	49
A.1	3D Figures of the Simulink Model	49
A.2	Global System	50
A.3	Subsystem: Segment 1	51
A.4	Subsystem: Segment 2	51
A.5	Subsystem: Segment 3	52
A.6	Subsystem: Segment 4	52
A.7	Subsystem: Frame	53
A.8	Subsystem: Path Belt	54
B	2D Simulation Sinusoidal Wave	55
C	Conceptual Designs	59
D	Motor Torque Calculation	63
E	Belt Speed Calculation	65
F	Final Prototype Design	67
F.1	Pictures	67
F.2	SolidWorks Drawings	67
G	Model Parameters in Matlab	85
H	Simulation Parameter: Wheel Axis Length	87
H.1	Assessed Situations	87
H.2	Assessment Results	88
I	Simulation Parameter: Sinus Amplitude	91
I.1	Assessed Situations	91
I.2	Assessment Results	92
J	Simulation Parameter: Sinus Frequency	95
J.1	Assessed Situations	95
J.2	Assessment Results	97

Introduction

1.1. Navigation Challenges

Over the years, the development of technology took some significant steps to achieve a higher quality of human life. Moreover, completing tasks which were assumed to be impossible formed a basis of research and development. One field of research was dedicated to navigation through tight and delicate environments. In those environments, the space to make a manoeuvre is limited.

When a human wants to reach a specific area in this environment, the dimensions of the body define the dimensions of the space through which the body is able to move. Moreover, a human is limited by its flexibility to move in certain shapes; the limbs have only a limited number of degrees of freedom. In many different areas it is requested to have more freedom in motion than a human is physically able to, for example in search and rescue, military uses, space applications, pipe inspections, and surgeries [1–4]. In these situations the available space is narrow. Moreover, in fields as search and rescue and surgery the environment is delicate, and the surrounding structures need to be preserved. For example, surgery is shifting more and more from open towards minimally invasive surgery and the available space of motion is very limited. Instruments are inserted via small incisions into the body; those incisions function as a pivoting point of the instrument, limiting the reachable area as well. When touching the surrounding tissue to reach a specific area, damages to delicate organs can result in complications or a bad recovery for the patient [1].

In the field of search and rescue it is all about finding survivors of a disaster as quickly as possible. However, safety is also an important aspect in this field. When for example a building collapsed, rescuers search for survivors in the unpredictable debris. The spaces are often so tiny that a human body does not fit through. Moreover, touching debris during the search could result in

a second collapse; killing possible survivors [5, 6].

Therefore, steerable tools would help in those situations, because they could steer around obstacles, increasing the reachable area of the user. The current challenge is to improve these tools to navigate properly through the tight and delicate environments. Steerable tools are usually composed of rigid elements with joints that provide degrees of freedom depending on the number of elements. However, the ability to navigate through tight and highly variable environments requires a high number of degrees of freedom. For this reason, hyper-redundant structures are usually proposed as a solution [7]. However, creating and controlling those structures is challenging.

Moreover, steering often means that the orientation of the first element (head) is given to the tool, while the other elements are dragged along. The first element may be able to steer around an object, but the rest of the tool cuts the corner by being dragged along. As a result the tool can still touch the surroundings and cause unwanted damage.

1.2. Snake Locomotion

The movement of the tool should be controlled in such a way that the first element moves along a curved path, while the rest of the tool follows the same path. The desired motion is comparable to the motion of a biological snake; a snake steers its head and the rest of the body follows the created path [8]. This motion is also known as the Follow-the-Leader (FTL) locomotion. A snake is able to propel itself forward using four different movement patterns: lateral undulation, rectilinear locomotion, sidewinding, and concertina progression [9, 10]. Each pattern has specific characteristics which are interesting in the research to FTL locomotion.

The undulatory motion, also called **serpentine motion**, is a frequently studied way of propulsion [11, 12]. It is interesting due to multiple reasons:

a serpentine robot is able to traverse rough terrain and is stable due to its low potential energy [13]. Hirose studied the undulatory movement of a snake and modelled it as a continuous curve that was not able to move sideways due to an sideslip constraint [14]. The resulting curve (Figure 1.1) is called the *serpenoid curve*, the origin of the serpentine motion [12]. Hirose found out that the body of a snake during serpentine motion can be described by a curve whose curvature varies sinusoidally [15]. The following equations give the serpenoid curve:

$$x(s) = \int_0^s \cos(acos(b\sigma) + c\sigma) d\sigma \quad (1.1)$$

$$y(s) = \int_0^s \sin(acos(b\sigma) + c\sigma) d\sigma \quad (1.2)$$

in which $(x(s), y(s))$ describes the coordinates of a point along the serpenoid curve with an arc length of s from the origin and a, b , and c are positive scalars [15]. The snake uses this wave to push itself against the environment's irregularities [16]. While pushing against the surroundings, a reaction force is generated at the contact points. The analysis of the serpenoid curve showed a distribution of the normal forces along the body of the snake. The forces are not directed parallel to the traveling direction of the snake. Since the forces oppose each other every half cycle, the net normal force is directed in the traveling direction [12]. The sum of the reaction forces from the contact points together form the total propulsive force in the direction of the motion [9, 17–19]. Due to this characteristic, serpentine motion is known as locomotion which is applicable to rough and complicated terrains and would be useful in the field of search and rescue.

Besides serpentine motion, also the **rectilinear motion** of a snake is interesting locomotion. The motion is based on waves of muscular contraction followed by relaxation of the ventral cutaneous musculature [20].

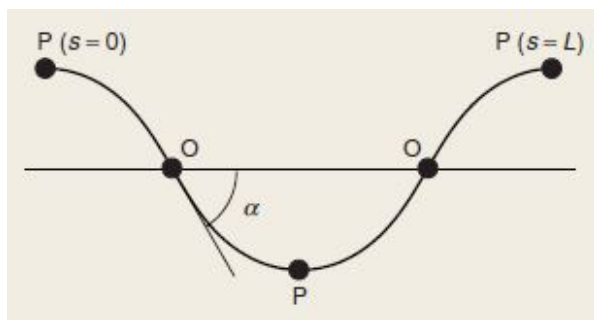


Figure 1.1: Serpenoid curve: The body of a snake is modelled as a continuous curve described by a sinus [12].

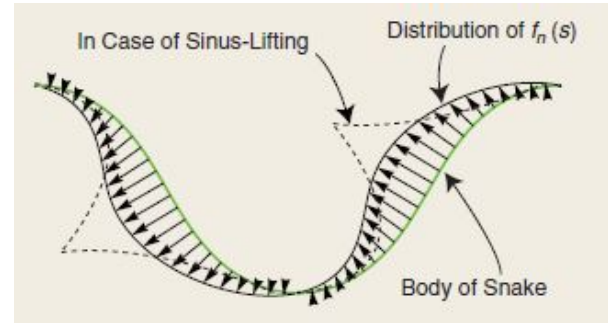


Figure 1.2: Reaction force distribution: The distribution of reaction forces between environment and serpenoid curve during undulatory movement [12].

During this way of motion, the snake moves forward in a straight line and it is able to move around obstacles by steering its head while the body follows the initiated orientation of the head: the earlier discussed FTL locomotion. The shape of the head and body is shifted backwards when the snake moves itself forward [1], also known as the travelling wave.

In both serpentine and rectilinear motion, a shape of the head is passed through the body. In serpentine motion, the wave is described by a sinus which is passed through the body. During rectilinear motion, the path is adaptable; the path is described by the position of the head. Both types of motion require a certain type of shape memory control.

1.3. Goal of this Study

This study is based on a conceptual design of static shape memory control. The aim of this study was to investigate if the static, non-moving, shape memory control could be used in a snake-like system which is actually able to move forward; a dynamic system. Since the biology of the snake is so interesting, many research groups have tried to develop a robot being able to move like a snake. Chapter 2 provides an overview of the current state-of-the-art. Delft University of Technology currently performs research in shape control systems; Chapter 3 addresses the current projects about mechanical shape memory control. Thereafter, the motion possibilities were investigated by model, generated with the software Matlab and Simulink (Chapter 4). The model is validated with the design of a prototype in Chapter 5, after which the model is used to assess different configurations of the snake-like system (Chapter 6).

State-of-the-Art of Shape Control

2.1. Categorization

A wide range of snake-like robots has been developed, each with a different purpose. In order to find voids in the state-of-the-art and analyze the related problems, the currently available robots were divided into categories, shown in Figure 2.3. Note that this Chapter provides examples for each category and is not a complete overview of all existing robots.

Focusing on the shape control system, the **first categorization** was made between *pre-defined* and *adjustable* shape control. In the pre-defined shape control, the path of the snake-like robot is defined before the actual movement starts (Figure 2.1a). In those situations, it is important to have a clear image of the surroundings prior to using the snake-like robot. The user defines the optimal path by using this information. The path is defined in the robot itself, after which the head of the robot will follow this path and the shape is passed along the body. Devices belonging to the adjustable shape control mechanisms have more freedom in movement choices; in this category it is not required to define the path of the robot before the movement (Figure 2.1b). The user chooses directions during movement; the rest of the body follows the shape of the first element.

A **second categorization** was made between the type of systems: *electrical* or *mechanical*. The electrical category contains all systems using electronics as computers, motors, and sensors to obtain shape memory control.

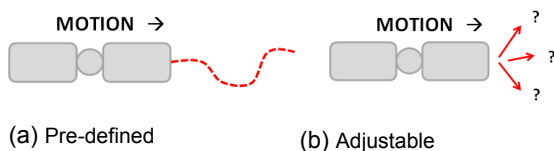


Figure 2.1: Path division: Pre-defined path (red) prior to movement or adjustable path (red) during movement of the snake-like robot (grey).

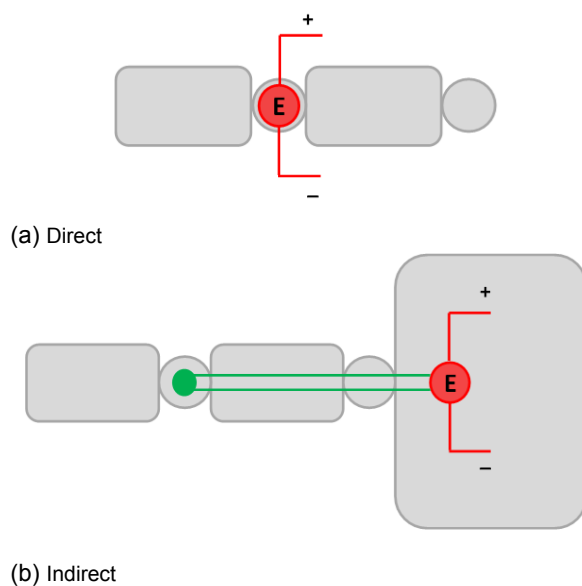


Figure 2.2: Electrical division: The electric component (red) is at the joint where shape is passed through (direct) or component (red) is located elsewhere and connected via transmission (green) to the joint (indirect).

Note that only the system of shape control was considered. To make a distinction between robots using electric components in the joints and robots using electric components located elsewhere, a **third categorization** was made between *direct* and *indirect* electrical shape control. In the direct group, the electronic equipment is directly connected to the segment of the snake and the motor directly drives the orientation of the segment with respect to the connected segment (Figure 2.2a). In the indirect group, a mechanical transmission is used to connect the electric components with the point of the segment where the orientation is controlled. By using a mechanical transmission as cables, the output of the motors is passed along the body to the right segment of the snake-like robot (Figure 2.2b).

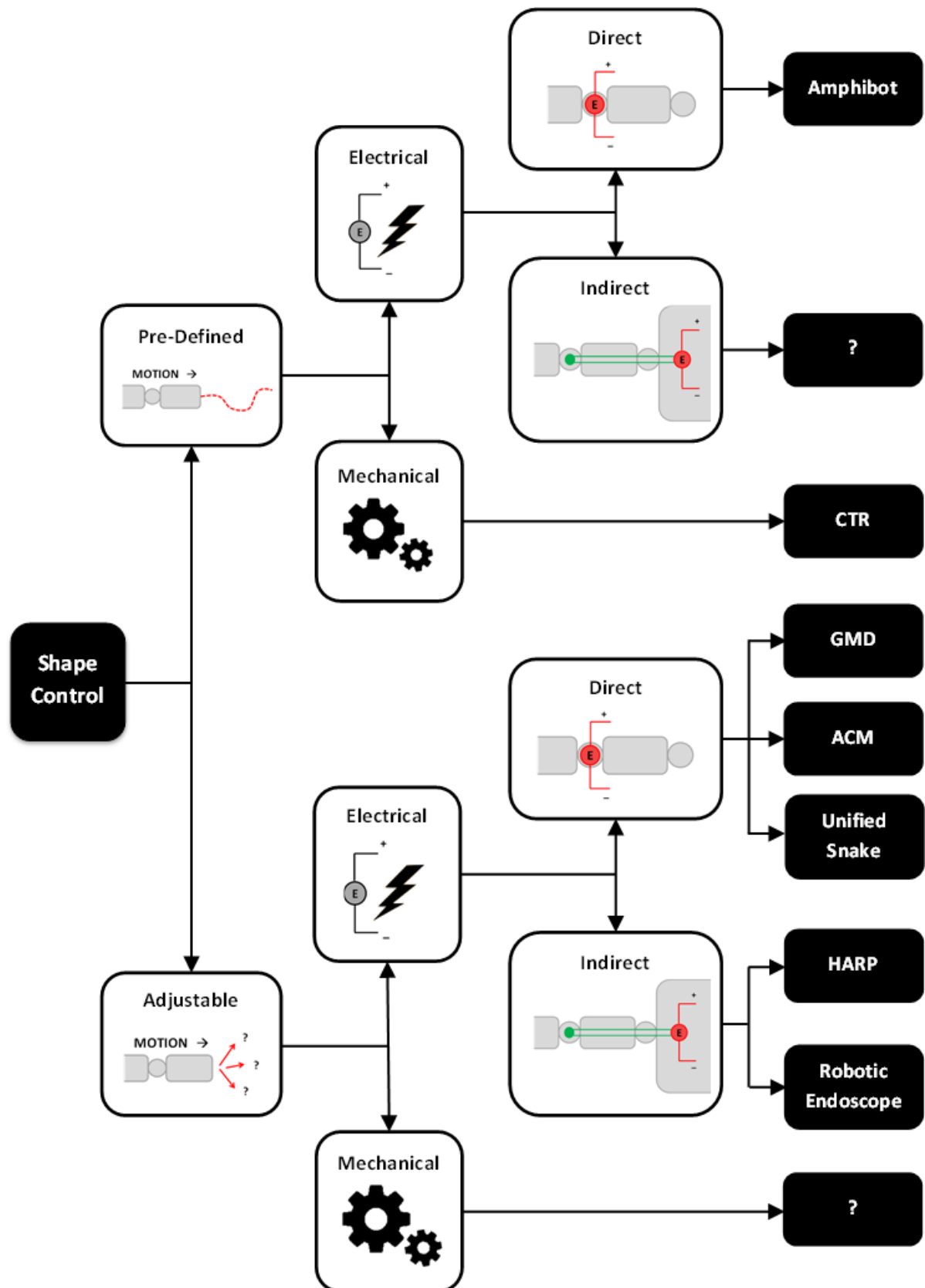


Figure 2.3: Categorization of the state-of-the-art of shape control: Two segments (grey squares) of a snake-like-robot are shown with joints (grey circles) in between. The current shape control systems are either adjustable or pre-defined and further divided into electrical and mechanical. Electrical can either be direct (red electrical component at the joints) or indirect (red electrical component elsewhere and connected with the joint via green transmission). The right column contains the available snake robots in which the voids are indicated with a "?". CTR = Concentric Tube Robot, HARP = Highly Actuated Robotic Probe, ACM = Active Cord Mechanism, GMD = Gesellschaft für Mathematik und Datenverarbeitung (German for "society for mathematics and information").



(a) AmphiBot I, configuration with wheels [21]



(b) AmphiBot II, configuration without wheels [22]

Figure 2.4: AmphiBot I and II: A snake consisting of multiple segments, being able to perform serpentine motion.

Besides snake-like robots using electric components to control their pose, some robots do not use electronics, but use a mechanical solution instead. Examples of this category are the usage of materials with shape memory abilities or applying gears to pass along the shape. In this category, no electronic devices are used.

2.2. Pre-defined Shape Control

2.2.1. Electric Control Systems

Direct Connection

In the category of direct electric pre-defined shape control, only one example was found: the *AmphiBot* [10, 23]. Two versions of this snake-like robot exist; AmphiBot I and AmphiBot II. The first version, the AmphiBot I, was developed to exploit new robot types. The inspiration was taken from the neuronal control mechanisms of snakes and similar looking animals (Figure 2.4a). The robot is able to move in the water when no wheels are connected and on dry terrain when wheels are connected to the robot. The robot contains DC motors in each segment, controlling the orientation of one segment with respect to the next segment. In that way a wave is passed through the body, creating serpentine motion.

AmphiBot II, as shown in Figure 2.4b, was mechanically simplified with respect to the first version and had wireless communication capabilities [22]. The robot was built in such a way that more elements could be added in a simple way to elongate the snake [10]. The locomotion of the segments is controlled by central pattern generators. The input of these generators

consists of the oscillation amplitude, frequency and phase difference of the sinusoidal movement. The pattern generators generate the oscillatory output signals and provides smoothing of possible discontinuities in the input [22].

Indirect Connection

In the category of indirect electric pre-defined shape control, no robots were found in the literature search. This is the first void in the overview.

2.2.2. Mechanical Control Systems

The mechanical category of the predefined shape control contains one example: the *Concentric Tube Robot* (CTR). The CTR, also called “active cannulas” in medical applications, is a robot using telescoping, concentric, pre-curved elastic tubes [24]. The robot was designed to be used in Minimally Invasive Surgery (MIS). The tubes can be translated or rotated with respect to each other, allowing the tip to move in different directions. The CTR does not derive bending actuation from pulling wires along the instrument, instead the elastic interaction of the pre-curved tubes generates the bending actuation [25]. The tubes are the backbone of the device.

The cannula from Figure 2.5 consists of three elastic tubes, in this situation referred to as “segments”, each with two degrees of freedom. The tubes are curved prior to the actual procedure. Then, the three pre-curved tubes are pushed into each other. In this situation, the more rigid tube will keep its shape while the other two are forced to follow that shape.

When the second tube is translated along the outer tube, the translating tube will reshape to its pre-curved shape. This phenomenon is achieved due to the elastic properties of the tube materials. The same happens when the third tube is translated along the second tube. By adapting the amount of translation and rotation, a small variety of paths could be created with the tubes.

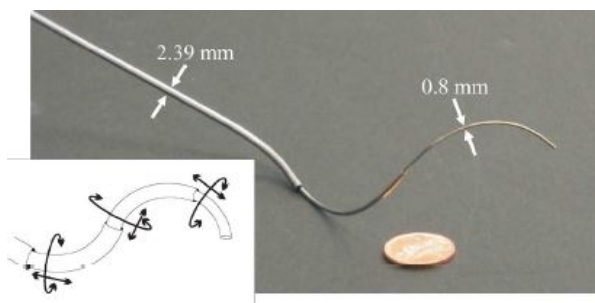


Figure 2.5: Concentric Tube Robot (CTR): Three tubes, inserted in each other, can be translated, and rotated with respect to each other, enabling the tool to steer [24].

2.3. Adjustable Shape Control

2.3.1. Electric Control Systems

Direct Connection

The second main branch of Figure 2.3 categorizes the robots which are able to adjust their path while moving. In the category of direct electrical drive multiple options were found. First, the two versions of the *GMD snake*; a robot developed at GMD (Gesellschaft für Mathematik und Datenverarbeitung, German for “society for mathematics and information”) in Germany to perform inspection tasks in areas difficult to access by humans [26].

The first version consists of short sections, free to move in between the joining segments where the motors were positioned. The fact that the joining segments were not able to bend or move, created difficulties in varying the locomotion. The bending sections contain cable winding mechanisms so that curvatures are affected along multiple segments [13]. The second version of the robot, the *GMD-snake2*, is an improved version of the *GMD snake*; it was built more rigidly using universal joints [26]. The robot is shown in Figure 2.6. Three motors in each joint section control the position of the robot. These motors use small ropes to move the joint [10]. Furthermore, a processor was added in each section, being able to calculate the position of the segment in front and the delay required before moving the following segments [27].

Another example of direct electrical robots is a result of one of the most famous researchers of snake-like robots. Back in 1971, Hirose started the studies on snakes and their locomotion, trying to implement this in a robot. One year later, the first prototype had already been built: the *ACM (Active Cord Mechanism)* [12, 28, 29]. The development kept improving and one of the later versions of the ACM robots is the *ACM-R3*, shown in Figure 2.7a. This robot is capable of performing three-dimensional movement while the servomotors obtain the bending motion in each joint. Furthermore, the servo-motors are radio-controlled to adjust the path [12].



Figure 2.6: GMD-snake2 robot: The second version of the snake-like robots being developed by the GMD group. The robot consists of cylindrical segments with 12 electrical driven wheels around each segment [10].



(a) ACM-3: third version with many larger wheels



(b) ACM-5: fifth version with wheels and paddles

Figure 2.7: Active Cord Mechanism (ACM): Results of the snake research of Hirose [12].

A later version is the *ACM-R5*, shown in Figure 2.7b. This is a snake-like robot having a dust- and waterproof body structure [12]. The robot uses friction forces with respect to the surface to propel itself forward. The mechanism contains paddles and passive wheels making the robot suitable for moving into the water as well as on ground [10]. Furthermore, the robot contains a central processing unit and motors, so that it automatically recognizes its position with respect to the head and being able to describe the next required position.

The third example of direct electrical shape control was found in the *Unified Snake*. The snake-like robot was developed with the purpose to have a robust and reliable modular snake robot which can be used in both the field of search and rescue as well as in research areas. The robot consists of different linked modules.



Figure 2.8: Unified Snake: A fixed camera is clearly visible in the head segment. The head provides sensing information [30].

Each module contains a motor, a gear train, sensors, and a custom connector between the modules [30]. The Unified snake is shown in Figure 2.8. Due to the presence of sensors, the robot can perform motion control tasks and report sensor feedback information. The accelerometer and gyroscope are sensors being used to determine the orientation of the robot so that the motion of the robot can be adapted by the shape control software [30].

Indirect Connection

In the indirect electrical category, two robots were found which use a mechanical transmission between the electric drive and steering section. One of the examples is the *Highly Actuated Robotic Probe (HARP)*. The HARP is a probe designed to be used in cardiac surgery. The probe contains two tubes and is actuated by four cables. The FTL locomotion is generated by alternately stiffening the inner and outer tube, caused by pulling the corresponding cables [31]. In order to steer the head of the snake, the outer tube is made limb and moved forward with one segment.

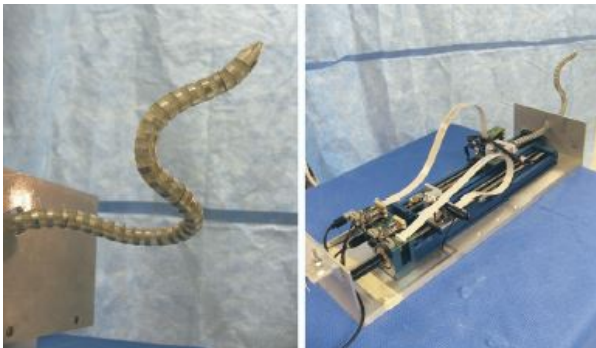


Figure 2.9: HARP: The left picture zooms in onto the steerable probe itself and the right picture shows the feeding instrumentation box, the unit which implies the stiffening of the different tubes [32].



Figure 2.10: Robotic Endoscope: A prototype of a robotic endoscope. As for the HARP, a feeding instrumentation box is visible in which the motors drive the tensioning cables [33].

This segment can be steered while the other segments of the snake maintain their pose, since the inner snake is still rigid. Now, the outer snake is made rigid in the new pose, while making the inner snake limb. The inner snake is moved equally far as the head of the inner snake; it catches up with the steered head. Then, the inner snake is made rigid again so that the process can start all over again [31, 34]. The links of the probe are held together by one cable in the inner snake and three in the outer snake, making it possible to steer the outer snake in any direction (left section of Figure 2.9). The probe has a feeding instrumentation box as well (right section of Figure 2.9). Both the inner and outer snake are driven independently by two separate linear motion systems [34]. The systems contain motors to control the tension on the cables [32].

The second found snake robot in the category of indirect drive in the adjustable shape memory control is the *Robotic Endoscope*, developed to improve the comfort of the patient during endoscopic procedures. The robot, shown in Figure 2.10, is a prototype and consists of five segments, each driven by four cables. Two DC servo motors drive the four cables (one motor per two cables). The project of the novel endoscope is medical related. However, the steering technology could be used in robots with other purposes as well [33].

2.3.2. Mechanical Control Mechanisms

A shape control system which passes the shape through the body with a mechanical principle is another category. In this category no robots were found. This is the second void in the overview.

2.4. Void Evaluation

As a result of the literature search two voids were found: one in the category of *indirect electrical pre-defined shape control* and one in the category

of *mechanical adjustable shape control*. The last category is an interesting research area in fields where the environment is not fully defined before entering with a snake-like tool. For example, in surgeries and the field of search and rescue it would be favorable to have the option to adjust the path of the robot while moving through the environment. Simulating the FTL locomotion with an adjustable mechanism is challenging to establish; it requires a shape control system of which the first element is steerable. Moreover, this system can be used to generate a traveling wave through the snake-like robot; serpentine motion.

Focusing on the current state-of-the-art, it was concluded that there is one issue: the systems are too complex and expensive, caused by the number of motors. Often, each segment contains a motor to remember and pass on the shape (as seen in the electrical mechanisms). Motors, in each segment of the instrument, have some disadvantages; first of all, complexity. When a robot requires additional length or a higher number of segments than designed, it is complex to add another element. Second, motors limit the miniaturization of the elements.

By providing a mechanical shape memory control system, dimensions can decrease and it would be easier to connect more segments to the snake. Furthermore, a simple mechanical solution is less susceptible to reliability issues than electrical solutions. For these reasons, the group of Bio-Inspired Technology (BITe) of Delft University of Technology is performing research in the area of mechanical shape control.

Background Projects

3.1. Mechanical Shape Control

Current snake-like robots do not fulfil the requirements of simplicity and minimizing dimensions. Finding a mechanical solution to shape memory control would eliminate the electric components and improve simplicity. The void of *mechanical adjustable shape control*, found in Chapter 2, is a popular research area at Delft University of Technology. Research has been performed with the aim to eventually implement the shape memory control in a steerable medical instrument. Multiple research projects with shape control were done. In the research group of Bio-Inspired Technology, four projects are known.

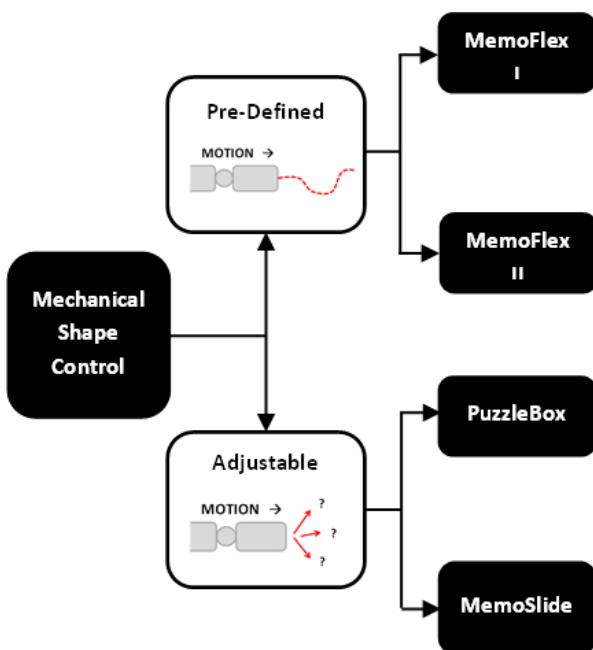


Figure 3.1: State-of-the-art in mechanical shape control: The overview of current research projects at the Delft University of Technology performed to implement mechanical shape memory control in medical instruments.

As for Chapter 2, the projects were divided into pre-defined and adjustable mechanisms. In this case the overview is simplified with respect to the previous Chapter, since only mechanical shape control systems are discussed (Figure 3.1).

3.2. Pre-defined Shape Control

3.2.1. MemoFlex I

One of the earlier projects is the MemoFlex, in which T. Krijger (2012) created an instrument of which the tip follows the predefined path given at the handle [35]. This is a system using a master-slave relation between the handle (control unit) and the tip (steerable shaft). The project of the MemoFlex was further developed into a version in which the path is passed through the system with a lever: the MemoFlex I [36].

A path is pre-defined and fixed with a rigid rod (the track in Figure 3.2). The rod is pushed through the handle, causing the handle to take over the shape of the rod. Wires, running through the shaft, connect the handle parts with the tip parts. These wires are pulled/released when the shape of the handle changes. The shape is passed to the tip due to wires pulling on the tip segments, as shown in Figure 3.3.

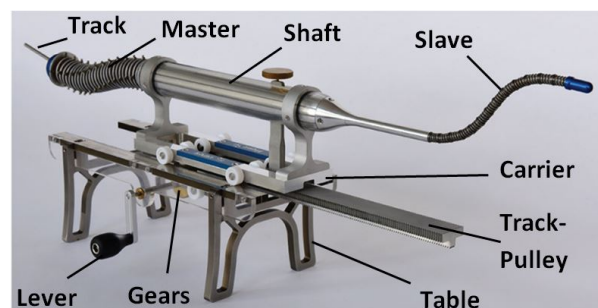


Figure 3.2: MemoFlex I: Schematic overview of the mechanism with the steerable shaft as the slave and the control unit as the master [36].

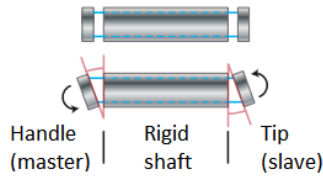


Figure 3.3: Master-slave relation: Cables connect the master to the slave. Steering the master results in pulling of the cables, ending up with a steered slave [35].

3.2.2. MemoFlex II

Besides the Memoflex I, there is a Memoflex II, which can be seen as a follow-up of the MemoFlex I. The MemoFlex II (Figure 3.4) allows FTL behavior: the steerable shaft (slave) of the instrument follows the shape given in the cylindrical mechanism of the device (master). The principle of motion is the same as in MemoFlex I: as the orientation of the parts at the master changes, the determined shape is transferred to the slave via pulling cables. The shape is controlled by memory elements in the cylindrical mechanism of the device. These memory elements contain a pre-defined path in the shape of a slot. Ball bearings are slid in these slots of the memory elements. The ball bearings are placed on sliding fingers that are connected to the steerable tip via cables. Note that the memory elements only describe a part of the total required motion. In total, four memory elements are needed: two memories control the motion in the vertical plane and the other two memories control the motion in the horizontal plane. The displacement of the ball bearings in the memory elements is changed by moving them forward or backward through the memory elements.



(a) MemoFlex II assembly



(b) Pre-defined memory elements

Figure 3.4: MemoFlex II: The cylindrical mechanism (master) controls the shape of the steerable shaft (slave) with pre-defined memory elements.

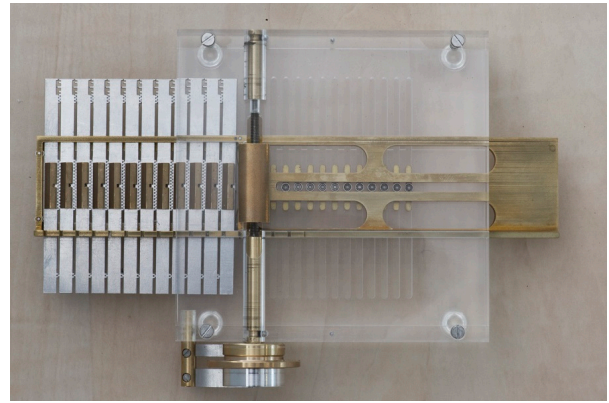


Figure 3.5: PuzzleBox: Puzzle elements describe the shape.

By moving the ball bearings, the sliding fingers are slid as well, and the cables connected to the steerable tip are pulled/released. The mechanism moves forward and backward by turning a lever. The ball bearings are forced to follow the shape of the memory elements resulting in pulling of the cables linked to the steerable shaft. The translational movement of the lever is therefore coupled to the vertical and horizontal motion of the steerable tip. The three 2D motions together form the 3D motion of the steerable tip.

3.3. Adjustable Shape Control

3.3.1. PuzzleBox

In MemoFlex II, a small pre-defined memory bank was shown. The mechanical memory bank mechanism was further developed in the PuzzleBox (sometimes called the “MemoBox”), as shown in Figure 3.5. The real improvement is the fact that the path no longer has to be pre-defined, because the control is in real-time. The mechanical shape memory was achieved with so-called puzzle elements; the elements contain teeth which enable the elements to interlock with each other, fixing the shape. The location of the first element can be changed by pulling this element apart from the rest, orientating the new position, releasing, and interlocking it again with the rest of the elements. This means that the shape is adjustable during movement; an improvement with respect to the mechanisms used in the MemoFlex I and the MemoFlex II. The PuzzleBox is, therefore, categorized in the mechanical adjustable shape memory control in Figure 3.1. The shape is again passed to the tip with the use of ball bearings and connected wires. The ball bearings are moved through a tunnel created by specially designed leaf spring cups fixed under the teeth fingers. These leaf spring cups move along with the puzzle elements and because of their elasticity, a clear tunnel guide for the ball bearings is created. This prevents the ball bearing to get stuck or run out of order.

3.3.2. MemoSlide

Introduction

The MemoSlide is a device created by the BITE group to obtain adjustable shape memory control [1]. As Figure 3.6 shows, it is a complex system. Since this mechanism functions as the basis of this design project, the sequence of motion is explained step by step before going deeper into the parts of the mechanism. The mechanism is based on two parallel rows of so-called fingers (elements): a **memory bank** and the **shape**. They are grouped into two rows.

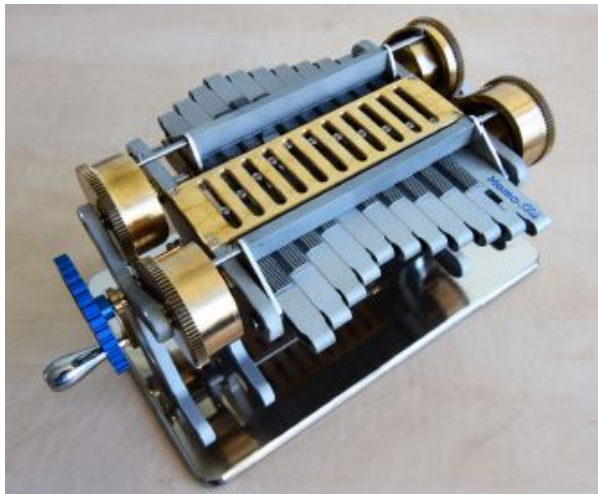


Figure 3.6: MemoSlide: Final prototype. [1].

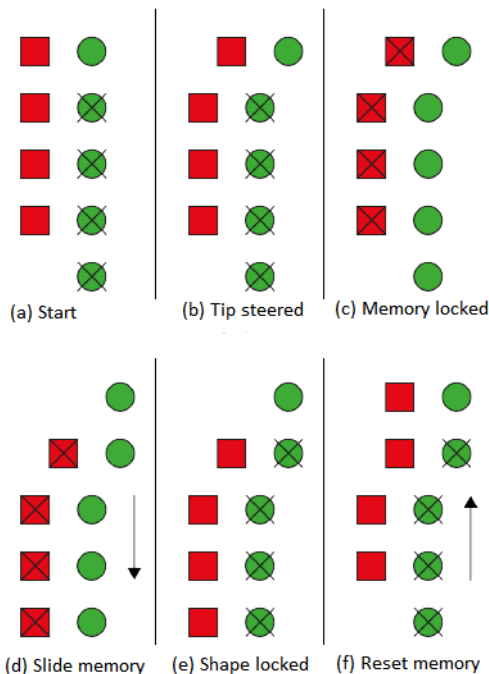


Figure 3.7: Schematic illustration of the sequence: The red squares represent the memory elements and the green circles represent the shape elements. A cross in an element means it is locked in position [1].

Motion Sequence

By alternately locking either the shape or the memory bank, the shape of one row could pass to the other row. To explain the sequence of the two rows, a schematic overview was made (Figure 3.7). The figure shows four memory elements (red squares) and five shape elements (green circles).

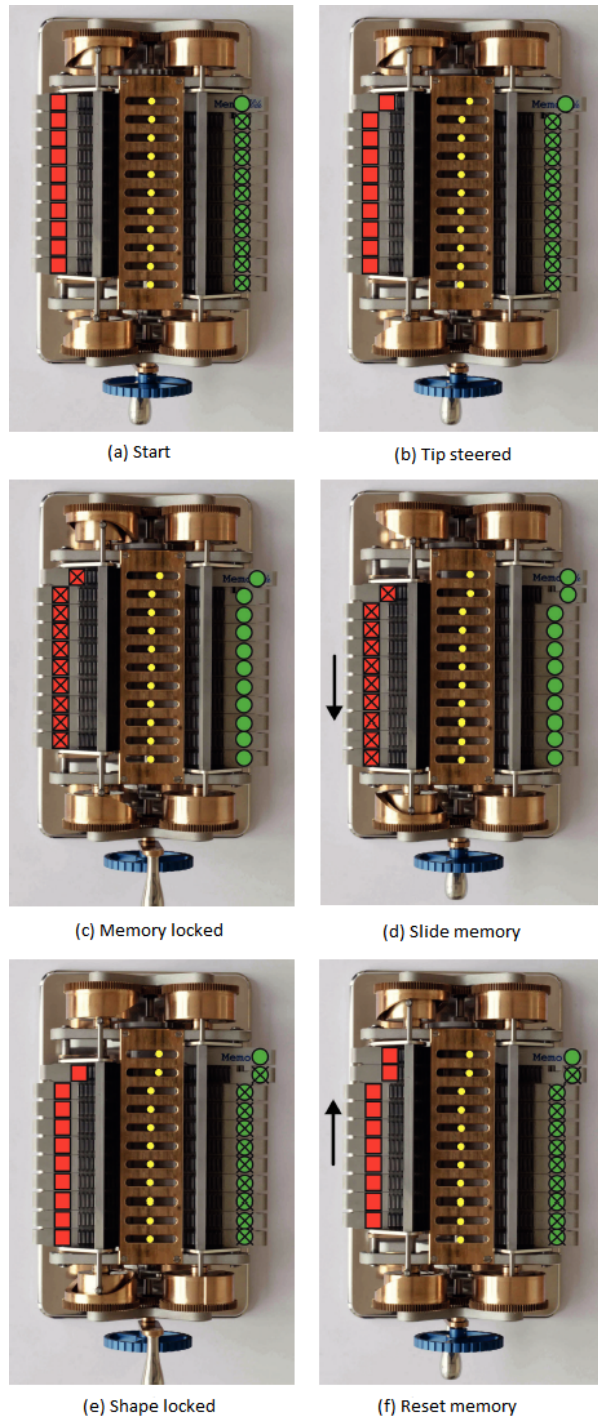


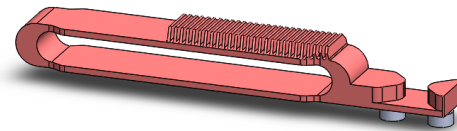
Figure 3.8: MemoSlide sequence: The green circles represent the shape fingers and the red squares represent the memory fingers. A cross in an element means it is locked in position. [1].

A cross in the elements represent the locking of the elements. Once the elements are locked, the shape of the entire bank is fixed. The shape is locked in the initial position (a), except for the first element. This allows the user to choose the new position of the first element. By sliding the position of the first element sideways, the tip is steered (b). The first element of the memory bank follows this shape. This new shape of the mechanism should be memorized; the memory bank is locked and the shape unlocked (c). To pass the orientation of the shape elements to the next elements, the memory bank slides one element backward (d). Since the shape of the memory bank is locked, the memory bank forces the shape elements to take over the shape; the shape is passed one element backward. This shape is locked in place and the memory bank is unlocked (e). The memory is now reset by sliding forwards again (f). The memory bank is unlocked and free to move and takes over the new position of the shape elements.

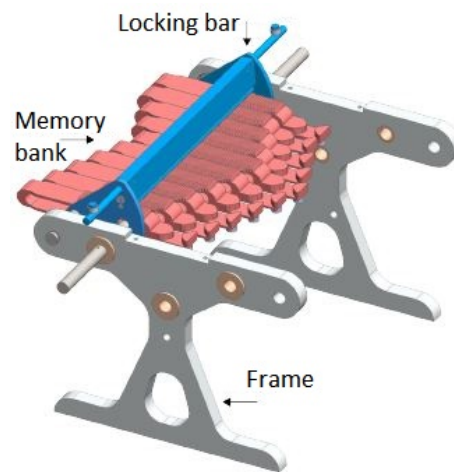
The MemoSlide is capable of performing this motion sequence. The working principle of the MemoSlide can be explained in the same way as the schematic sequence of Figure 3.7; by locking the shape and memory bank at the right time, the shape is passed from one bank to the other. Steering is done by turning the steering wheel (blue wheel at the bottom of pictures in Figure 3.8).

Parts of the Mechanism

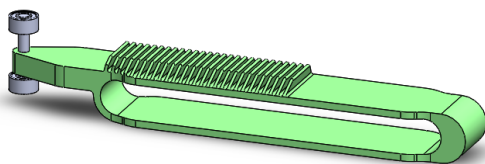
The sliding of the memory bank is obtained by turning a crank handle (Figure 3.8). Locking is done by a locking bar, located above each row of elements. Detailed views of the shape and memory elements are shown in Figures 3.9 and 3.10, respectively. The fingers look similar but there are some main differences.



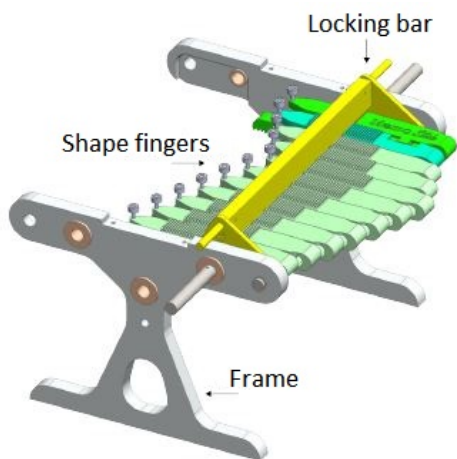
(a) Single memory finger with grey ball bearings



(b) Row of memory fingers in the MemoSlide

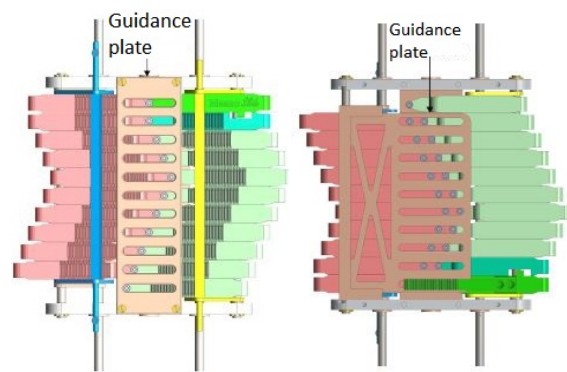


(a) Single shape finger with grey ball bearings



(b) Row of shape fingers in the MemoSlide

Figure 3.10: Schematic illustration of the memory fingers (the memory bank): A locking bar is able to lock the entire row of fingers in its position; locking the shape of that row [1].



(a) Top view

(b) Bottom view

Figure 3.9: Schematic illustration of the shape fingers (the shape bank): A locking bar is able to lock the entire row of fingers in its position; locking the shape of that row [1].

Figure 3.11: Guidance plate: The ball bearings of the shape (green) end memory (red) fingers run through the slots in the guidance plate, allowing them to move sideways only [1].

The shape finger contains a pin with two ball bearings connected to it. The lower ball bearing run through the groove feature of the memory fingers, while the upper ball bearing runs through the guidance plate of the MemoSlide, allowing the element to move sideways only (illustrated schematically in Figure 3.11a). The memory finger contains the groove feature through which the lower ball bearing of the shape finger is running. Underneath the groove, two ball bearings are attached to the memory finger. These ball bearings run through the bottom guidance plate (Figure 3.11b).

Interaction between Shape and Memory

The shape and memory elements have a specific interaction with each other; they are connected but also free to move. As seen in the sequence, the memory bank slides back and forward. This type of interaction is obtained by the lower ball bearing of the shape element and the groove of the memory element (Figure 3.12a). That is the point of interaction between the elements. At that point, the shape of one element is passed to another element.

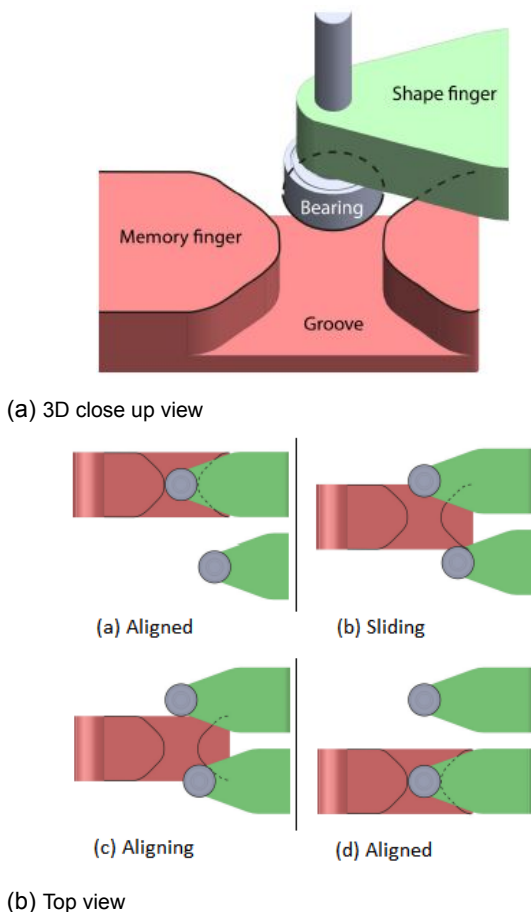
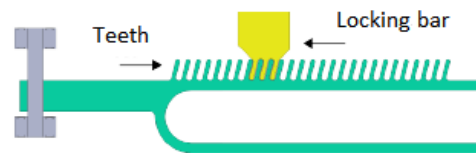
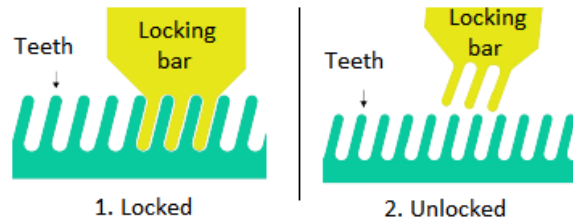


Figure 3.12: Schematic illustration of the interaction between Shape and Memory: The ball-bearing of the shape finger runs through the groove of the memory finger [1].



(a) A finger locked by a locking bar



(b) Locked and unlocked configuration

Figure 3.13: Schematic illustration of the locking principle: The top figure shows one finger with the locking bar locking the position using the teeth on the finger. Left down figure is the locked configuration, while the right down figure is the unlocked configuration [1].

The interaction is shown schematically in Figure 3.12b. A memory element passes the shape from one shape element (a) to the next shape element by sliding to that element (b) and forcing the shape element to take over the shape. The forcing is obtained with the groove and the ball bearing of the shape element (c). Once they are aligned (d), the memory bank is reset to the initial state by sliding forwards again.

Locking the Shape

Note that each finger contains teeth on top of the element. These teeth are used to lock the position. The locking bars contain similar teeth. The locking bar is placed above the memory bank and shape bank. A schematic view of the locking bar is shown in Figure 3.13a. When the locking bar is moved down, the teeth interlock with the teeth of the element, keeping its position fixed. During the sequence and while turning the crank, the locking bar is driven as well; the locking bar moves down, locking the fingers underneath and up, unlocking the fingers underneath (Figure 3.13b).

3.4. Design Perspective

Focusing on the mechanical shape control, the MemoSlide and PuzzleBox are the two most interesting projects. They give more freedom in motion since they have the option to adjust the shape in real-time. The MemoSlide shows a clear and understandable way of passing the shape to the next element in a mechanical way. However, to reach the goal of implementation in medical instruments, the system has to be made less complex. The goal of the PuzzleBox was to simplify and improve the mechanism of the MemoSlide

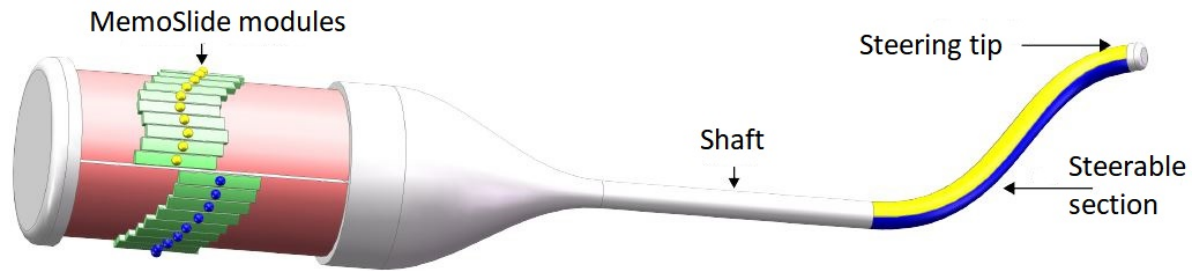


Figure 3.14: Idea of MemoSlide application: The system is implemented in a steerable medical instrument so that the shape of the instrument is controlled during surgery [1].

and eventually implement the mechanism in the MemoFlex II, as shown schematically in Figure 3.14. The MemoSlide modules would replace the master device, shifting from pre-defined to adjustable path planning.

As explained in Chapter 1, it would have an added value when the mechanical shape memory control of the MemoSlide can be implemented in both FTL locomotion (implementation in a steerable medical instrument) and in serpentine motion (moving on rough terrain). Since the implementation of FTL behavior in medical instruments was already part of the topic in the PuzzleBox project, this thesis focused on the serpentine motion.

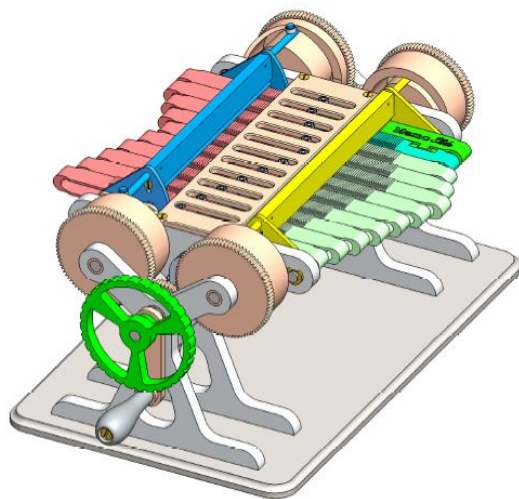
During this thesis an analysis was done to investigate the motion behavior of a dynamic snake-like robot using the static MemoSlide system as shape memory control. The shape memory control could be used to pass a wave along the body of a snake-like robot. In order to have a functioning robot, this should result in forward motion by serpentine movements. The project investigated if the snake was able to propel itself forward with this type of motion; the ground contact points itself must not be directly driven by motors, even as the interaction between the segments. The whole robot should be driven by only one motor driving the shape memory control system.

An important step was the translation of a static mechanism (MemoSlide) to a dynamic snake-like robot. This involved factors as interaction with the environment and moving masses.

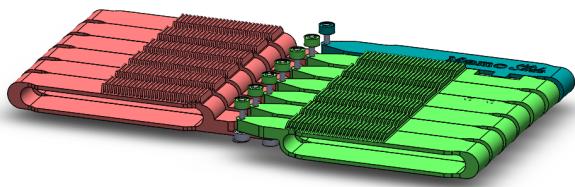
3D Simulink Model

4.1. MemoSlide Simplification

An analysis was done to investigate if the static MemoSlide mechanism from Chapter 3 could be used to propel a dynamic system forward by passing a traveling wave through the system. Remember that the MemoSlide mechanism was developed to create mechanical shape memory control. The traveling wave is created by the shape and memory fingers of the mechanism.



(a) MemoSlide system, schematically shown



(b) Simplification

Figure 4.1: Simplifying MemoSlide: Only the memory fingers (red) and shape fingers (green) are kept visible, while the rest of the mechanism is neglected for this moment.

Since the aim of this thesis was to analyze the possibilities of forward motion, only the parts of the mechanism describing the wave were considered. Therefore, a simplification was made from the system. Figure 4.1b shows the **memory fingers** and **shape fingers**. The rest of the mechanism was neglected in this research. In order to make a snake-like robot, adapting the MemoSlide mechanism, two parallel systems were created; the **snake-like mechanism** below and the **shape control system** on top. The snake-like mechanism consists of several connected segments, forming a train (blue bars in Figure 4.2). Each segment interacts with the surroundings at the contact points with the ground; wheels or other passive elements (e.g. paddles). The shape control was kept as in the MemoSlide mechanism, see Chapter 3. The two systems work together. The shape control system creates a certain shape by orientating the fingers in a specific way. Note that the shape and memory fingers are connected with a pin with ball bearings. These ball bearings form an important part in the connection between the two systems.

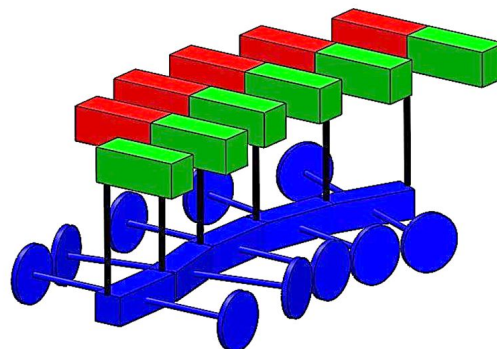


Figure 4.2: Segments connected to the MemoSlide: Segments with wheels (blue) are connected between two consecutive shape fingers (green) via the pins (black). The red beams represent the memory fingers of the shape control system.

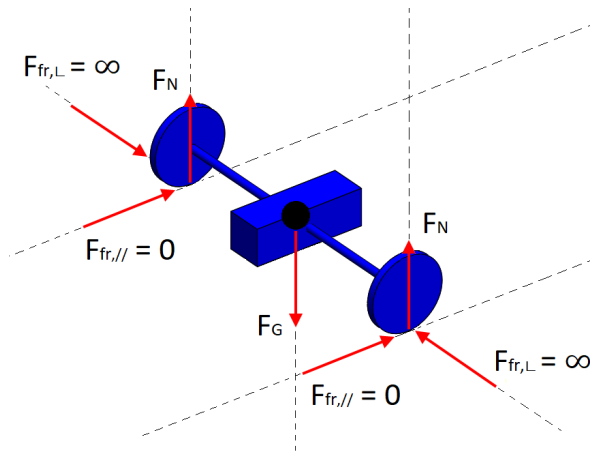


Figure 4.3: Friction on one segment: The friction perpendicular to the wheels ($F_{fr,\perp}$) is desired to be infinite while there is no friction wanted in parallel direction of the wheel ($F_{fr,\parallel}$).

The end-points of each segment of the snake-like mechanism can be connected with the ball bearings from two consecutive shape fingers, as shown in Figure 4.2. In that way, the element is forced to follow the shape created by the shape control mechanism. The shape control mechanism is illustrated schematically with green and red bars (representing the shape and memory fingers). The snake-like mechanism (blue) is connected below. One segment of the snake-like mechanism is connected between two consecutive shape fingers. If the fingers are moved sideways with respect to each other, the snake-like segments are rotated.

The orientation of the fingers with respect to each other is described by a certain wave or path. While the path is pushed through the frame, the segments are forced to follow the initiated path; a traveling wave is generated. However, to obtain forward motion like a snake there should be an interaction with the ground. As explained in biology, a snake moves forward by pushing itself against the surroundings. The reaction force of the surroundings against the body causes forward motion. To mimic this motion with a snake-like robot, the contact points should have an important characteristic: the segment encounters high (theoretically infinite) friction with the ground perpendicular to the wheel ($F_{fr,\perp}$ in Figure 4.3) and low (theoretically zero) friction with the ground parallel to the wheel ($F_{fr,\parallel}$ in Figure 4.3). This characteristic could be generated by using wheels; due to the use of ball bearings between the wheel and the wheel axis, it encounters zero friction in rotating. Moreover, the material of the tire causes friction with the ground in the direction of the wheel axis; in the model to be assumed high.

Furthermore, the wave, generated by the shape fingers of the shape control system, is adaptable. However, to investigate if a system is able to move itself forward due to the input wave, in this model

the adaptable path was simplified to a pre-defined wave; described by a sinus. The standard equation of a sinus was the basis of the wave description:

$$y = A * \sin(B(x + C)) + D \quad (4.1)$$

In this equation, $(-C, D)$ describes the starting point of the sinus. In this case the starting point was equal to $(0, 0)$, so both the C and D canceled out of the equation. Therefore, the equation of this sinus wave became:

$$y = A * \sin(B * x) \quad (4.2)$$

In this equation, the A expresses the amplitude of the sinus and the B is related to period and frequency, $2\pi/B$ is equal to a period of the sinus. This means that the frequency equals $B/2\pi$. However, the units of the period and frequency are different than the usually used *sec.* and *Hz.*. The period is given in *mm*, so that it could be implemented with respect to the length of the system. The frequency is therefore given in $1/mm$.

4.2. Simulink Model Explanation

4.2.1. Parts of the Model

The basic mindset was used as a start of the analysis with computer software Matlab and Simulink. In the 3D Simulink model a snake-like robot of four segments was generated, connected to a frame. The pre-defined sinus wave was pushed with a certain relative speed through the frame.

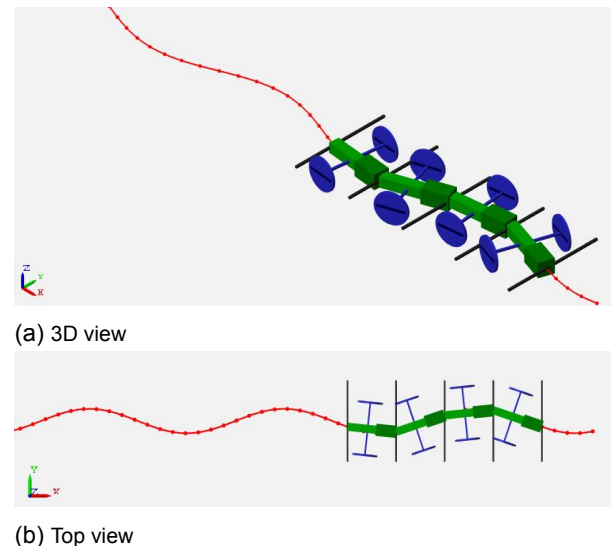


Figure 4.4: 3D Simulink Model: Four segments (green) are connected with their end points to a simplified frame (grey). Each segment has a wheel axis with two wheels (blue). A path (red) moves over the frame from left to right, with the segment end points forced to follow this path.

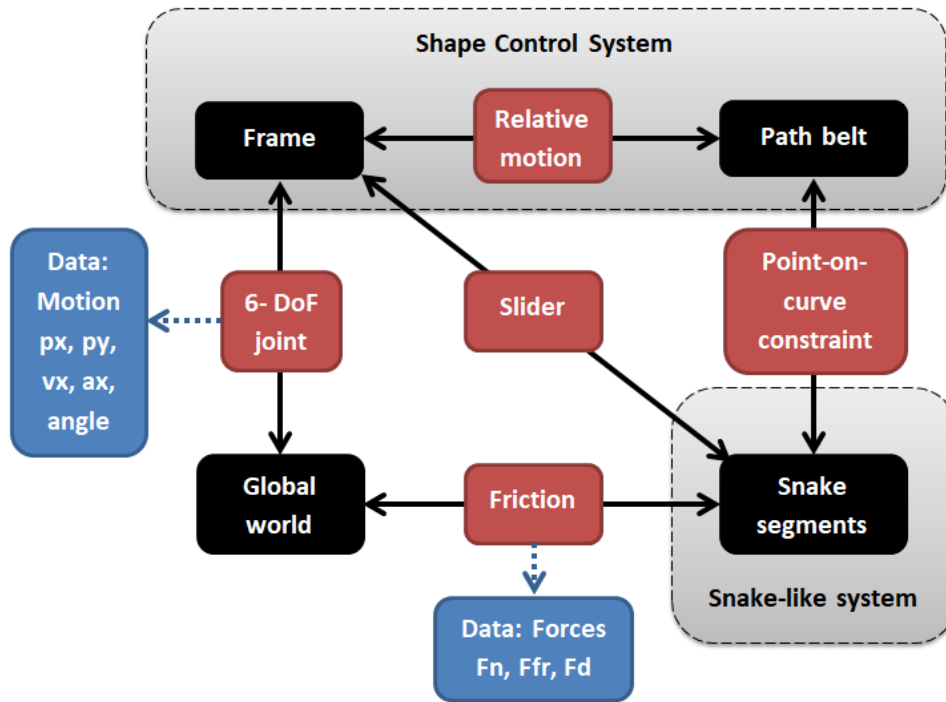


Figure 4.5: Schematic illustration of Simulink model code: Subsystems are black, relations are red and data collection is blue. The subsystems frame and path belt form the shape control system and are linked to the snake-like system (containing snake segments). Data about the motion and contact forces were logged.

The model was generated by a Simulink code, in which the system (snake-like robot) is composed of three subsystems that are linked together; the **frame** (grey beams), the **path belt** (red sinus wave) and the **four snake segments** (green elements). The model includes also a **global world** (white plane) that represents the plane on which the snake-like robot is moving. Figure 4.4a shows the result.

Note that the grey beams mimic the guidance plate of the MemoSlide (Figure 3.11). The distance between the beams should therefore stay equal during the motion; the frame is one fixed total. Moreover, from the geometrical relation of a triangle was noted that the length of a segment increases when the segment is steered; the long side of the triangle increases when the angle of the segment with respect to the central axis increases. In the model, this is taken into account by implementing a slider in the subsystem of the segments. This slider is generated by two beams per segment; the thicker part is able to slide over the thinner green beam. In Figure 4.4b, the red path is pushed through the system from left to right.

4.2.2. Relations and Parameters

In order to represent a real system, the subsystems and the global world were linked to each other by means of relations, as shown schematically in Figure 4.5. The code can be

found in Appendix A. The shape control system consists of the frame and the path belt. The frame acts as a sliding mechanism on which the end points of the segments are connected and able to slide sideways, illustrated with a “slider” relation between the frame and the snake segments. The end-points of the segments are also constrained to stay on the wave, described by the path. These “point-on-curve” constraints are the interaction between the path belt and the elements of the snake-like system. The path belt moves through the frame with a relative velocity with respect to the frame. A 6-degrees of freedom (DoF) joint was added between the global world and the frame. This allows the frame to move freely with respect to the world.

In the 6-DoF joint block, the forward displacement (**px**), forward velocity (**vx**), forward acceleration (**ax**), sideways displacement (**py**) and angle of rotation (**angle**) were logged during a simulation. Furthermore, the normal force (**Fn**), friction force in x- and y-direction (**Ffr**), and damping force (**Fd**) at the contact points were logged at the friction relationship. The logged data was used to analyze the behavior of the mechanism.

4.2.3. Subsystems in the Code

The first subsystem represents the path belt, which describes the wave and the relative velocity of the path with respect to the frame (Figure 4.7).

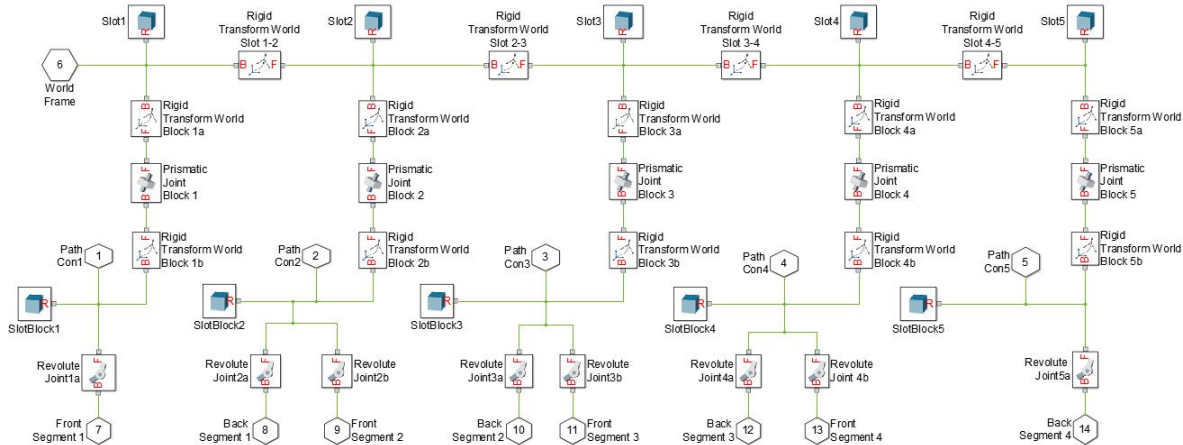


Figure 4.6: Subsystem frame: Five slots with a fixed distance in between them, each having a slotblock sliding over it which is hinge connected to the segment ends. The slotblocks are constrained to follow the described path.

The path should be able to move over the frame; an imaginary sliding joint between the path and the frame was introduced (“prismatic joint block” in Figure 4.7). Moreover, the sliding joint is moved with a constant relative velocity with respect to the frame. The path is the output of the system which is linked to the snake segments via the point-on-curve constraint (Figure 4.5).

The second subsystem is the frame, shown in Figure 4.6. This subsystem is more complex than the path belt. First of all, a geometry was given to the five grey beams, the blocks called “slots” in Figure 4.6. A fixed distance between the slots was generated by the rigid transform blocks in between them. The connection between two snake segments is a complex joint, since three functions are combined; the connection should be able to slide over the frame slots, the segments should be able to hinge with respect to each other, and the connection should follow the traveling wave. In the model, this complex joint is build out of several parts and joints:

- “Slotblocks” are placed on the slots. These blocks are able to slide over the slots (“prismatic joint” block in Figure 4.6).
- The end-points of one segment and the start-point of the next segment are connected to the same slotblock; the slotblock forms the connection element and the segments are not connected directly to each other.
- A hinge is added as relation between the segments and the slotblock (“revolute joint” block in Figure 4.6).
- The “slotblocks” are connected to the path via “point on curve constraints”.

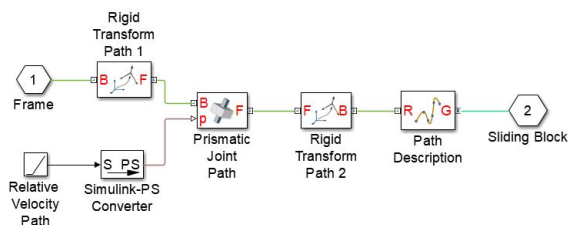


Figure 4.7: Subsystem path belt: A path and the constant relative velocity with respect to the frame were described.

So, when the path moves through the system, the slotblock is forced to slide left or right on the slots. This will cause the segment to rotate due to the wave that is pushed through the system.

Besides the frame and path belt, there were four segments described in equal subsystems. One of the subsystems, segment 1 in this case, is shown in Figure 4.8. As told before, the segment contains a sliding mechanism, which in this model, is represented by the prismatic joint between the base of the segment and the slider. Furthermore, the wheel axis was connected to the base of the segment. Wheels were connected on each end of the wheel axis. Note that Figure 4.8 shows a “wheel line” as well. This generated a line on the disk wheel, visible in Figure 4.4 with a black line. In this way, it was made visible when the wheel rotated (the line rotated as well) or slid (the line did not rotate) during a simulation.

Another important aspect of the segment subsystem is the friction with respect to the ground (global world). The friction was described as the relation between a sphere and a plane. Assuming that the tire of the wheel has a cylindrical cross section, the tire has a point of contact with the ground; equal to the point of contact between a sphere and a plane (Figure 4.9).

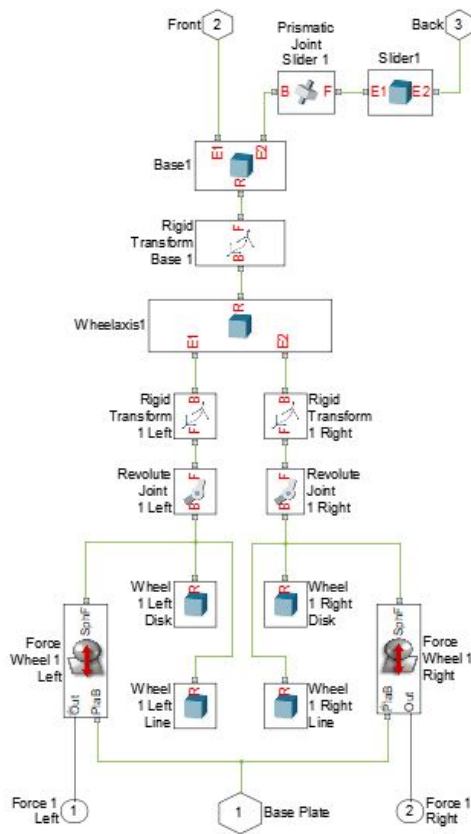


Figure 4.8: Subsystem segment 1: The segment consists of a sliding mechanism in which the slider is sliding over the base. A wheel axis is fixed to the base, with wheels on both ends of the axis. The friction relation is described with respect to the base plate and the data is logged.

The sphere in the friction relation has the radius of the wheel and the plane is the global world. The relation was established by giving values to the kinetic and static friction coefficients. Since high friction was required, these friction coefficients were chosen to be high as well. Moreover the plane stiffness and plane damping were described; these values should be chosen so that the wheels do not penetrate the global world. To make sure the wheel has no friction perpendicular to the wheel axis, a revolute joint was added between the wheel and the wheel axis. This joint equals the behavior of a ball bearing; the wheel is free to rotate around the wheel axis.

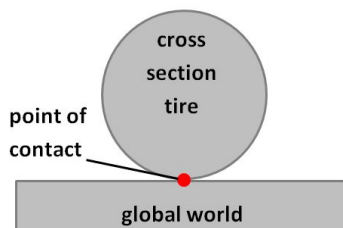


Figure 4.9: Point of contact: Cross section of the tire in contact with the global world.

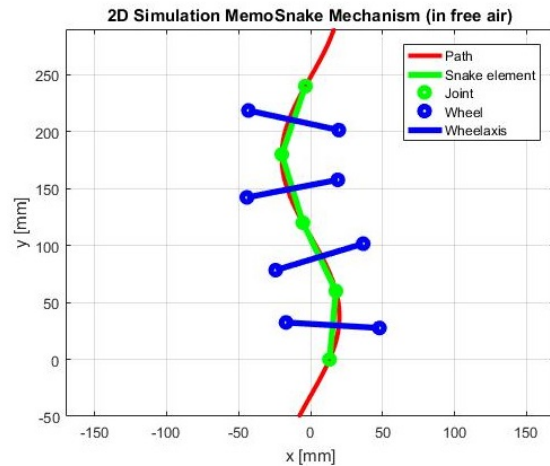


Figure 4.10: 2D simulation: The path (red sinus) is moved through a system of snake-elements (green), each having a wheel axis (blue) with wheels (blue dots).

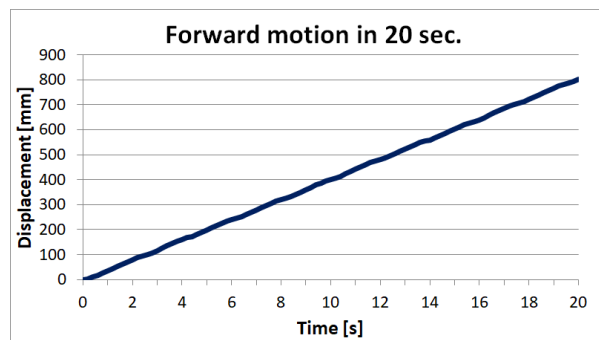


Figure 4.11: Forward motion: The resulting forward displacement of basic analysis over 20 seconds, with wheelbase=65mm, segment length=60mm, amplitude=20mm, frequency= $\frac{1}{300}$ /mm.

Considering the relationships listed above, the wheel is free to move in the direction perpendicular to the wheel axis and encounters infinite friction in the direction parallel to the wheel axis. The values of the force relation were given as output of this subsystem, so that the data could be logged and possibly analyzed in a later stadium.

4.3. Basic Analysis

The Simulink code and the detailed subsystems can be found in Appendix A. With the code, the first basic research question was answered: is the system able to generate forward motion? First, a wave was chosen which shows a smooth traveling wave through the system. A Matlab code was used to check the wave. This code does not include dynamics and friction, but shows how the wave moves through the snake-like system in free air. The code can be found in Appendix B. Figure 4.10 is the result; a path (red) is moved through the snake-like system (green), showing the motion of the system in free air.

In the code, basic dimensions were given to the parameters as segment length, wheelbase length, relative velocity, sinus amplitude and sinus frequency. In this basic analysis, only the forward motion was plotted; the result clarified if the system was able to move forward or not (Figure 4.11). The result of this basic analysis is clear; according to the model, forward motion is possible when a wave is pushed through the snake-like body. A point of discussion is the validity of the model. Since this model was built with basic blocks and a uniform mass distribution, there may be another situation in reality. Furthermore, it is hard to validate the values of the static and dynamic friction coefficients. Typically, they are between 0 and 1. However, in the model the static and dynamic friction coefficients were set to be 10. It can be concluded that the model requires validation with a prototype before the results of the model can be valued.

5

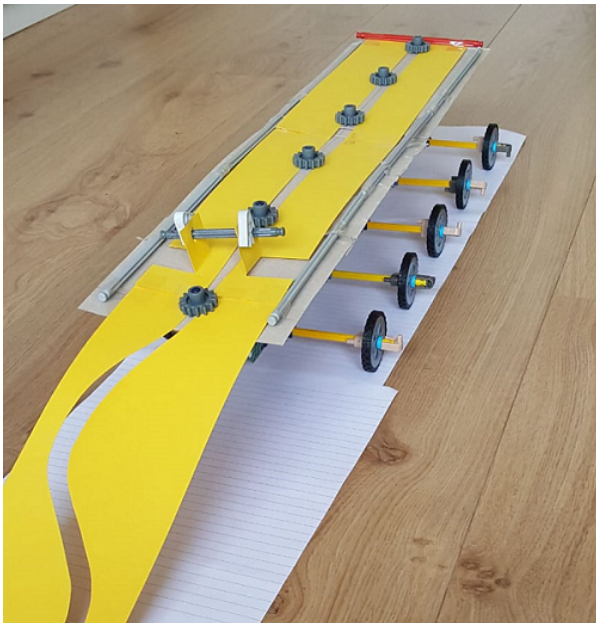
Design and Prototyping

5.1. Design Goal & Requirements

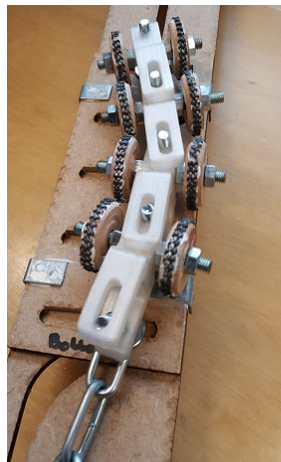
According to the model of Chapter 4, forward motion is possible with a snake-like robot if a sinus wave is pushed through the system. A prototype was developed to validate the Simulink model, the used values for the static and dynamic friction coefficients, and to have a real-life confirmation of the behavior.



(a) Total assembly



(a) Total assembly

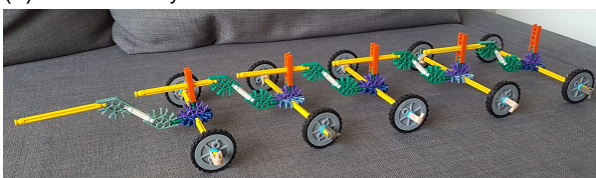


(b) Train



(c) Path

Figure 5.2: Wooden model: Wooden plate used as path, pulled through the system of 3D printed segments.



(b) Snake-like train

Figure 5.1: LEGO model: Cardboard used as path, pulled through the system of LEGO parts.

In the Simulink model of Chapter 4, an imaginary plane with a sinus wave was pushed through the system. However, while the Simulink model provides a simplification of the wanted behavior, prototyping must include practical solutions to solve problems such as the one for the path that cannot float in the air. To see the behavior of the system while a long plane with a random path moved through the system, two **"quick and dirty" models** were assembled

with the available material. First, a LEGO model was assembled (Figure 5.1) in which cardboard was used as path material. Since the path and snake-like train were too fragile, the model did not give any insight into motion behavior. Therefore, a quick improvement was made with a wooden plate and 3D printed snake-like train segments (Figure 5.2). The model gave insight into the behavior of the different snake segments of the snake-like train while the wooden path was pushed through the system. The hypothesis was: “while holding the snake-like train in place and pushing the wooden path through the system, the snake-like train would be able to slide a sheet of paper forward or backward.” Speaking in relative displacement, sliding a paper backward with a static snake-like train would in principle be the same as the snake-like train moving forward on a static plane.

However, these models did not give the desired insight into motion capabilities. As found out in the early models, driving the shape memory system by hand can be difficult and does not give a reliable knowledge of the behavior of the snake-like robot. Therefore, the decision was made to create a motorized model keeping low the cost of the entire robot, thus the following **requirements** were settled:

- Only a single motor must be used; to drive the mechanical shape memory system.
- The length of the robot must be approximately 300 mm; this makes the robot easy to handle on a table.
- Use a sinus path as pre-defined path which could be modelled in Chapter 6 to allow comparison of results between the Simulink model and the prototype.
- Use 3D printing to manufacture as many parts of the prototype as possible.
- Preferable to use the already available LEGO motor and battery box.
- The prototype should be able to move forward over a distance of at least one times his length in 30 seconds.

5.2. Design Ideas in Categories

The first step of conceptualization was related to the path; the type of system used as an imitation of the shape memory system determined the design direction of the whole snake-like robot. Therefore, the **first design choice** concerned the path feature. Figure 5.3 gives four options:

- One large forward and backward moving plate, similar to the wooden model.
- Multiple sideways moving plates along, similar to the MemoSlide mechanism, but with a predefined moving sequence.

- Multiple axes, rotating in such a way that a path is created.
- A belt that contains a path, positioned on two rolls; one at each end of the snake-like robot.

The concept of one large forward and backward moving plate would result in instability since the top plate would be significantly longer than the supporting snake-like robot underneath, or the robot should be significantly larger than in other designs. Multiple sideways moving plates would result in a high number of parts (as in the MemoSlide) and would be difficult to control in a simple prototype.

The concept of multiple axes could result in difficulties with aligning the path features in the rolls. Furthermore, rolls are more difficult to 3D print than flat surfaces. The most simple and effective solution seemed to be the belt concept. Note that the belt mechanism is stable since the mass distribution stays the same when the belt moves, assuming the belt has a uniform mass distribution. Furthermore, a single motor would be able to drive the belt, fulfilling the requirement. As for manufacturing, this concept seemed easy to manufacture; two rolls and a belt gave the total shape memory system.

With the choice of the belt concept, other design choices were taken. A **morphological overview** was used to picture the different categories of the snake-like robot, each with their own functions. Since the prototype contains two subsystems (shape control system and snake-like system), a morphological overview of each subsystem was made.

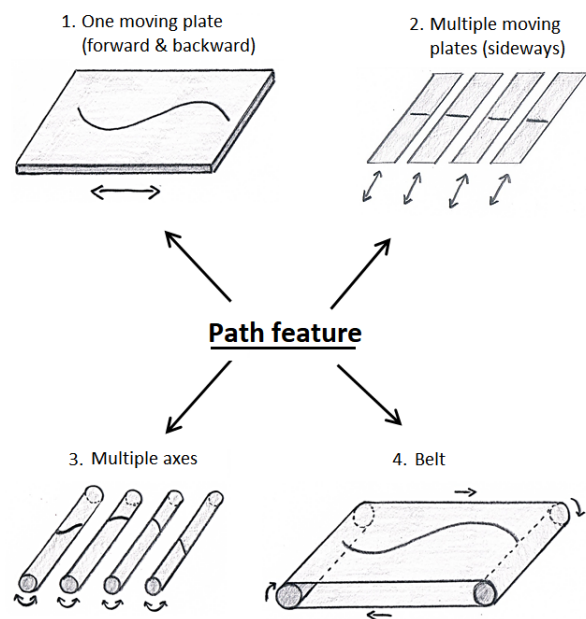


Figure 5.3: First design choice: How to pass the desired path through the system? Four options are given.

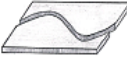


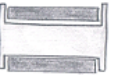
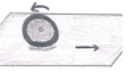




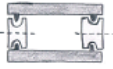
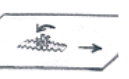

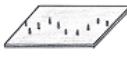


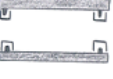

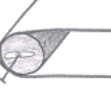

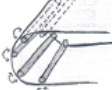




Category	Belt structure	Belt end guidance	Belt mid guidance	Belt slide prevention	Belt drive	Belt adjuster
Options	1. Flexible belt with all-through path cut-out 	1. Full static cylinder 	1. None 	1. Larger diameter roll end 	1. Rubber tire on belt 	1. Spring at guide 
	2. Flexible belt with engraved path 	2. Half static cylinder 	2. Large wheels 	2. Wheels with slot and pin on belt 	2. Sprocket wheel on belt with teeth 	2. Wheel spring 
	3. Flexible belt with pins 	3. Rolling cylinder 	3. Small wheels 	3. Slots on frame and pin on belt 	3. Sprocket wheel at frame end 	3. Bolt on guide axis 
	4. Inter connected links with engraved path 	4. Rolling axes 	4. Small sprocket wheels 			4. Bolt through guide axis 
	5. Inter connected links with pins 	5. Sprocket wheel 				

Figure 5.4: Morphological overview for the shape control system: A solution in each category leads to a concept idea.

The overview of the shape control system contains six categories (Figure 5.4):

- Belt structure: design of the belt, containing a path.
- Belt end guidance: how the belt would be guided at the two ends of the frame.
- Belt mid guidance: the belt may require guidance along the frame.
- Belt slide prevention: the belt is not allowed to slide sideways.
- Belt drive: connection between the motor and the belt.
- Belt adjuster: equipment to adjust the distance of the belt loop.

Looking at the first category, three of the five options in the category "belt structure" consist of a flexible belt with a path cut-out. However, as seen in the LEGO model, a flexible belt with the cut-out path would open up when a pin is moved through the path. The belt should be stiff to keep the shape of the path while a pin moves

through. The three flexible belt options therefore require a special material structure; flexible in one direction to bend at the rolls and stiff in the other directions to prevent opening up. This is difficult to establish with 3D printing. Therefore, the three options were cancelled out. The remaining two options can be stiff in all directions, with hinges in between to simulate the flexibility. Since the prototype had to be easy to manufacture and 3D printing would be used as manufacturing process, the inter connected links are the best options.

The belt end guidance options are based on the "belt on a role" idea. Besides regular rolls, a half role was also considered; the idea requires less space, and therefore, dimensions could be minimized. Another option is replacing the half-circle by multiple rolling axes. In that case friction between the guide and the belt could be minimized. A sprocket wheel was also considered. This type of wheels can be found in bicycles.

The belt mid guidance options are all inspired by tanks. Large guiding wheels were used in the design of the Soviet Christie-type BT-

7 tank, described by Ogorkiewicz (1991). The German Pz.Kpfw.IV tank contained multiple small guiding wheels [37]. The sprocket wheel as a driving mechanism was also used in the Vickers-Armstrongs Six-Ton tank [37]. Using small sprocket wheels, for mid guidance, are a similar idea to the end guidance option with sprockets in the previous category.

To prevent the belt from sliding sideways, three options were considered. An alternative is that the belt guidance could have a larger diameter at the two ends; the belt is restricted to move sideways. Another option has been found in the literature of tanks: Soviet Christie-type BT-7 tank showed wheels with a slot, through which a pin of the belt is navigated [37]. Static slots connected to the frame are a derivative of the last option.

In the category of belt drive, three options were considered. The most simple option is a rubber tire on the belt. The motor is linked to the axis of the wheel and friction between the belt and tire causes belt drive. Another option is a sprocket wheel on the belt; the sprockets would have more grip on the belt but still a limited contact area with the belt.

Positioning the sprocket wheel at the belt end guidance results in a larger contact area. Moreover, two functions are combined: belt drive and belt end guidance.

As a belt adjuster, a spring pushing the guide is an idea. Also, an extra wheel with a spring elsewhere at the belt is an option, inspired by the US M47 medium tank [37]. Moreover, adjusting the position of the belt by using a bolt can be considered as an option. That idea is inspired by the chain adjuster of a bicycle. Similar options were given in the morphological overview of the snake-like train. The overview of the snake-like system contains only three different categories (Figure 5.5):

- The number of snake segments
- Segment length; variable length systems and connection between segments
- Ground contact point: type of interaction element with surroundings

The number of segments is related to the number with which snake-like motion could be accomplished. Also, stability plays a role here; more segments would result in more ground contact points.

As for the segment length, four options were considered. The first option is a fixed length of elements. A mathematical analysis showed however, that a variable length is required. The other three options have variable length mechanisms. An upper (single) slider is considered, in which a pin is the connection between the two segments. To prevent jamming of the sliding mechanism, a double slider is considered as third option. The fourth option is elastic material between the rigid segments; a spring is an example.

As explained in Chapter 4, the ground contact is an important part in obtaining forward motion by friction. In this category, three options are considered. Non-rotating elements are the first option, paddles for instance. A second option is a rotating wheel axis with two wheels. The wheels are fixed to the wheel axis and not able to rotate with respect to the other wheel. In the third option, the wheel axis is fixed and the wheels are free to move individually.

5.3. Preliminary Concept Design

By combining solutions of each category of the morphological overview, **preliminary concepts** were made (Figure 5.7). The different combinations in the morphological overview can be found in Appendix C.

In the choice of the number of snake segments, the model of Chapter 4 was used. The model was simulated with one, two, three, and four segments. The resulting forward displacement shows that at least three snake segments are required to

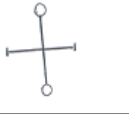
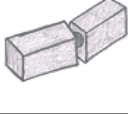

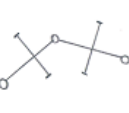
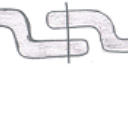





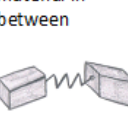
Category	Number of snake segments	Segment length	Ground contact point
Options	1. One 	1. Fixed length 	1. Non-rotating element 
	2. Two 	2. Upper slider 	2. Rotating wheel axis 
	3. Three 	3. Double slider 	3. Rotating wheels 
	4. Four 	4. Elastic material in between 	

Figure 5.5: Morphological overview for the snake-like system: A solution in each category leads to a concept idea.

generate forward displacement with snake-like motion (Figure 5.6). The aim of the prototype was to show the behavior and validate the motion. To get a better view on how the wave passes through the system, the four segments were chosen. This choice requires only a few additional parts, but provides a better visual insight.

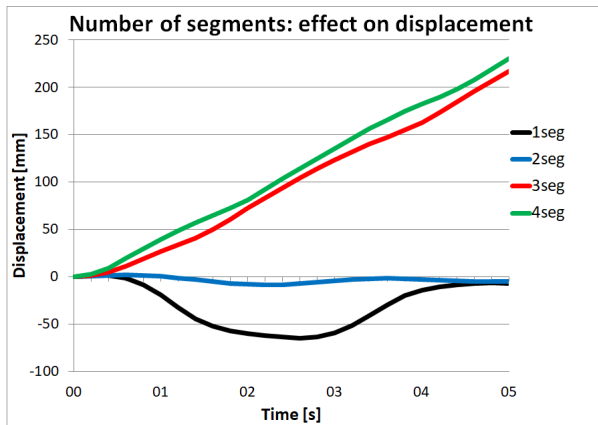
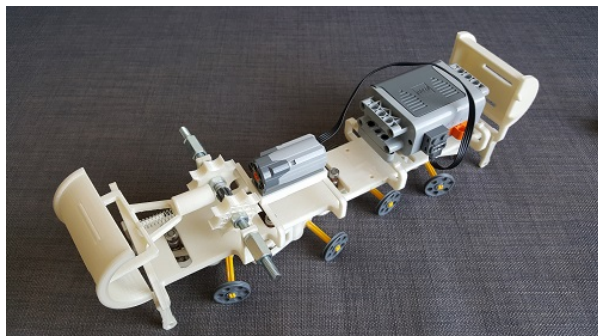


Figure 5.6: Segment analysis: Investigating the minimum number of segments to obtain forward displacement with snake-like motion.

During the preliminary design, 3D printing was used to obtain more insight into the parts and to quickly review dimensions. **Concept 1** uses two half static rolls as frame end belt guides. Moreover, a sprocket wheel on the belt is the driving mechanism, while the belt is adjusted by a spring at one guide. The belt is obtained by inter connected links with an engraved path and is prevented from sliding sideways by larger diameter ends of the static rolls (Figure 5.7a). Further guidance of the belt along the frame was not taken into account. The wheels and axes of the underlying snake-like train were not able to rotate; they were just non-rotating passive elements.

In contrast to the concept 1, **concept 2** focused on the guidance of the belt along the frame. The belt was supposed to move in between two rows of wheels. Moreover, sprocket wheels replaced the half static rolls at the end of the frame (Figure 5.7b). The large sprocket wheels were connected to the motor as well, to generate more contact area with the belt.

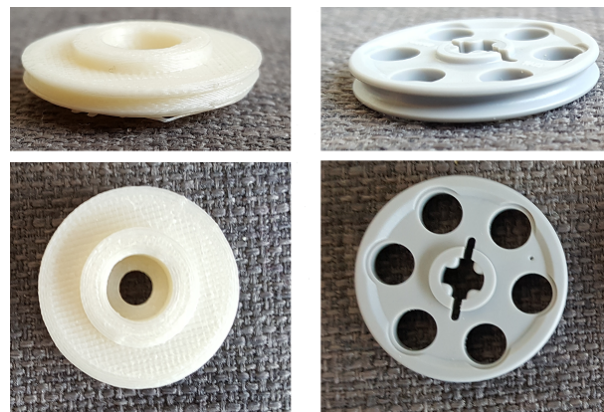
Both concepts had issues. These issues were analyzed, and as a result, multiple parts were re-designed. In particular, in concept 1, the wheels and their axes were not able to move. However, the snake-like motion includes making multiple curves. In a curve, the inner wheel rotates less than the outer wheel. Therefore, the concept idea of individual rotating wheels was chosen.



(a) Concept 1: two half-cylinders as belt end guidance, a spring as belt adjuster, two small sprocket wheels as belt drive and non-rotating elements as ground contact points.



(b) Concept 2: two sprocket wheels as both belt end guidance and belt drive, belt mid guidance by two rows of wheels along the frame.



(a) Wheel concept: New design and LEGO wheel



(b) Snake segment concepts: Early and improved design

Figure 5.7: Concept ideas: Two different versions from the morphological overviews are further developed.

Figure 5.8: Concept solutions: Proposals to solve the problems with the previous wheel and segment concept.

In order to use wheels of similar dimension as the used LEGO wheels, so that the LEGO tires could be used, a design was made with the same characteristics (Figure 5.8a). The diameter is the same as the LEGO wheel and the outer edge contains a groove where a LEGO tire could fit on. Moreover, at the center of the wheel a ball bearing could be placed, which should result in minimal friction at the wheel rotation.

Another issue noted in concept 1 was at the segments of the snake-like robot. In the concept, a ball caster was fit into the segment. The ball caster had the goal to decrease the friction between the frame of the shape memory system and the segments of the snake-like system.

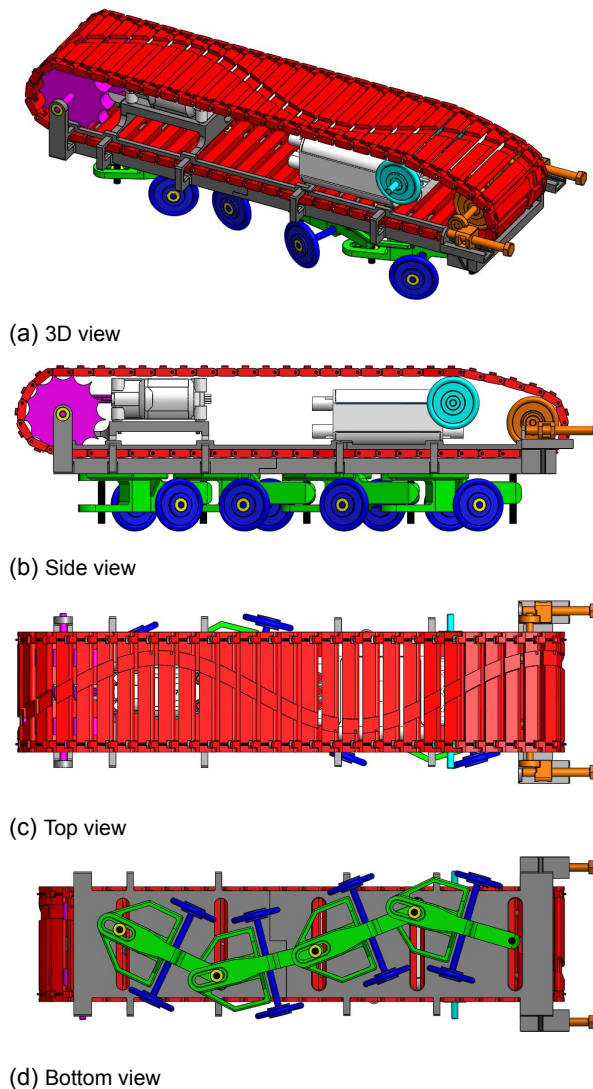


Figure 5.9: Detailed final design: Frame (grey) of the shape control system resting on four segments of the snake-like system (green) with the belt (red) being driven by sprocket wheels (magenta), connected to the motor (white), and adjusted with bolts (orange). The snake-like system uses (wheels) with ball bearings (yellow). The belt is guided over the battery box (white) with an extra set of wheels (cyan).

However, this resulted in the frame to rest only on the four ball casters, creating an unstable frame when the ball casters approached a straight line. Moreover, trying to slide the segments directly on the frame showed less friction than expected. A second concept eliminated the ball caster, adding frame support wings (Figure 5.8b).

Concept 2 was characterized by two parallel rows of small wheels as belt mid guidance. However, as Figure 5.7b shows, this would result in an large amount of wheels, raising the costs of the concept. Since one of the design requirements was to design a low-cost prototype, another design of belt mid guidance had to be found. Fixed slots on the frame and pins on the belt were chosen as the solution.

5.4. Final Prototype Design

By resolving the found problems, a **detailed design** was made. The resulting design (Figure 5.9) can be analyzed considering the two subsystems; the shape control system and the snake-like system. The shape control system consists of a frame (grey) on which a belt with the pre-defined path (red) is mounted. A LEGO motor (white) drives the mechanism via two sprocket wheels (magenta). A mechanism with two bolts (orange) could adjust the belt position. The snake-like system (green) consists of four segments, positioned underneath the frame. Pins (black) with ball bearings (yellow) form a first connection between the segments of the snake-like system and a second connection between the snake-like system and the shape control system.

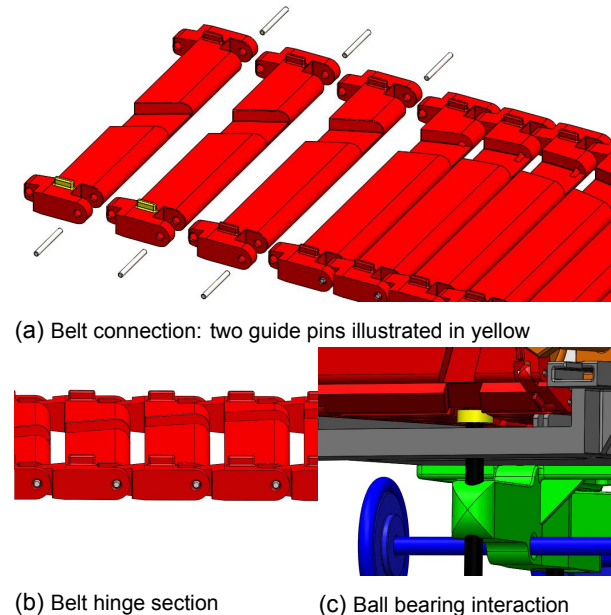
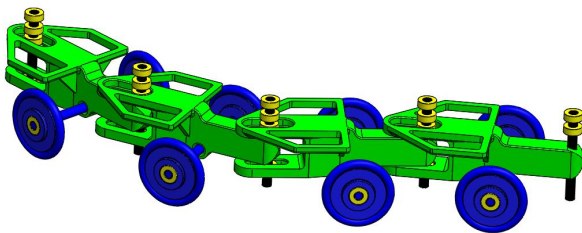
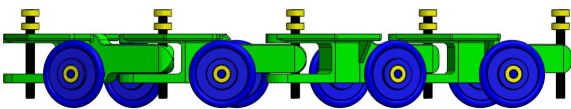


Figure 5.10: Belt design: Parts of the belt (red) are connected by using pins (white). Ball bearings (yellow) of the snake-like system run through the engraved path.

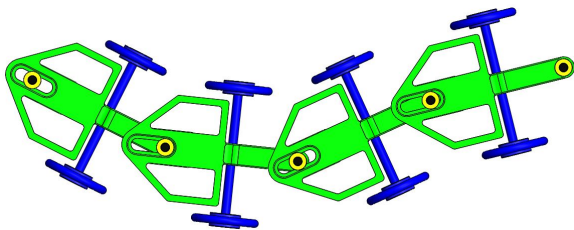
The **belt** is an assembly of rigid parts and small press pins (Figure 5.10a). The pins act as a hinge and the belt parts were designed so that hinge motion is possible; one part has a flat side, while the other part has a spherical side (Figure 5.10b).



(a) 3D view

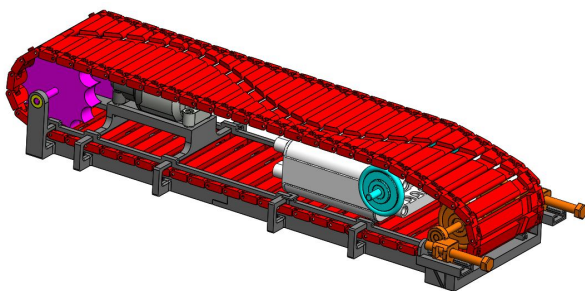


(b) Side view

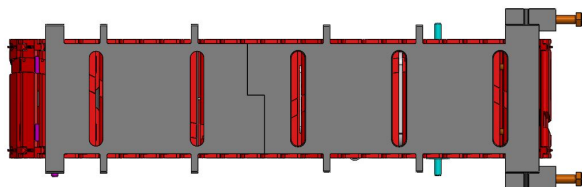


(c) Top view

Figure 5.11: Snake-like system design: Four segments connected with slider mechanism.



(a) 3D view



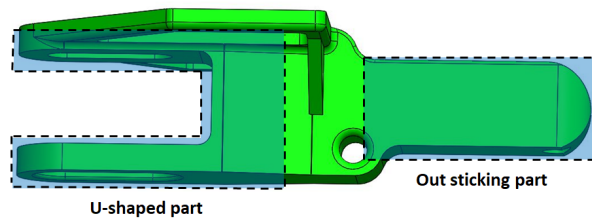
(b) Bottom view: slots in frame (grey) visible

Figure 5.12: Shape control system design: Belt with the engraved path (red), driven by sprocket wheels (magenta) and positioned with adjusting mechanism (orange).

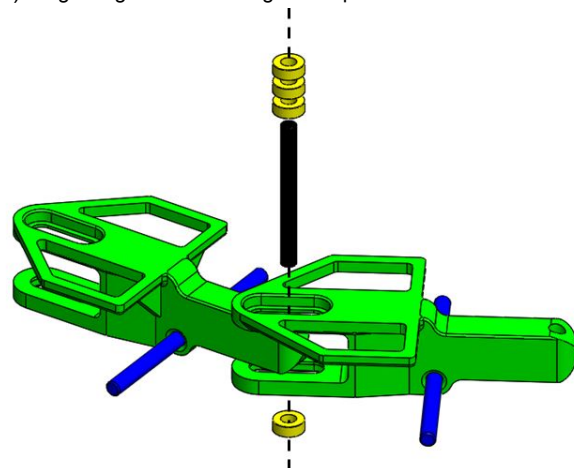
A spacing between the belt parts is created in between the hinges. This enables the sprocket wheels of the drive mechanism to fit with their teeth in between the segments. The design of the sprocket wheels is therefore dependent on the width of the belt parts. Moreover, the engraved sinus path was chosen so that one period of the sinus equals the width of a certain number of belt parts. This provided the option to manufacture the same period multiple times and connect them afterwards. The chosen sinus, with an amplitude of 20mm and a period of 228mm, is given by:

$$y[mm] = 20 \times \sin\left(\frac{\pi}{114} \times x\right) \quad (5.1)$$

Each pin of the snake-like segment has two ball bearings sticking out above the segment bases (Figure 5.11b). The upper ball bearing is the connecting element between the snake-like system and the shape memory system; the ball bearing runs through the engraved path of the shape memory system (Figure 5.10c). The lower ball bearing on the pin is the interaction element between the snake-like robot and the frame of the shape memory system; the ball bearing runs through the slots of the frame (Figure 5.12b). The slots are similar to the guidance plate of the MemoSlide (Figure 3.11).



(a) Single segment consisting of two parts



(b) Two segments with pin connection

Figure 5.13: Segments design: Detailed view of the base (green) with wheel axis (blue), but without wheels. Ball bearings (yellow) run in the slider slots, while a pin (black) connects the ball bearings and both segments with each other.

Each pin of the snake-like system is positioned in such a slot. The ball bearings result in low friction motion of the snake-like system in the slots of the frame. Two other ball bearings were used in the sliding mechanism of the **segments** of the snake-like system. Each segment contains two parts: a U-shaped part and an out sticking smaller part (Figure 5.13a). The smaller out sticking part of the segment fits in between the U. Slots in the upper and lower arm allow the connection of the segments; a pin runs through the slots and a hole in the other segment (Figure 5.13b). A ball bearing is placed in each slot. These ball bearings have two functions: smoothing the sliding and preventing jamming of the segments. The earlier discussed printed wheels with LEGO tires (blue) are connected to the segment with a fixed wheel axis (blue). are fit on the segments. As the given solution, ball bearings in the wheels (yellow) allow free rotation of the wheel on the axis (Figure 5.11a).

Another aspect to note is the **belt adjusting mechanism** (orange). The mechanism consists of an axis with two wheels guiding the belt. The axis is connected to the frame with a slider on each end of the axis. The mechanism enables adjusting of the belt path. It is similar to the principle used in bikes; the belt cannot be put under tension but the distance between the frame end guides of the belt should be defined in such a way that the belt runs smoothly. Adjusting happens by two bolts. By rotating the bolts the adjusting mechanism slides on the frame, increasing or decreasing the distance of the belt.

Focusing on the shape control system, the frame is designed in such a way that the electric components can be placed at the center of the belt. By doing this, no exterior components were required. The stability increased since the mass is located above the wheels of the snake-like system. Note that an extra set of wheels was added at the battery box. These wheels prevent the belt from sliding over the battery box, which would result in jamming of the total mechanism. The **drive mechanism** of the belt is the same as the one seen in concept 2 of the preliminary design. The LEGO motor is connected to two sprocket wheels via a worm wheel and a small gear wheel (Figure 5.14a). The motor is located in between two sprocket wheels to make the system symmetrical and eliminate the possibilities of jamming due to the system to bend sideways when only one sprocket wheel is located on one side of the motor. The sprocket wheels “grasp” the belt parts and force the belt to move (Figure 5.14c-d).

Since electric motors generally have high-speed and low-torque specifications, the worm gear is used to reduce the speed and increase the available torque. Moreover, a worm gear is compact in dimensions, which was required to place the motor and drive mechanism in the center of the belt. To prevent the worm wheel from losing

connection with the gear wheel when the axis of the worm wheel bends upward under the load of forces of motion, the axis of the worm wheel is supported by the frame (Figure 5.14b).

In order to choose a suitable LEGO motor, a calculation was done (Appendix D). The required motor torque was calculated to drive the belt: 0.52×10^{-2} Nm. This result is significant less than the available motor torque (6.48×10^{-2} Nm). However, it has to be taken into account that the pins of the snake-like system will cause resistance to the belt motion. The maximum allowable resistance load is calculated to be $23.8N$. Since this is a large buffer, it is assumed that the LEGO motor is suitable to use in this snake-like robot.

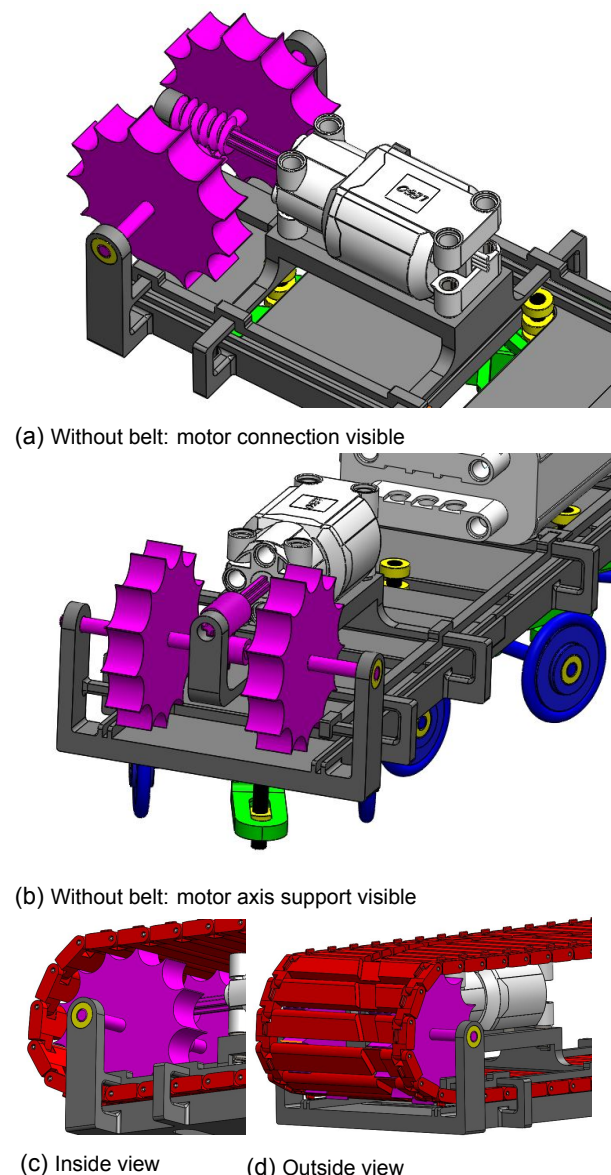
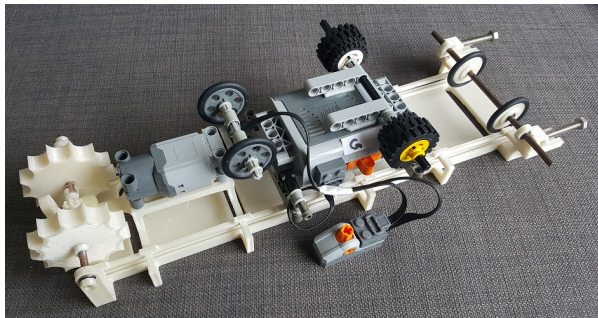


Figure 5.14: Drive mechanism design: Two sprocket wheels (magenta) with a gear wheel (magenta) in between, connected to the motor (white) via a worm wheel (magenta). The sprocket wheels fit with their teeth in between the belt parts (red).



(a) Total assembly



(b) Shape control system without belt

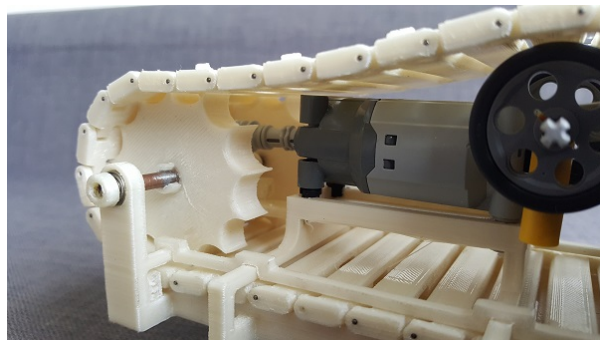


(c) Snake-like system

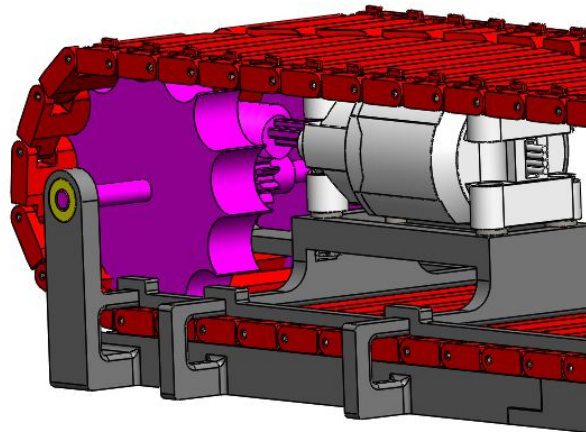
Figure 5.15: Prototype subsystems: Shape control system and snake-like train with 3D printed parts (white).

5.5. Prototype Manufacturing

The drawings of the detailed design can be found in Appendix F. The final design was manufactured by using 3D printing. Furthermore, 3D printing was a quick solution to the manufacture of the frame of the shape control system. 3D printing allows complex shapes to be produced, increasing freedom in the design process. The only aspect to take into account was that the dimensions of the printer did not allow the frame to be printed as a single part but in two separated parts. The Ultimaker 3 was the available printer. During the prints, a layer height of 0.15mm and a fill level of 20% were used. These specifications are stated as “normal printing” in the 3D printer. Polylactic Acid (PLA) AA 0.4 was used as material. This thermoplastic polyester is a commonly used material in prototyping due to its ease of use. Figure 5.15 shows the resulting assembly of the prototype. Note that the white-colored parts are the PLA parts manufactured with a 3D printer.



(a) Prototype



(b) CAD model

Figure 5.16: Drive mechanism: Resulting prototype compared to design.

Table 5.1: Prototype specifications: The calculation of the belt speed can be found in Appendix E.

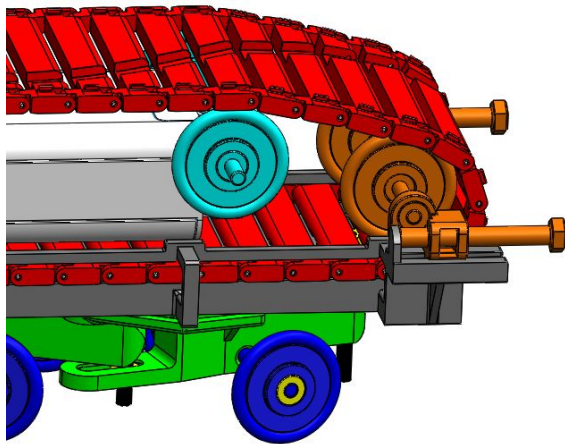
Parameter	Value
Weight	0.706 kg
Length	330 mm
Width	106 mm
Height	110 mm
Belt speed	62.7 mm/s

Moreover, a switch was added between the motor and the battery box. This enables easy turning on and off of the system. The main specifications of the prototype are summarized in Table 5.1.

Focusing on the comparison between prototype and design, it can be noted that, instead of one extra pair of wheels, two extra pairs of wheels were added to guide the belt over the battery box and motor. Another adjustment made in the prototype compared to the CAD model, are the pins on top of the belt parts. As shown in Figure 5.17a, the even number of parts contain guiding pins at the outside. These pins run through the slots of the frame.



(a) Prototype



(b) CAD model

Figure 5.17: Belt adjuster: Prototype compared to the design.

In the design, each belt part had those pins (illustrated in Figure 5.10a). However, during manufacturing and assembling it was noted that this caused too much friction. Also, fewer pins were needed to guide the belt in the right way, so half of the pins were removed.

The belt parts were connected via pins at each hinge. However, to adjust motor settings or change the batteries of the mechanism, it should be possible to open the belt again. It is difficult and time consuming to get the pins back out of the hinge. Therefore, one pair of hinges was made in such a way that the belt can be opened up at that point: the belt part is shorter so that the pin can stick out without being longer than other belt parts. Jamming was prevented and the belt can be opened and closed whenever needed.

5.6. Evaluation and Validation

5.6.1. Evaluation Method

The motion of the system was analyzed with the model of Chapter 4. With one set of parameters, the design and prototype were made with the aim

to validate the model by comparing the results of the model with the reality. Furthermore, it was investigated what type of surface belongs to the used values of the static and dynamic friction coefficients. The friction parameters in the model were defined to describe high friction between the wheels and ground surface. In reality, the friction depends on the structure of the surface; rough surfaces create more friction than smooth surfaces. Therefore, the prototype was tested on four different surfaces, each with their own roughness:

- Laminate flooring
- Sheet of Paper
- Carpeting
- Wallpaper

Both laminate flooring and paper were described as smooth surfaces in which the paper is a fraction less smooth than the laminate flooring. Significant rougher surfaces were found with carpeting and wall paper.

The prototype was tested on the four described surfaces (Figure 5.18). The starting position was marked with a pencil on the surface. Thereafter, the motor of the prototype was turned on and moved for 20 seconds. The prototype was turned off and the end position was marked. The displacement from start to finish position was measured and logged. Furthermore, the displacement from the straight line to the side was measured to evaluate the deviation between the predicted motion and reality.

5.6.2. Results and Assessment

For each of the four surfaces, forward displacement (p_x) and displacement to the side (p_y) were measured (Table 5.2). The model from Chapter 4 was used to simulate the same specifications as the prototype, so that the model could be validated by comparing results.



(a) Laminating Floor

(b) Paper



(c) Carpeting

(d) Wallpaper

Figure 5.18: Test on different surfaces: Motion behavior and displacement were analysed on four different surfaces. The pencil marks the starting position.

Table 5.2: Displacement comparison: Prototype on surfaces with different friction rates.

Surface	Friction	px [mm]	py [mm]
Laminate flooring	low	550	350
Paper	low	620	270
Carpeting	high	960	90
Wallpaper	high	980	150

The simulation of the specifications resulted in a forward displacement of 840mm and a sideways displacement of 40mm. Comparing these values with the results in Table 5.2, it can be concluded that the forward displacement of the model is close to the high friction surfaces. Since the forward displacement of the model lies in between the values for the low and high friction, it was assumed that the friction values in the model are realistic. With that finding, it was concluded that the model is valid to use during further assessment.

6

Parameter Assessment

6.1. Parameter Selection

Since the prototype of Chapter 5 validated the model of Chapter 4, the model could be used to assess different configurations easily. However, each block of the model needs to set specific parameters of the components. For instance, the wheels need to know the dimensions of the radius and their thickness. Furthermore, choosing a sinus wave as input, amplitude and frequency are parameters that can be varied. A simulation time, the time span over which the model runs, also had to be given. To be able to change those values in a fast and controlled way, a Matlab script was written. This script contains all parameters of the Simulink model.

Values were given to the parameters and the script had to be run before starting the simulation. The script with all parameters can be found in Appendix G. The dimensions of the segments and wheels are fixed; the wheels are described by the available Lego wheels and the segment length is set to fit with the desired frame length of approximately 300mm. Instead, the **wheel axis length**, the **sinus amplitude**, and the **sinus frequency** were changed during simulations, to check the effect of the specific parameter on the forward displacement. Moreover, the extreme situations of each of the three selected parameters were assessed.

Table 6.1: Simulation parameters: Values that did not change during simulations.

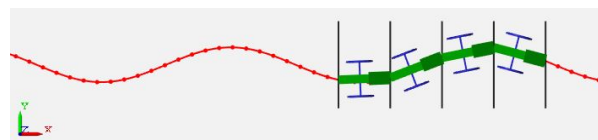
Parameter	Value
Wheel diameter	31 mm
Wheel axis diameter	2 mm
Slot spacing	60 mm
Frame width	100mm
Number of segments	4
Relative Path speed	60 mm/s
Simulation Time	20 s

For all simulations, the dimensional parameters which did not change are shown in Table 6.1. Each situation was simulated for 20 seconds and the data of motion were logged. One simulation with this simulation time would take approximately three to four hours to run. In total, 50 different simulations were done.

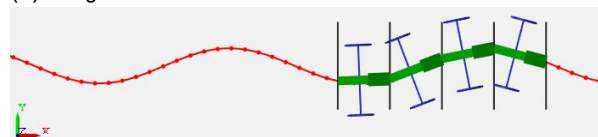
6.2. Wheel Axis Length

6.2.1. Assessment Range

One of the parameters of which the effect on forward displacement was checked during the simulation is the wheel axis length. A longer wheel axis would provide better stability of the robot, but it is unclear what effect a longer wheel axis would have on the forward displacement. In order to analyze this effect, nine different wheel axis lengths were simulated: from 40mm to 80mm with steps of 5mm. The effect of doubling the wheel axis length could be assessed. Note that during this simulation, the path is not changed; the same amplitude (20mm) and frequency ($\frac{1}{300}$ /mm) were used in all nine cases.



(a) Range minimum: 40mm



(b) Range maximum: 80mm

Figure 6.1: Wheel axis length range: The minimum and maximum of the selected wheel axis lengths which were simulated.

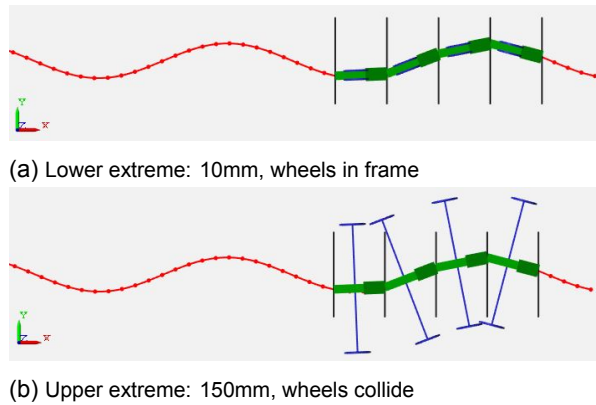


Figure 6.2: Wheel axis length extremes: The two extreme situations.

Figure 6.1 shows the minimum and maximum wheel axis length to get an idea of the changing parameter. The other cases can be found in Appendix H.

6.2.2. Extreme Configurations

Besides the analysis of the realistic range of wheel axis lengths, the extreme values could also give interesting information. Two extremes were analyzed:

- The wheels are located in the frame due to the small wheel axis (Figure 6.2a).
- The wheels collide with other wheels due to the large wheel axis (Figure 6.2b).

6.3. Sinus Amplitude

6.3.1. Assessment Range

Another parameter that was assessed is the amplitude of the sinus wave. Since both the amplitude and frequency influence the motion of the snake-like robot directly, these parameters were interesting in the analysis of forward displacement. In the case of the amplitude, eight different cases were assessed: an amplitude of 4mm to 28mm in steps of 4mm.

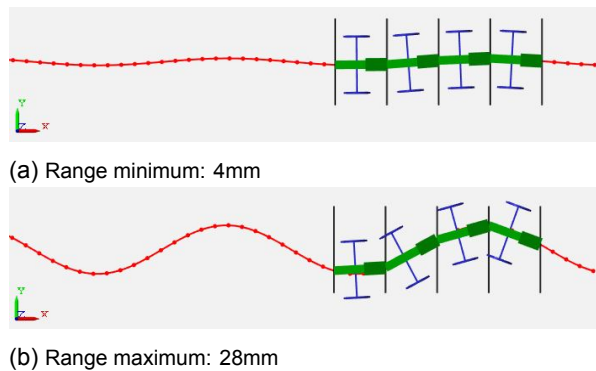


Figure 6.3: Sinus amplitude range: The minimum and maximum of the selected amplitudes which were simulated.

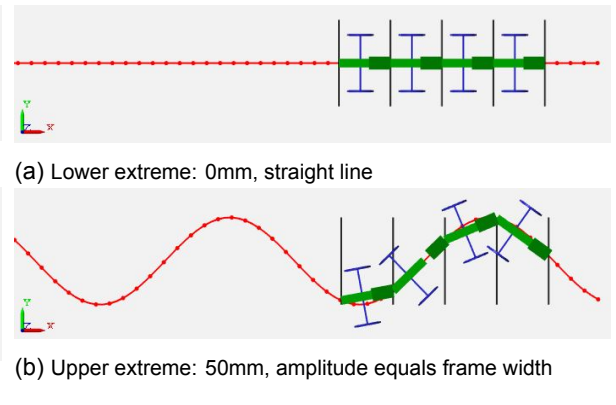


Figure 6.4: Sinus amplitudes extremes: The two extreme situations.

To give insight into the changing parameter, Figure 6.3 shows the minimum and maximum value. The other situations can be found in Appendix I. It can be seen that the small amplitude (4mm) approaches a flat line. The difference with the largest amplitude (28mm) is significant, so that the relationship between amplitude and forward displacement could easily be found. Equal to the situation of the wheel axis lengths, the other parameters were kept the same during the simulation. In this case, one specific wheel axis length (65mm) and frequency ($\frac{1}{300}$ /mm) were taken, while the amplitudes changed.

6.3.2. Extreme Configurations

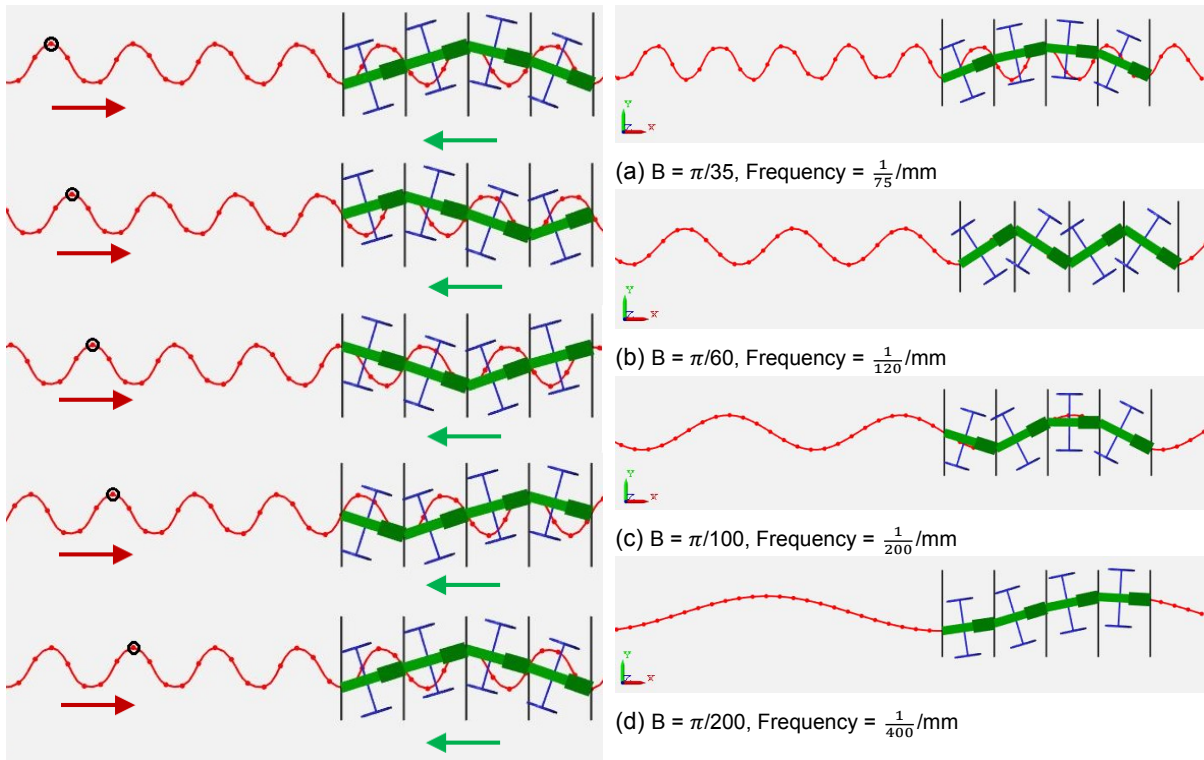
Furthermore, the behavior of the snake-like system was also analyzed in two extreme situations:

- Zero amplitude, resulting in a straight line (Figure 6.4a).
- The amplitude equals the frame width, the maximum possible amplitude since the path is pushed through the frame (Figure 6.4b).

6.4. Sinus Frequency

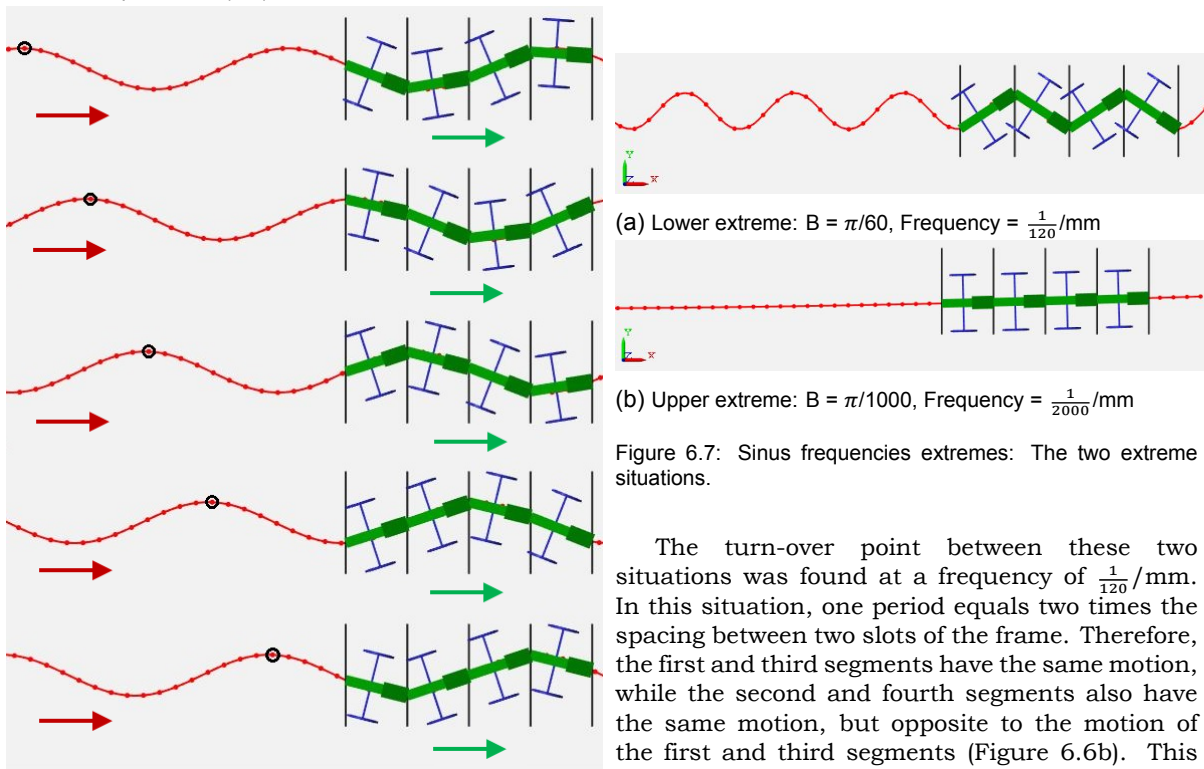
6.4.1. Assessment Range

In the case of the frequency, more cases were assessed due to the large variety of possibilities. Figure 6.6 shows a selection of the simulated frequencies, but in reality different cases were simulated, ranging from $\frac{1}{75}$ to $\frac{1}{1000}$ /mm. All cases can be found in Appendix J. Again, the amplitude (20mm) and wheel axis length (65mm) were taken constant during this simulation. The snake-like system creates two types of motion: “forward” and “backward” motion (Figure 6.5). With lower B 's in the $y = A \cdot \sin(B \cdot x)$ relation (high frequencies), the snake-like robot does not follow the shape of the pre-defined wave; the snake-like robot created a new wave on its own (Figure 6.6a), which moves in opposite direction of the path wave. When taking higher B 's, the snake-like robot follows the wave (Figures 6.6c and d).



(a) Backward motion: shape wave (green) moves in opposite direction as path wave (red)

Figure 6.6: Sinus frequencies: A selection of the frequencies which were simulated while other parameters stayed the same.



(b) Forward motion: shape wave (green) moves in same direction as path wave (red)

(a) Lower extreme: $B = \pi/60$, Frequency = $\frac{1}{120}$ /mm
 (b) Upper extreme: $B = \pi/1000$, Frequency = $\frac{1}{2000}$ /mm

Figure 6.7: Sinus frequencies extremes: The two extreme situations.

Figure 6.5: Backward and forward motion: The black dot shows how the sinus wave moves. The motion of the path is indicated with a red arrow and the wave inside the shape is indicated with a green arrow.

The turn-over point between these two situations was found at a frequency of $\frac{1}{120}$ /mm. In this situation, one period equals two times the spacing between two slots of the frame. Therefore, the first and third segments have the same motion, while the second and fourth segments also have the same motion, but opposite to the motion of the first and third segments (Figure 6.6b). This means that the snake-like robot does not have a wave, but counteracting segments.

6.4.2. Extreme Configurations

Besides the chosen assessment range of frequencies, the extremes were also investigated. One extreme was found already: the turn-over

point between forward and backward motion. The other extreme is an infinitely high B (low frequency), which would result in a straight line. However, to investigate the motion when there is still a wave, a significant higher B was described as extreme: $B = \frac{\pi}{1000}$ (Figure 6.7).

6.5. Simulation Results

6.5.1. Wheel Axis Length Results

After completing the different simulations, the logged data of contact forces, rotation angle, displacement, velocity, and acceleration were collected and plotted. The data of forward displacement showed two parts of information:

- How much the system was translated after a 20 second simulation
- How the progress in displacement was during the simulation

The velocity also gave insight into two parts of information:

- How the wave pattern influenced the velocity pattern
- The velocity of the system compared to the velocity of the belt

If the velocity of the system equals the relative velocity of the belt with respect to the system, the belt would not be moving with respect to the global world. The acceleration was logged to see if the system experienced highly variable acceleration and, as a consequence, did not move smoothly. The sideways displacement could give insight in the deviation of the motion with respect to the expected straight forward motion.

The resulting displacements from the simulations with different wheel axis lengths, 40mm till 80mm, showed two relations: the forward displacement stayed equal for all situations (960mm), while the sideways displacement increased with an increasing wheel axis length (Figure 6.8).

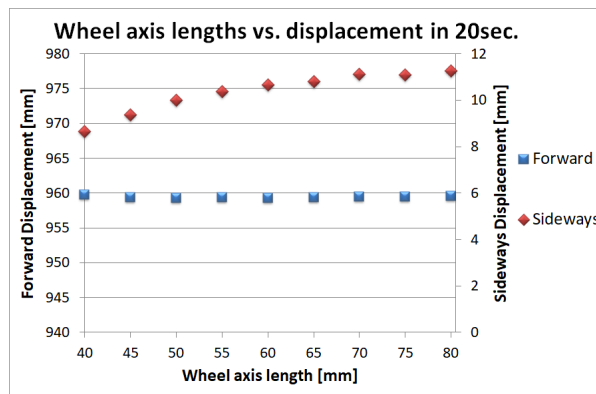
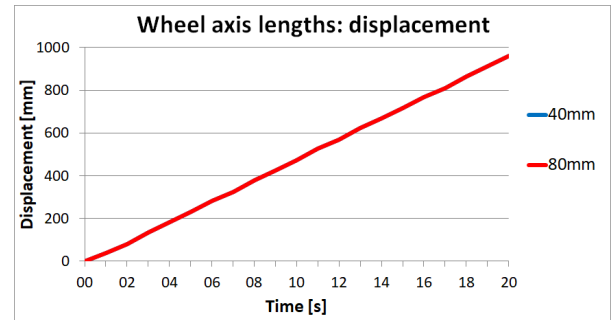
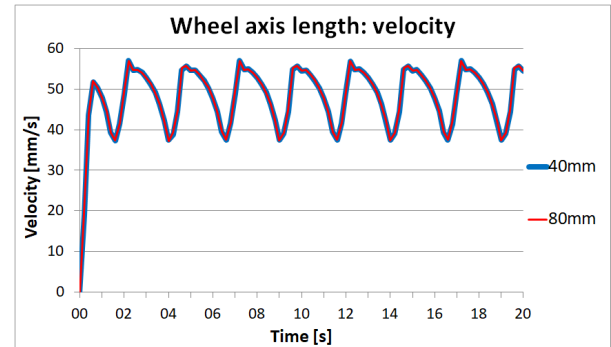


Figure 6.8: Displacements vs. wheel axis length: The results of forward and sideways displacement with different wheel axis lengths, during a 20 second simulation.

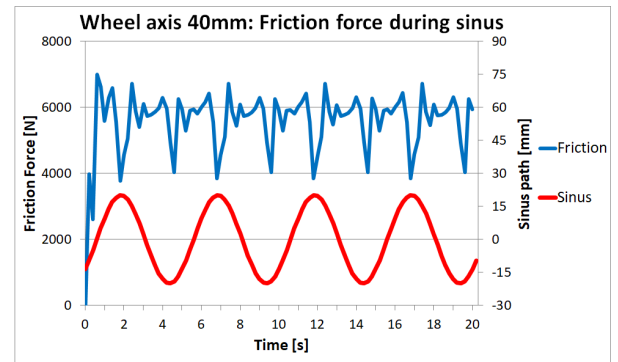


(a) Forward displacement vs. time

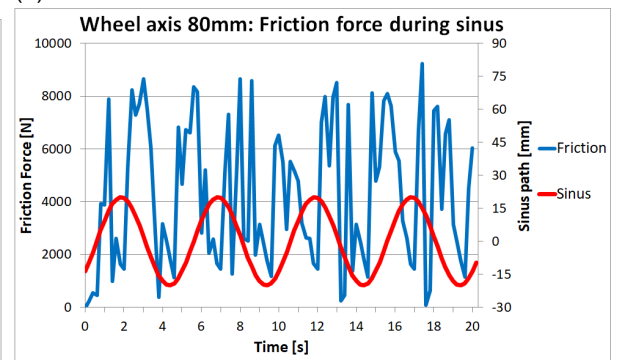


(b) Velocity vs. time

Figure 6.9: Effect of wheel axis length on motion: Forward displacement and velocity during a 20 second simulation.

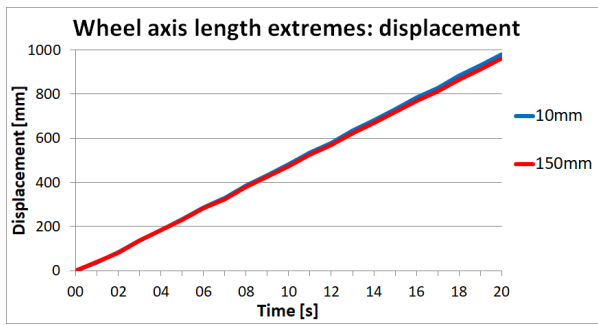


(a) Friction vs. time

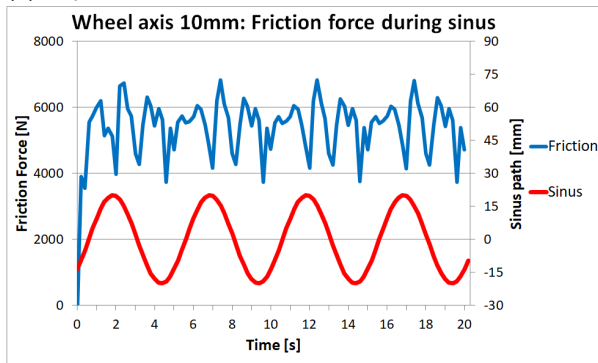


(b) Friction vs. time

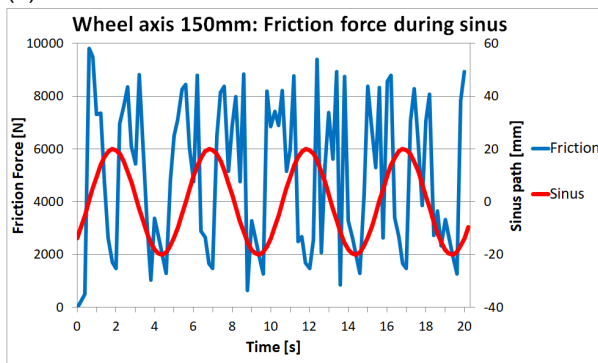
Figure 6.10: Effect of wheel axis length on friction: The resultant friction force on one wheel during the sinus wave in the 20 second simulation.



(a) Displacement vs. time



(b) Friction vs. time for a wheel axis of 10mm



(c) Friction vs. time for a wheel axis of 150mm

Figure 6.11: Extreme wheel axes: Forward displacement and friction forces during a 20 second simulation.

The effect of the wheel axis length on the motion is shown in Figure 6.9. Since the forward displacement is not affected by an increasing wheel axis length, the displacements of both the upper and lower limit of the assessment range shows similar progress in displacement (Figure 6.9a). The effect on the velocity is shown in Figure 6.9b; similar patterns were obtained for the upper and lower limit of the assessment range. The pattern of the velocity shows that the snake-like robot was not moving at a constant speed. The velocity varies between 37 and 57mm/s. The data of the acceleration did not give useful information. The plots can be found in Appendix H.

The contact forces gave information about the resultant friction on the wheels during motion. For the lower and upper limit of the assessment

range, the resultant friction force on one wheel is shown in Figure 6.10. The sinus is plotted to compare the friction pattern with the phase of the wave the wheel was in. The friction pattern shows peaks in a similar period as the sinus (Figure 6.10a). Moreover, the friction of the situation with a large wheel axis length shows a pattern with a larger variety (Friction 6.10b). In both situations, the friction value drops when the sinus reaches its extremes. The simulations of the extreme situations show similar results as the assessment range (Figure 6.2). The lower extreme (10mm) shows similar friction values as the 40mm situation and the upper extreme (150mm) is similar to that of the 80mm situation. Both situations result in a displacement of 960mm.

6.5.2. Sinus Amplitude Results

The simulations of the different sinus amplitudes resulted in the displacement of Figure 6.12. The forward displacement shows a slightly increasing displacement when the amplitude increases: 4.8% increase in displacement when the amplitude increases from 4 to 28mm. The sideways displacement, deviation with respect to the expected straight forward displacement, shows a pattern with a peak around 12mm. After that peak, the forward displacement increased while the sideways displacement decreased.

Figure 6.13a shows the forward displacement of different amplitudes over time. It can be noted that the pattern is similar and the lines seem to run parallel. The only significant difference is noted at the start of the simulation; the configuration with a larger amplitude accelerates faster than smaller amplitudes. Figure 6.13b supports this observation. The 4mm amplitude shows a different pattern at the start of the sequence. Moreover, the velocity curve again shows a wave pattern instead of a constant velocity. The velocity varies between 36 and 59mm/s.

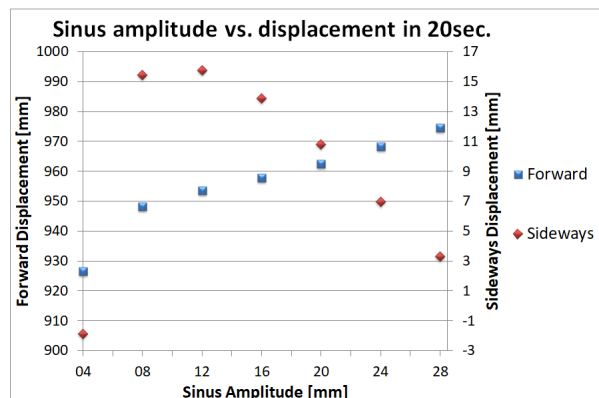
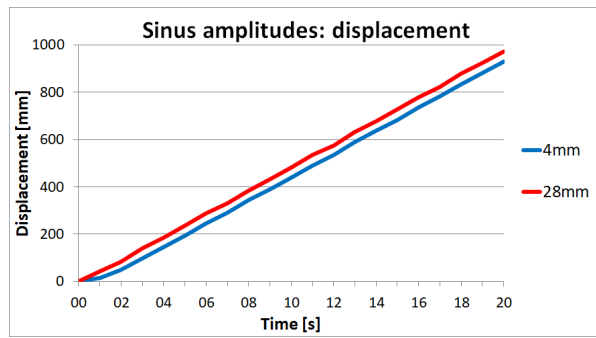
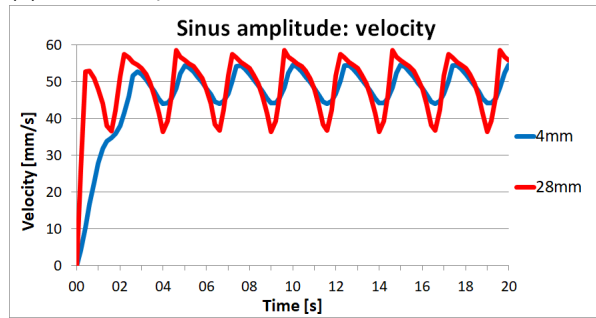


Figure 6.12: Displacements vs. sinus amplitude: The results of forward and sideways displacement with different sinus amplitudes, during a 20 second simulation.



(a) Forward displacement vs. time

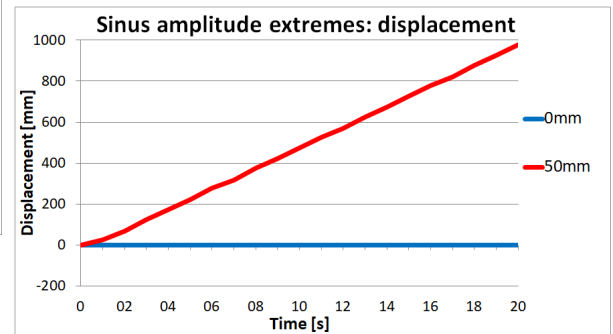


(b) Velocity vs. time

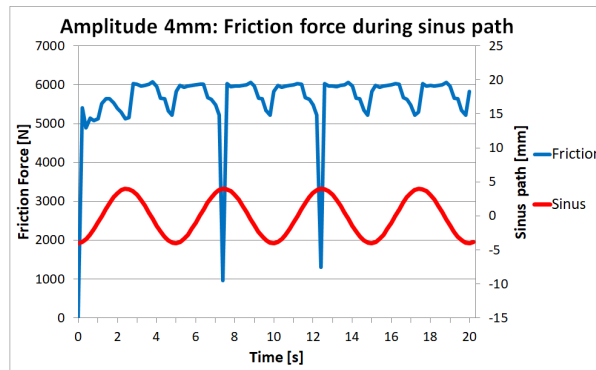
Figure 6.13: Effect of sinus amplitude on motion: Forward displacement and velocity during a 20 second simulation.

The friction on one wheel shows a pattern with a similar period as the sinus wave. The friction results of the 4mm sinus amplitude are approximately as high as the friction results of the 28mm sinus amplitude (Figure 6.14a-b).

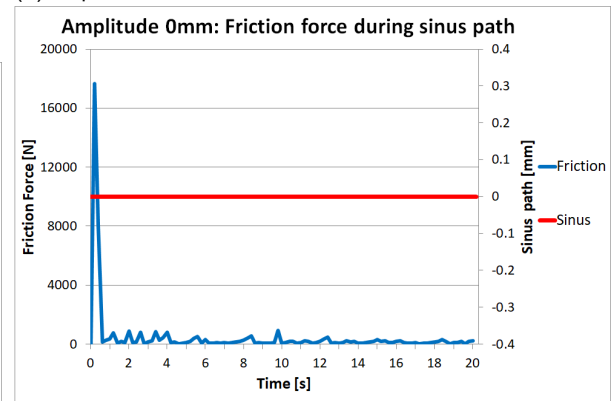
A straight-line, instead of a wave, was one of the extreme situations of the sinus amplitude. This situation resulted in zero displacement (Figure 6.15a). The other extreme situation (50mm) shows a similar displacement as the assessed range of sinus amplitudes: approximately 980mm in 20 seconds. In terms of friction, the straight line showed a different result than the non-zero sinus amplitudes.



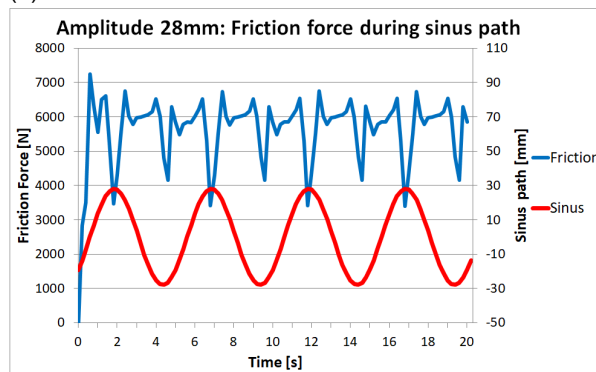
(a) Displacement vs. time



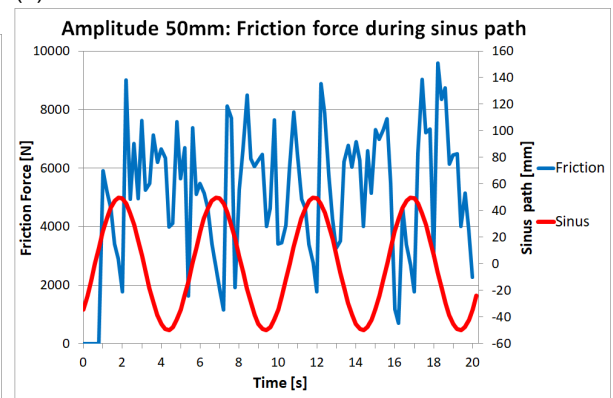
(a) Friction vs. time



(b) Friction vs. time



(b) Friction vs. time



(c) Friction vs. time

Figure 6.14: Effect of sinus amplitude on friction: The resultant friction force on one wheel during the sinus wave.

Figure 6.15: Extreme sinus amplitudes: Forward displacement and friction forces during a 20 second simulation.

A straight-line results in very low friction, with the exception of the first second (Figure 6.15b). The situation with a large sinus amplitude (50mm) results in similar friction values as the other assessed sinus amplitudes. However, less of a pattern was noted in this situation.

6.5.3. Sinus Frequency Results

The relation between the sinus frequency and forward displacement shows a pattern with an optimum (Figure 6.16). At a frequency of $\frac{1}{450}$ to $\frac{1}{600}$ /mm, the forward displacement reaches a certain optimum. However, the results of the sideways displacement are highly variable in that region and seems to influence forward displacement:

1. High forward displacement and low sideways displacement.
2. High sideways displacement and lower forward displacement than surrounding results.

Focusing on the forward displacement, negative and positive displacements were noted (Figure 6.17a); both forward and backward motion was created. The higher frequencies, in which the period is larger than the length of a snake segment, results in a negative displacement. The frequency in which the segments counteract each other ($\frac{1}{120}$ /mm) results in a slightly backward motion. The results of lower frequencies ($\frac{1}{200}$ and $\frac{1}{400}$ /mm) shows forward displacement with an increase in displacement when the frequency decreased and the period increased.

The frequency of $\frac{1}{75}$ and $\frac{1}{120}$ /mm shows another behavior at the velocity as well. A negative velocity was seen at a frequency of $\frac{1}{75}$ /mm with a maximum velocity of -272mm/s. The frequency of $\frac{1}{120}$ /mm shows a velocity between 0 and -58mm/s.

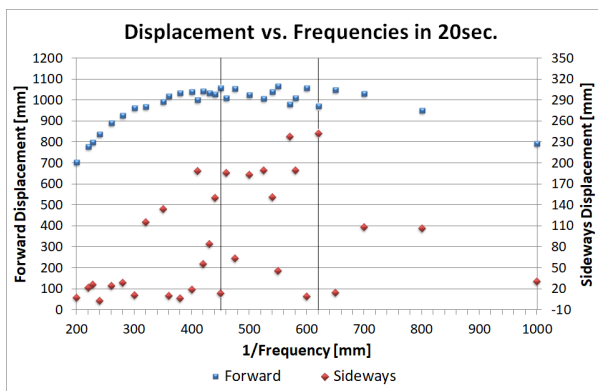
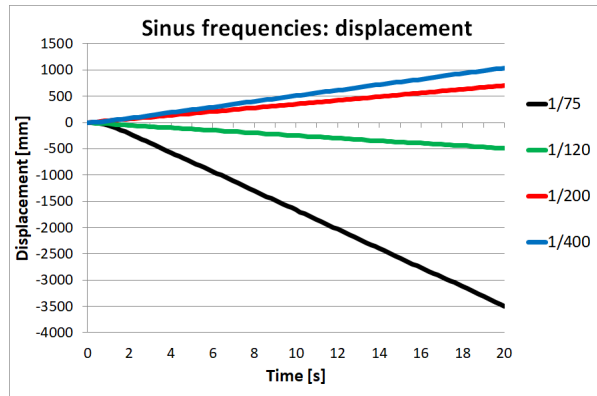
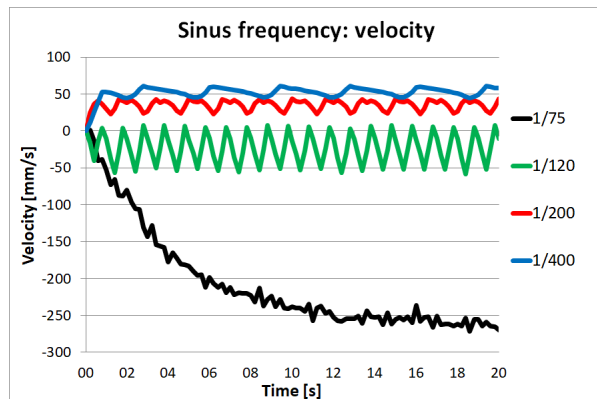


Figure 6.16: Displacements vs. 1/sinus frequency: The results of forward and sideways displacement with different sinus frequencies, during a 20 second simulation. 1: a high forward displacement and low sideways displacement. 2: a high sideways displacement and a lower forward displacement than surrounding results.



(a) Forward displacement vs. time



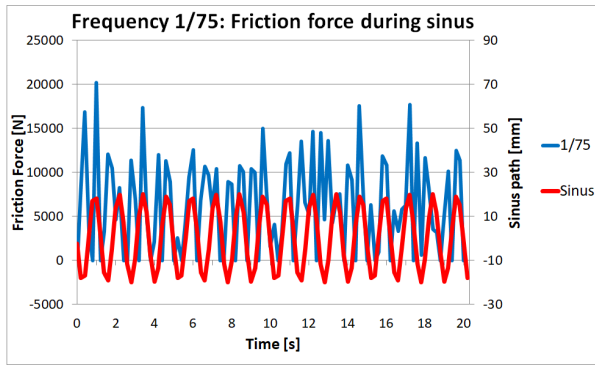
(b) Velocity vs. time

Figure 6.17: Effect of sinus frequency on motion: Forward displacement and velocity during a 20 second simulation.

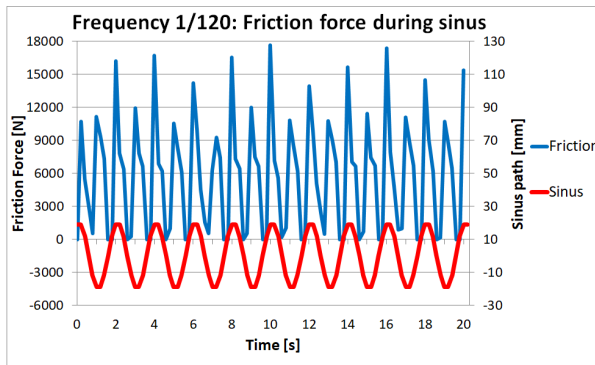
The frequency of $\frac{1}{200}$ /mm results in a maximum velocity of 44mm/s, compared to the 60mm/s of the $\frac{1}{400}$ /mm frequency. All four velocity plots show a variation in speed. The sinus wave seems to influence the velocity pattern.

Focusing on the friction forces on one wheel during the simulation, significant higher friction forces are noted in the frequencies of $\frac{1}{75}$ and $\frac{1}{120}$ /mm (Figure 6.18a-b). The frequency of $\frac{1}{400}$ /mm shows the lowest friction values (Figure 6.18d). All four friction plots show certain patterns, linked to the sinus wave. As noted before, the friction values are seen to be lower when the sinus wave reaches its extremes. However, a particular situation is found in the frequency of $\frac{1}{120}$ /mm: the friction force reaches zero when the sinus wave is at its center line.

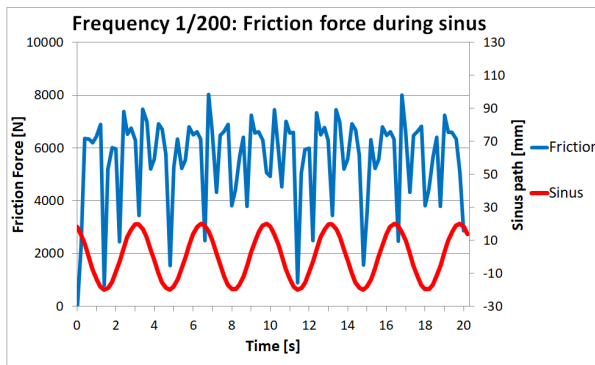
One of the extremes was already found: $\frac{1}{120}$ /mm, since this is the turn-over point between forward and backward motion. The upper extreme is a very low frequency, simulated with a frequency of $\frac{1}{2000}$ /mm. This frequency resulted in only 93mm forward displacement (Figure 6.19a). The friction relation shows similar behavior as the higher frequencies; low values at the extremes of the sinus (Figure 6.19b).



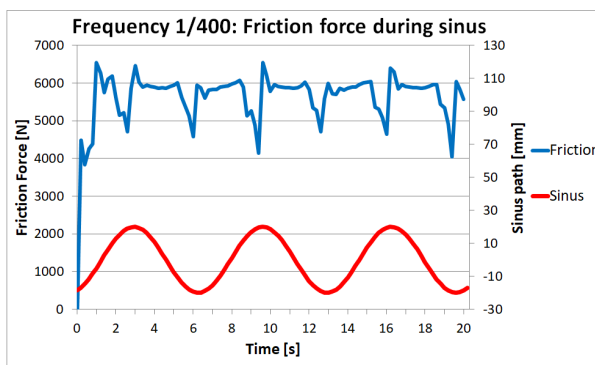
(a) Friction vs. time for a frequency of $\frac{1}{75}$ /mm



(b) Friction vs. time for a frequency of $\frac{1}{120}$ /mm

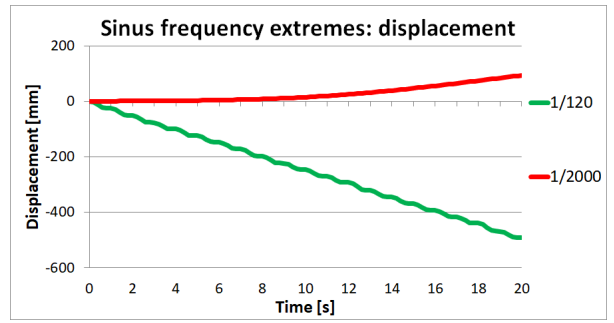


(c) Friction vs. time for a frequency of $\frac{1}{200}$ /mm

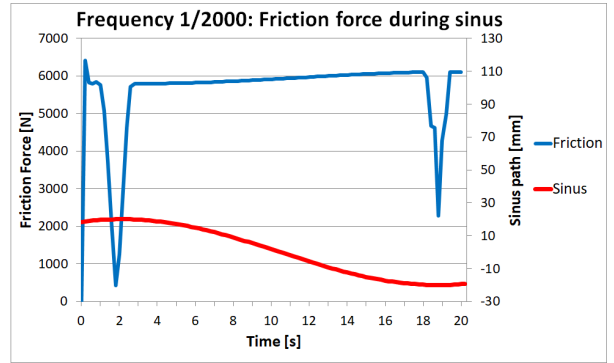


(d) Friction vs. time for a frequency of $\frac{1}{400}$ /mm

Figure 6.18: Effect of sinus frequency on friction: The resultant friction force on one wheel during the sinus wave.



(a) Displacement vs. time



(b) Friction vs. time

Figure 6.19: Extreme sinus frequencies: Forward displacement and friction forces were plotted during 20sec. simulation.



Discussion

7.1. Model and Validation

The 3D Simulink model was validated with a low-cost, 3D printed, prototype. The belt concept was chosen as pre-defined path, because of the simplicity of the concept; only two rolls and a belt were required. During design and prototyping, however, the belt was made up of 57 parts and 114 pins, in contrast to the predicted one part. By creating a belt from multiple linked, rigid, parts, it was easier to manufacture in the available settings.

The sinus shape can explain the noted sideways displacement in the model and prototype. The smoothness of motion is strongly related to the dimensions of the wave with respect to the snake segments. In the case of the prototype, the wave creates sharp turns of the segments. When the first segment reaches the turn-over point between steering to the right and steering to the left, the wheel rotation changes as well. This effect causes irregularities in the motion. However, a significant difference was noted: the model encountered 40mm sideways displacement and the prototype between 90mm and 350mm.

The difference between the model and prototype can be explained by the design of the prototype and the theoretical model. The path was simulated by a floating plane. In the prototype, however, a complete system was built to generate the motion. Moreover, in the model, the friction inside the system was neglected. In the prototype, ball bearings run through slots of the frame and the slot in the belt. When one of the parts creates more friction than the same part at another location, deviations in motion are the result. The large variety in the sideways displacement of the prototype is related to the surface type: surfaces with high friction coefficients result in less sideways displacement. When the friction coefficients are low, it becomes easier to slide sideways. With an irregularity in the prototype,

creating internal friction, the system tends to choose the way of lowest friction (slide sideways).

7.2. Parameter Assessment

Forward displacement is obtained when the system creates friction with the surroundings. The effect of the wave parameters and wheel axis length was assessed. The wheel axis length did not affect the forward displacement. Increasing the wheel axis length does not change the orientation of the segments; the friction relation does not change. Equal forward displacement in all simulated configurations corresponds to the non-changing friction relation.

On the other hand, changing the wave parameters does result in another forward displacement. When the amplitude is changed, the orientation of the snake-like system changes as well. With a larger amplitude, the sinus has a bigger gradient in between the extremes, which causes the snake-like system to make sharper steering motions. Since the gradient increases, the friction force perpendicular to the wave obtains a bigger component in forward motion. Therefore, the snake-like system is able to push itself further forward in situations with large amplitudes. This effect is supported by the increasing values of the friction force when the amplitude increases. The wave becomes a straight line when the amplitude is set to zero. Since this results in a zero gradient, the friction component in the forward direction is eliminated, and the system is not able to push itself forward.

In the frequency analysis another interesting behavior was observed, since three different situations can be described:

- Period sinus $> 2 \times$ segment length: the snake-like system follows the shape of the sinus. The wave is passed through the system in the same direction as the belt. Forward motion is created in the opposite direction as the belt motion.

- Period sinus = $2 \times$ segment length: the first and third snake segments rotate in the opposite direction as the second and fourth segments. The odd and even segments counteract each other.
- Period sinus $< 2 \times$ segment length: the snake-like system creates another wave that the described sinus. The wave travels through the snake-like system in the opposite direction as the belt; backward motion is created in the same direction as the belt motion.

Moreover, the highest forward displacement was generated with a frequency between $\frac{1}{450}$ and $\frac{1}{600}$ /mm. However, because the frequency has a significant effect on the variation of sideways displacement, a clear optimum in displacement was not found.

The effect of the sinus wave is visible in the velocity curves. The velocity is directly related to the gradient of the sinus wave; the velocity is maximal when the gradient is maximal and the velocity is minimal when the gradient is zero. This can be explained by the steering motion; when the gradient is maximal, the rotation of the snake segments is also maximal and thus the forward push is maximal. In contrast to the wheel axis length, the sinus amplitude does influence the velocity curves. Increasing the amplitude results in a larger variance in the velocity pattern. This is explained by the gradient of the sinus; the gradient increases when the amplitude increases. A larger range of gradients results in a larger range of velocities along the wave.

In the assessment of the sinus frequency, different patterns were noted. The velocity curves also show the three different motions of the snake-like system with different frequencies:

- The frequency of $\frac{1}{120}$ /mm would not result in a sinus wave but counteracting snake elements.
- The frequencies of $\frac{1}{200}$ /mm and $\frac{1}{400}$ /mm result in similar velocity patterns as the described sinus wave.
- The frequency of $\frac{1}{75}$ /mm shows a shortage of data points; the high frequency sinus wave is not represented in the velocity plot, but more data points would result in the described sinus wave.

7.3. Limitations in the Project

The relationship of friction described the basic mindset of the Simulink model, infinite friction in the direction of the wheel axis and zero friction in the direction perpendicular to the wheel axis. However, using infinite friction in the Simulink model resulted in such a high calculation time, that only one simulation would take at least several days. In order to decrease the calculation

time, it was decided to use values for static and dynamic friction describing high friction instead of infinite. The results of the high friction model were similar to the rough surfaces of the evaluation, so the friction relation of the model was assumed to be equivalent to situations in reality. The values of static and dynamic friction were kept the same in all simulations so that the effect of one variable parameter could still be investigated. Besides using the right material properties with the aim to generate high friction, the configuration of the system can also generate more friction. The results showed that adapting the amplitude and frequency of the wave created different displacements. These are valuable results in real-life situations, where infinite friction is not available. It is expected that the found relationships do not count in the situation of infinite friction; the friction is equal in all configurations which would theoretically result in the same displacement. In order to analyze the effect of infinite friction, it is recommended to perform long lasting simulations with values for static and dynamic friction close to infinite.

A second limitation in the model relates to the measured friction forces. The friction was described by a standard “sphere on plane contact force” block of Simulink. The output data of forces is described in function of the global world reference frame, being (x,y) . However, it could be interesting to see if forces reach a certain limit during motion. The values of displacement, velocity, and acceleration showed the behavior of the system. It is recommended to rebuild a model in which friction could be measured parallel and perpendicular to the wheel axis, to get even more insight in the motion.

A third limitation was chosen before prototyping; a pre-defined sinus was used as a wave instead of using an adaptable wave as in the MemoSlide mechanism. The prototype with the pre-defined path looks unnecessarily complex with the shape control system on top of the snake-like system. However, this was an important first step in the investigation of snake-like robots with adaptable mechanical shape control. The pre-defined wave was used to demonstrate the possibilities on forward motion, the motion behavior, and to validate the Simulink model. Now, the next step can be taken: simulate random waves to investigate the motion when an adaptable path is used.

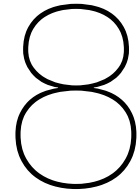
7.4. Personal Learning Process

During this thesis, I went through a personal learning process as well. One of the challenges was to filter and process the right information from feedback meetings. Discussions with different people result in different advises. Especially at the beginning of the project, it was hard to find

the right way to go in finding a suitable software package. Once the Simulink model was built, the right way was taken.

Prototyping was the second challenge. Especially building a robust prototype that would give reliable validation results was difficult. As discussed, the first models (LEGO and wood) were far from the desired outcome. Also, the first printed parts (Concept 1 and Concept 2) had too much noise: system instability and friction blurred the required information.

In the end, I can say that, with the support of my supervisors, I grew during the project as a technical student and as a person.



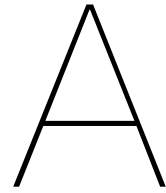
Conclusion

This thesis focuses on a snake-like system using mechanical shape control to generate forward motion. A 3D Simulink model was created and validated with a prototype to analyze the motion of the snake-like system. A pre-defined wave used to simplify the system and demonstrate the possibilities of forward motion with mechanical shape control. The model assessed different configurations with friction parameters corresponding to reality. When the configuration of the snake-like system creates high friction with the surroundings, the system is able to push itself further forward and generates more forward displacement. A sinus wave with a large amplitude and a frequency between $\frac{1}{450}$ and $\frac{1}{600}$ /mm provided the highest forward displacement. The research goal is accomplished: it is demonstrated that forward motion is possible when a snake-like system is connected to a mechanical shape control system. Now, the next step can be taken; simulate random waves to investigate the motion behavior when an adaptable path is applied.

Bibliography

- [1] S. Gottenbos. Mechanical Follow-The-Leader Principle, Validation Concept Design. *Master Thesis TU Delft*, 2016.
- [2] M. Neumann and J. Burgner-Kahrs. Considerations for Follow-the-Leader Motion of Extensible Tendon-Driven Continuum Robots. *IEEE International Conference on Robotics and Automation (ICRA)*, pages 917–923, 2016.
- [3] R. Buckingham. Snake Arm Robots. *Industrial Robot: An International Journal*, 29(3):242–245, 2002.
- [4] H.R. Choi and S.M. Ryew. Robotic System with Active Steering Capability for Internal Inspection of Urban Gas Pipelines. *Mechatronics*, 12(5):713–736, 2002.
- [5] J.C. McKenna, D.J. Anhalt, F.M. Bronson, H.B. Brown, M. Schwerin, E. Shammass, and H. Choset. Toroidal Skin Drive for Snake Robot Locomotion. *IEEE International Conference on Robotics and Automation*, pages 1150–1155, 2008.
- [6] A. Wolf, H.B. Brown, R. Casciola, A. Costa, M. Schwerin, E. Shamas, and H. Choset. A Mobile Hyper Redundant Mechanism for Search and Rescue Tasks. *Proceedings of the 2003 IEEE/RSJ International Conference on Intelligent Robots and Systems*, pages 2889–2895, 2003.
- [7] G.S. Chirikjian and J.W. Burdick. The Kinematics of Hyper-Redundant Robot Locomotion. *IEEE Transactions on Robotics and Automation*, 11(6):781–793, 1995.
- [8] P.W.J. Henselmans, S. Gottenbos, G. Smit, and P. Breedveld. The MemoSlide: an explorative study into a novel mechanical follow-the-leader mechanism. *Proceedings of the Institution of Mechanical Engineers, Part H: Journal of Engineering in Medicine*, 23(12):1–7, 2017.
- [9] C. Gans. How snakes move. *Scientific American*, 222:82–96, 1970.
- [10] J.K. Hopkins, B.W. Spranklin, and S.K. Gupta. A Survey of Snake-Inspired Robot Designs. *Bioinspiration Biomimetics*, 4(2):1–19, 2009.
- [11] S.M. Song and B.S. Choi. A Study on Continuous Follow-The-Leader (FTL) Gaits: An effective Walking Algorithm over Rough Terrain. *Mathematical Biosciences*, 97(2):199–233, 1989.
- [12] S. Hirose and H. Yamada. Snake-Like Robots, Machine Design of Biologically Inspired Robots. *IEEE Robotics Automation Magazine*, 16(1):88–98, 1989.
- [13] K.J. Dowling. Limbless Locomotion: Learning to Crawl with a Snake Robot. *Doctor Thesis*, 1997.
- [14] S. Hirose. Biologically Inspired Robots: Snake-Like Locomotors and Manipulators. *Oxford: Oxford University Press*, 1093, 1993.
- [15] P. Liljebäck, K.Y. Pettersen, Ø. Stavdahl, and J.T. Gravdahl. A Review on Modelling, Implementation, and Control of Snake Robots. *Robotics and Autonomous Systems*, 60(1):29–40, 2012.
- [16] L. Chen, Y. Wang, S. Ma, and B. Li. Analysis of Traveling Wave Locomotion of Snake Robot. *Proceedings of the 2003 IEEE International Conference on Robotics, Intelligent Systems and Signal Processing*, pages 365–369, 2003.
- [17] J.P. Gasc, D. Gattaert, C. Chasserat, and F. Clarac. Propulsive Action of a Snake Pushing Against a Single Site: its Combined Analysis. *Journal of Morphology*, 201:315–329, 1989.
- [18] C. Gans. Terrestrial Locomotion without Limbs. *American Zoologist*, 2:167–182, 1962.
- [19] J. Gray. The mechanism of locomotion in snakes. *Journal of Experimental Biology*, 23(2):101–120, 1946.

- [20] H.W. Lissmann. Rectilinear Locomotion in a Snake (*Boa Occidentalis*). *Journal of Experimental Biology*, 26(4):368–379, 1950.
- [21] A. Crespi, A. Badertscher, A. Guignard, and A.J. Ijspeert. AmphiBot I: an amphibious snake-like robot. *Robotics and Autonomous Systems*, 50(4):163–175, 2005.
- [22] A. Crespi and A.J. Ijspeert. AmphiBot II: An Amphibious Snake Robot that Crawls and Swims Using a Central Pattern Generator. *Proceedings of the 9th International Conference on Climbing and Walking Robots*, pages 19–27, 2006.
- [23] D. Krupke. Development of Bio-inspired Locomotion Using Modular Robotic Simulation and Control System. *Master Thesis*, 2013.
- [24] R.J. Webster, J.M. Romano, and N.J. Cowan. Mechanics of Precurved-Tube Continuum Robots. *IEEE Transactions on Robotics*, 25(1):67–78, 2009.
- [25] R.J. Webster, A.M. Okamura, and N.J. Cowan. Toward Active Cannulas: Miniature Snake-Like Surgical Robots. *Proceedings of the 2006 IEEE/RSJ International Conference on Intelligent Robots and Systems*, pages 2857–2863, 2006.
- [26] B. Klaassen and K.L. Paap. GMD-SNAKE 2: a Snake-Like Robot Driven by Wheels and a Method for Motion Control. *Proceedings of the 1999 IEEE International Conference on Robotics and Automation*, 4:3014–3019, 1999.
- [27] K.L. Paap, T. Christaller, and F. Kirchner. A Robot Snake to Inspect Broken Buildings. *Proceedings of the 2000 IEEE/RSJ International Conference on Intelligent Robots and Systems*, 4:2079–2082, 2000.
- [28] S. Hirose and M. Mori. Biologically Inspired Snake-Like Robots. *International Conference on Robotics and Biomimetics*, pages 1–7, 2004.
- [29] M. Mori and S. Hirose. Development of Active Cord Mechanism ACM-R3 with Agile 3D Mobility. *Proceedings of the 2001 IEEE/RSJ International Conference on Intelligent Robots and Systems*, 3:1552–1557, 2001.
- [30] C. Wright, A. Buchan, B. Brown, J. Geist, M. Schwerin, D. Rollinson, M. Tesch, and H. Choset. Design and Architecture of the Unified Modular Snake Robot. *2012 IEEE International Conference on Robotics and Automation*, pages 4347–4354, 2012.
- [31] A. Degani, H. Choset, A. Wolf, and M.A. Zenati. Highly Articulated Robotic Probe for Minimally Invasive Surgery. *Proceedings of the 2006 IEEE International Conference on Robotics and Automation*, pages 4167–4172, 2006.
- [32] T. Ota, A. Degani, D. Schwartzman, B. Zubiate, J. McGarvey, H. Choset, and M.A. Zenati. A Highly Articulated Robotic Surgical System for Minimally Invasive Surgery. *The Annals of Thoracic Surgery*, 87(4):1253–1256, 2009.
- [33] H. Hu, P. Wang, B. Zhao, M. Li, and L. Sun. Design of a Novel Snake-Like Robotic Colonoscope. *2009 IEEE International Conference on Robotics and Biomimetics*, pages 1957–1961, 2009.
- [34] A. Degani, H. Choset, B. Zubiate, T. Ota, and M.A. Zenati. Highly Articulated Robotic Probe for Minimally Invasive Surgery. *2008 30th Annual International Conference of the IEEE Engineering in Medicine and Biology Society*, pages 3273–3276, 2008.
- [35] T. Krijger, J. Dankelman, and P. Breedveld. Design of the MemoFlex: A Highly Manoeuvrable Backbone for a Dextric Manipulator. *Master Thesis TU Delft*, 2012.
- [36] P.W.J. Henselmans, G. Smit, and P. Breedveld. Mechanical Follow-the-Leader motion of a hyper-redundant surgical instrument: Proof-of-concept prototype and first tests. *Proceedings of the Institution of Mechanical Engineers, Part H: Journal of Engineering in Medicine*, 2019.
- [37] R. M. Ogorkiewicz. *Technology of Tanks I*. Jane’s Information Group Limited, Coulsdon, Surrey, 1991.



3D Simulink Simulation

A.1. 3D Figures of the Simulink Model

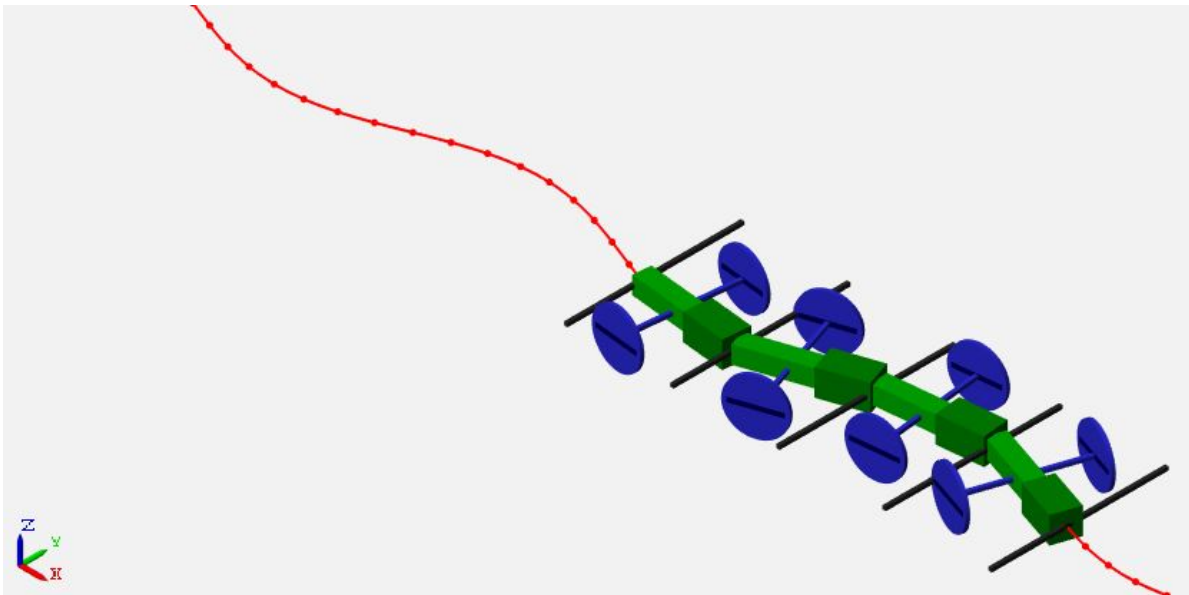


Figure A.1: 3D view of the Simulink model

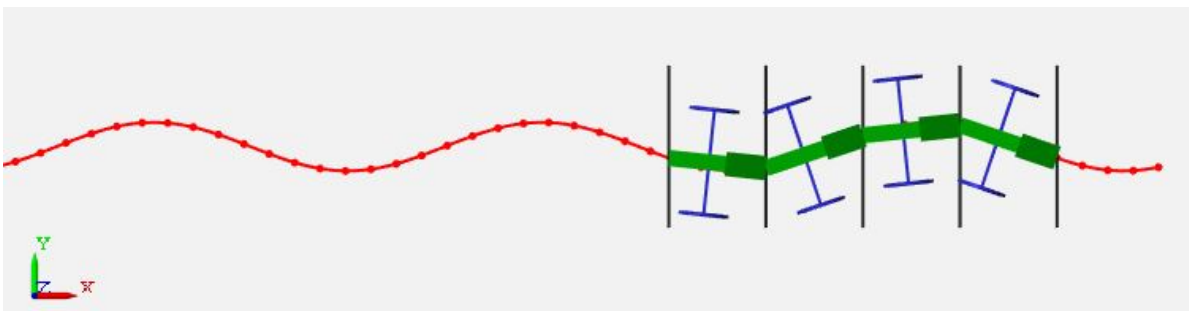


Figure A.2: Top view of the Simulink model

A.2. Global System

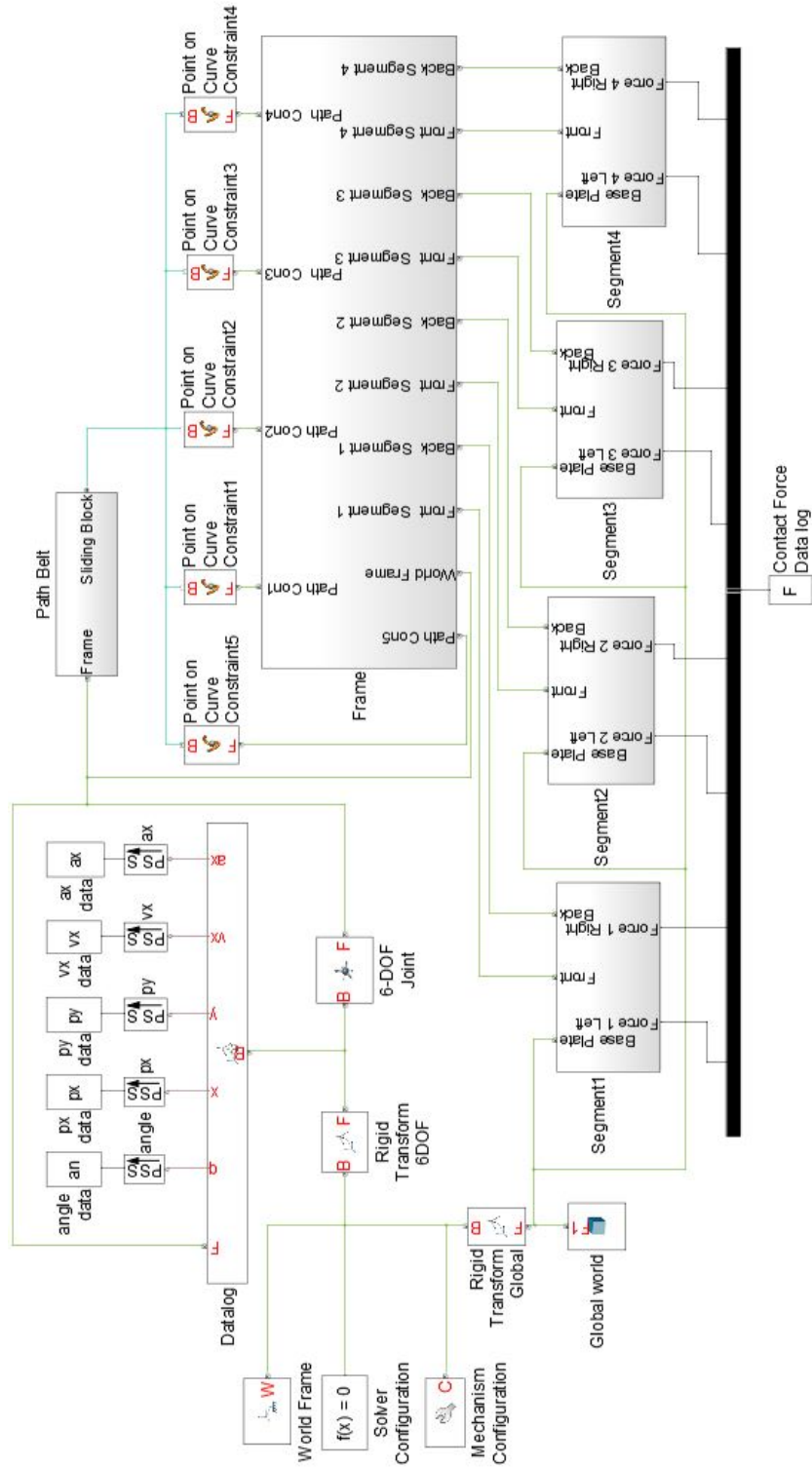


Figure A.3: Simulink blocks for the global system with subsystems: Path Belt, Frame, Segment1, Segment2, Segment3, and Segment4.

A.3. Subsystem: Segment 1

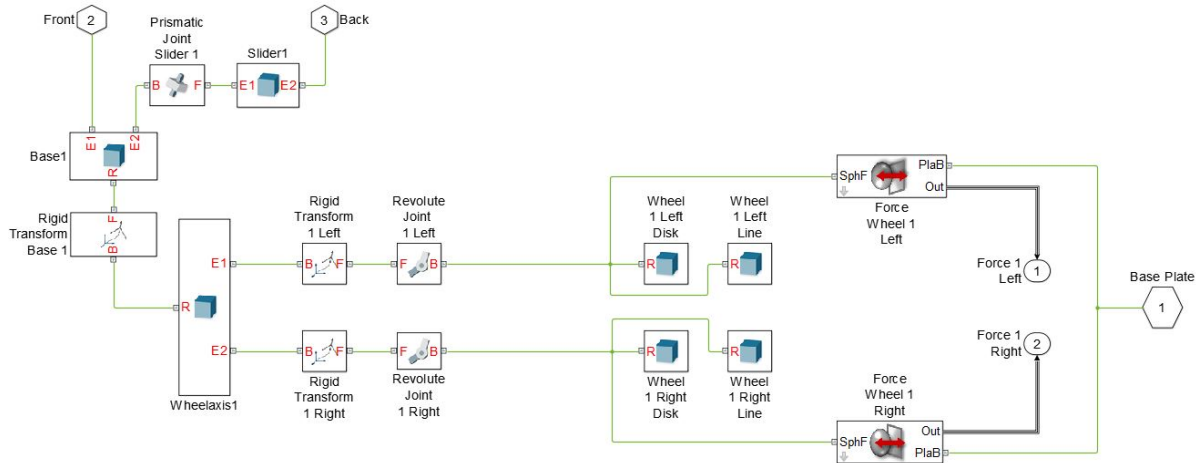


Figure A.4: Simulink blocks for the subsystem “Segment 1”.

A.4. Subsystem: Segment 2

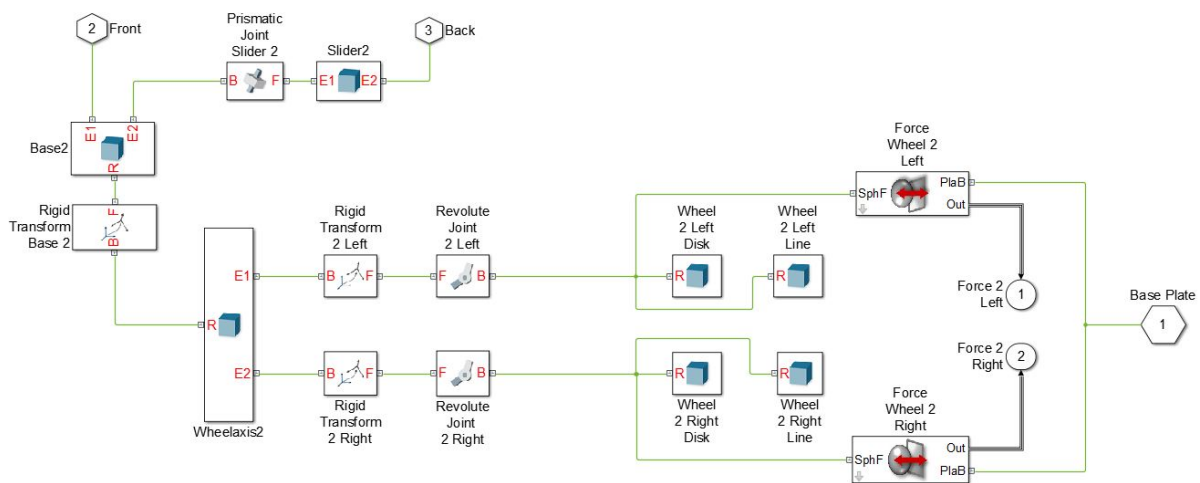


Figure A.5: Simulink blocks for the subsystem “Segment 2”.

A.7. Subsystem: Frame

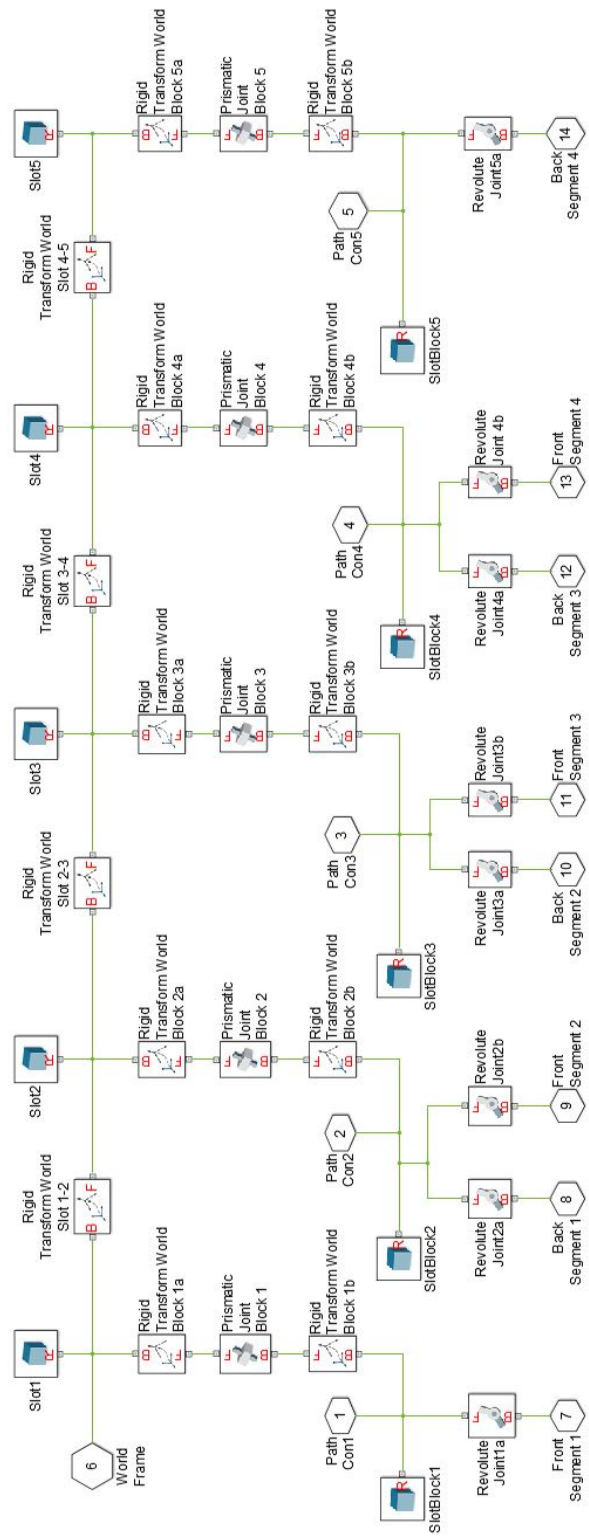


Figure A.8: Simulink blocks for the subsystem "Frame".

A.8. Subsystem: Path Belt

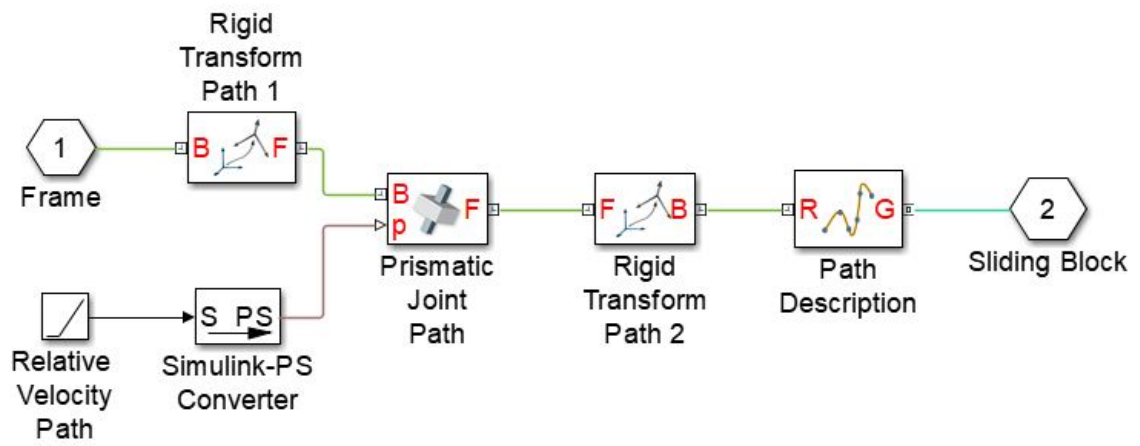
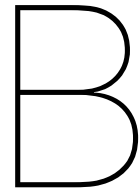


Figure A.9: Simulink blocks for the subsystem "Path Belt".



2D Simulation Sinusoidal Wave

```
%% 2D Simulation Sinusoidal Wave
%
% BMA0332 BME MSc - Thesis
%
% Sander d'Hont
% Studentnumber 4209893
% September 9th, 2019
%
% Train of 4 segments, connected between five pins, each having
% two wheels. The pins are forced to follow a sinusoidal path and
% with this model it is analyzed how the system behaves in free air.
% It is the goal to find a smooth wave. These parameters are used
% in a Simulink Simulation to investigate if the system will propel
% itself forward.
%
close all
clear all
clc

%% Constants
% Snake-like system constants
delta_y = 60; % Length between two joints [mm]
wb = 65; % Wheel axis length [mm]
s = 4; % Number of segments of the snake
j = s+1; % Number of joints of the snake

% Shape control system constants
A = 20; % Amplitude sinus [mm]
B = pi/150; % Frequency sinus = 2pi/B [1/mm]

% Simulation constants
time = 3600; % Time of running the path [s]
dt = 1; % Time step [s]
i = 10; % Starting time [s]
ymax = 50; % Spacing in plotting figure
xmax = ((s*delta_y)+2*ymax)/2; % Used in plotting figure

while i<time
    clear z J COM RC RC_p % Clears used matrices

    % Sinusoidal path
```

```

P      =   [];                                     % Empty Matrix P, filled below
for w = -ymax:dt:((s*delta_y)+ymax) % Path coordinates in Plot
    P = [P; A*sin(B*(w+i)), w]; % Path coordinates
end

% New positions of joints, using the sinusoid
WB = [];
for z = 1:j
    J(z,:) = [A*sin(B*(i+(z-1)*delta_y)), (z-1)*delta_y]; % Joints
    if z>1
        % Centers of Mass (COM) of each segment:
        COM((z-1),:)=[(J(z,1)+J((z-1),1))/2, (J(z,2)+J((z-1),2))/2];
        % Vectors describing each segments:
        V((z-1),:)=[(J(z,1)-J((z-1),1)), (J(z,2)-J((z-1),2))];
        % Calculating Lengths of vectors:
        L((z-1),1)=sqrt((V((z-1),1))^2 + (V((z-1),2))^2);
        % Calculating RC (direction) of each segment:
        RC((z-1),1)=V((z-1),2)/(V((z-1),1));
        % Calculating RC of each wheelbase, perpend. to segments:
        RC_p((z-1),1)=- 1/RC((z-1),1);
        % Positions of wheels:
        WB=[WB; COM((z-1),1)+(wb/2)/(sqrt(1+(RC_p(z-1))^2)), ...
            COM((z-1),2)+(wb/2)/(sqrt(1+(RC_p(z-1))^2))*RC_p(z-1);...
            COM((z-1),1)-(wb/2)/(sqrt(1+(RC_p(z-1))^2)), ...
            COM((z-1),2)-(wb/2)/(sqrt(1+(RC_p(z-1))^2))*RC_p(z-1)];
        % Center of mass times length (used to find COM local system)
        COM_xl((z-1),:) = [COM((z-1),1)*L(z-1),COM((z-1),2)*L(z-1)];
    end

end

% Calculating center of mass of local system
COM_loc = [sum(COM_xl(:,1))/(sum(L)), sum(COM_xl(:,2))/(sum(L))];

% Plotting joints in local frame
plot(P(:,1),P(:,2), 'r-', 'LineWidth', 3); % Path (red)
hold on
plot(J(:,1),J(:,2), 'g-', 'LineWidth', 4); % Snake elements (green)
plot(J(:,1),J(:,2), 'go', 'LineWidth', 4); % Snake joints (green)
plot(WB(:,1),WB(:,2), 'bo', 'LineWidth', 4); % Wheels (blue)
plot([WB(1,1) WB(2,1)], [WB(1,2) WB(2,2)], 'b', 'LineWidth', 4); % Axis
plot([WB(3,1) WB(4,1)], [WB(3,2) WB(4,2)], 'b', 'LineWidth', 4); % Axis
plot([WB(5,1) WB(6,1)], [WB(5,2) WB(6,2)], 'b', 'LineWidth', 4); % Axis
plot([WB(7,1) WB(8,1)], [WB(7,2) WB(8,2)], 'b', 'LineWidth', 4); % Axis

legend( 'Path', 'Snake_element', 'Joint', 'Wheel', 'Wheelaxis' );

% Plot layout:
title( '2D_Simulation_MemoSnake_Mechanism_(in_free_air) ' )
xlabel( 'x [mm] ' ) % Title of x-axis
ylabel( 'y [mm] ' ) % Title of y-axis
grid on % Grid in plot figure
axis([-xmax xmax -ymax ((s*delta_y)+ymax)]); % Limits of x and y

% Pausing figure to show plotted shape
if i == 0
    pause(0.1); % Pause longer at the start
else
    pause(0.01); % Pause before next step (to show movement)

```

```
end  
  
    clf('reset')    % Clears figure before plotting next movement  
    i = i + dt;     % Update time step  
  
end
```


C

Conceptual Designs





















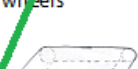



Category	Belt structure	Belt end guidance	Belt mid guidance	Belt slide prevention	Belt drive	Belt adjuster
Options	1. Flexible belt with all-through path cut-out 	1. Full static cylinder 	1. None 	1. Larger diameter roll end 	1. Rubber tire on belt 	1. Spring at guide 
	2. Flexible belt with engraved path 	2. Half static cylinder 	2. Large wheels 	2. Wheels with slot and pin on belt 	2. Sprocket wheel on belt with teeth 	2. Wheel spring 
	3. Flexible belt with pins 	3. Rolling cylinder 	3. Small wheels 	3. Slots on frame and pin on belt 	3. Sprocket wheel at frame end 	3. Bolt on guide axis 
	4. Inter connected links with engraved path 	4. Rolling axis 	4. Small sprocket wheels 			4. Bolt through guide axis 
	5. Inter connected links with pins 	5. Sprocket wheel 				

Figure C.1: Designs of shape control system: Red = Concept 1, Green = Concept 2, Blue = Final Design


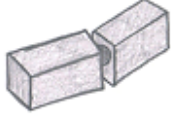

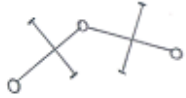

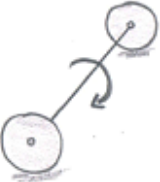
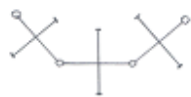

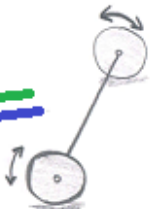


Category	Number of snake segments	Segment length	Ground contact point
Options	1. One 	1. Fixed length 	1. Non-rotating element 
	2. Two 	2. Upper slider 	2. Rotating wheel axis 
	3. Three 	3. Double slider 	3. Rotating wheels 
	4. Four 	4. Elastic material in between 	

Figure C.2: Designs of snake-like system: Red = Concept 1, Green = Concept 2, Blue = Final Design

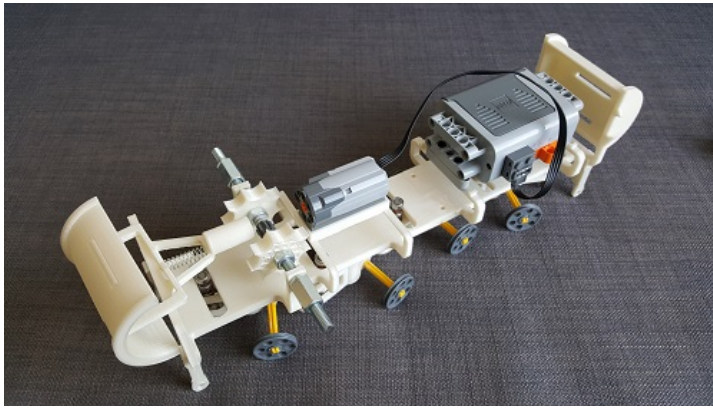


Figure C.3: Concept 1 of the MemoSnake

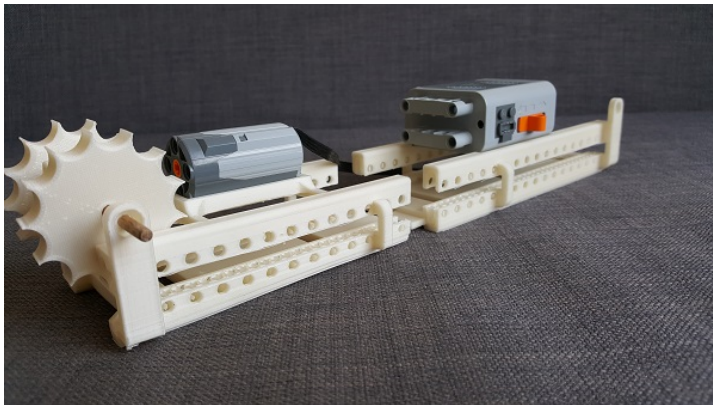
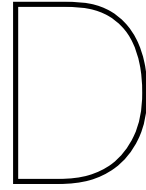


Figure C.4: Concept 2 of the MemoSnake



Figure C.5: Final Design of the MemoSnake



Motor Torque Calculation

The required motor torque was calculated for the situation with zero friction between the belt and the snake-like segments. This value was compared with the given motor specifications. The margin between the two values determines if the LEGO motor can be used in this design.

Table E.1 shows the specifications of the LEGO motor. 9V is the voltage delivered by the six 1.5 V batteries in the battery box.

Table D.1: Motor specifications: under loaded condition.

Parameter	Value
Voltage	9 V
Current	0.49 A
Torque	6.48 Ncm
Rotation speed	272 rpm
Mechanical power	1.85 W
Electrical power	4.41 W
Efficiency	42%

The gear ratio between the worm wheel and the gear wheel is described by the number of teeth of the gear wheel and the number of starts of the worm wheel. The used gear wheel has 10 teeth, while the worm wheel is a single start worm. Therefore, the gear ratio is 10:1. Moreover, the diameter of the belt on the sprocket wheel is approximately 50 mm.

The required motor torque is described by the following parameters:

- weight of the belt, $m_{belt} = 0.21kg$
- diameter of the sprocket wheel, $D_{sprocket} = 50mm$
- belt speed, $v_{belt} = 60mm/s$
- angular velocity of the gear wheel, $\omega = \frac{60}{25}$
- gear ratio between the worm wheel and gear wheel, $GR = 10$
- friction coefficient between belt and sprocket wheel, $\mu = 1$ (assumed)

The calculation is as follows:

$$Torque_{motor,required} = \frac{Torque_{sprocketwheel}}{GR} \quad (D.1)$$

$$Torque_{sprocketwheel} = \frac{Power}{\omega} \quad (D.2)$$

$$Power = m_{belt} \times g \times \mu \times v_{belt} \quad (D.3)$$

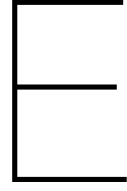
Substitution of these equations results in:

$$Torque_{motor,required} = \frac{m_{belt} \times g \times \mu \times v_{belt}}{\omega \times GR} = \frac{0.21 \times 9.81 \times 1 \times 0.060}{2.4 \times 10} \approx 0.0052Nm = 0.52Ncm \quad (D.4)$$

The maximum load of the belt with the given motor torque is found by:

$$Load_{max} = \frac{Torque_{motor,spec} \times \omega \times GR}{v_{belt} \times \mu} = \frac{0.0648 \times 2.4 \times 10}{0.060 \times 1} \approx 25.9N \quad (D.5)$$

The theoretical (no resistance) was set to be $0.21 \times 9.81 \approx 2.1N$ and the maximum allowable load is calculated to be $25.9N$. This means that the load can be 12.5 times larger than the load without resistance. Therefore, the LEGO motor is found to be sufficient.



Belt Speed Calculation

The belt speed of the prototype is described by three parameters:

- the rotation speed of the LEGO motor axis
- the gear ratio between the worm wheel and gear wheel
- the diameter of the sprocket wheel

Table E.1 shows the specifications of the LEGO motor. 9V is the voltage delivered by the six 1.5 V batteries in the battery box.

Table E.1: Motor specifications: under loaded condition.

Parameter	Value
Voltage	9 V
Current	0.49 A
Torque	6.48 Ncm
Rotation speed	272 rpm
Mechanical power	1.85 W
Electrical power	4.41 W
Efficiency	42%

The gear ratio between the worm wheel and the gear wheel is described by the number of teeth of the gear wheel and the number of starts of the worm wheel. The used gear wheel has 10 teeth, while the worm wheel is a single start worm. Therefore, the gear ratio is 10:1. Moreover, the diameter of the belt on the sprocket wheel is approximately 50 mm.

The calculation is as follows:

$$Rotationspeed_{motor}[rps] = \frac{Rotationspeed_{motor}[rpm]}{60} \quad (E.1)$$

$$Rotationspeed_{sprocketwheel}[rps] = \frac{Rotationspeed_{motor}[rps]}{gearratio} \quad (E.2)$$

$$Beltspeed[mm/s] = Rotationspeed_{sprocketwheel}[rps] \times perimeter_{sprocketwheel}[mm] \quad (E.3)$$

Substitution of these equations results in:

$$Beltspeed[mm/s] = \frac{Rotationspeed_{motor}[rpm]}{60 * 10} \times \pi D_{sprocketwheel} = \frac{272}{600} \times 50\pi \approx 71.2mm/s \quad (E.4)$$

F

Final Prototype Design

F.1. Pictures

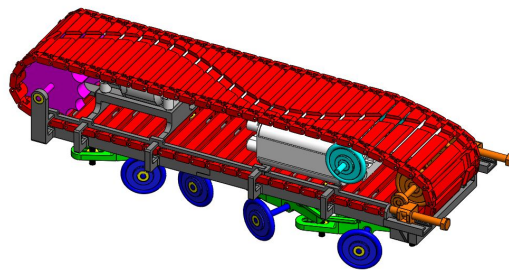


Figure F.1: 3D view of the total assembly of the CAD model.

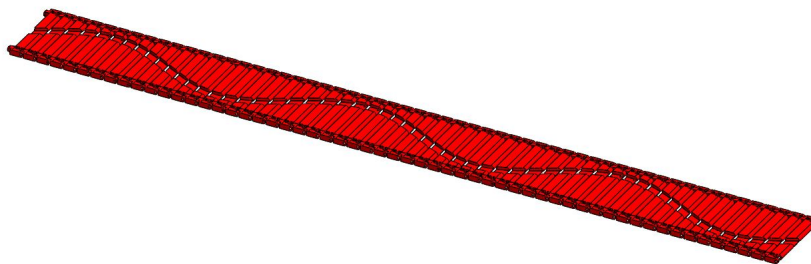


Figure F.2: Belt structure of the shape control system of the CAD model.

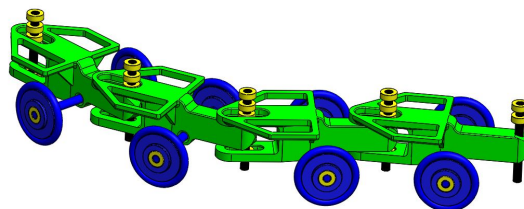
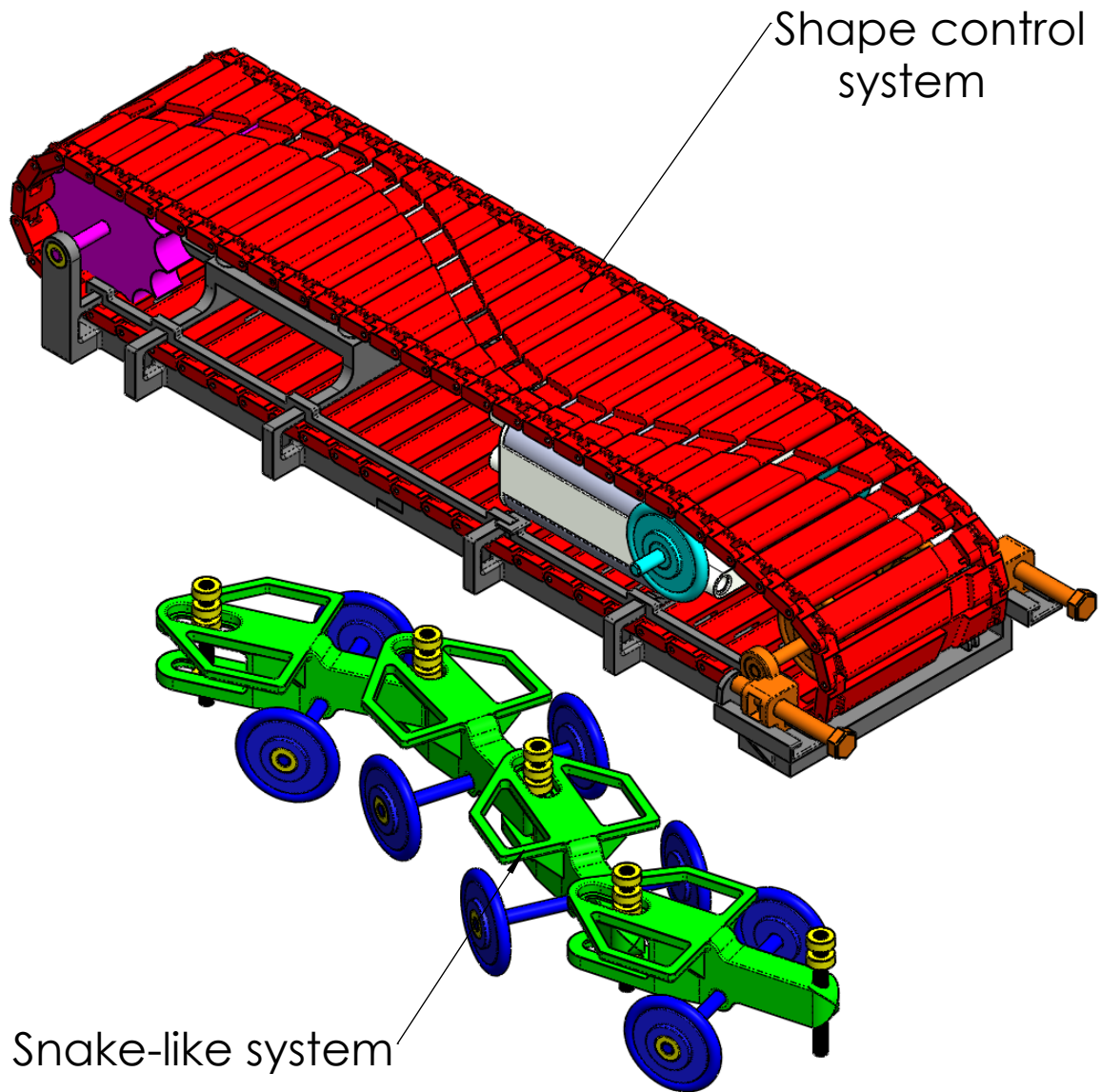



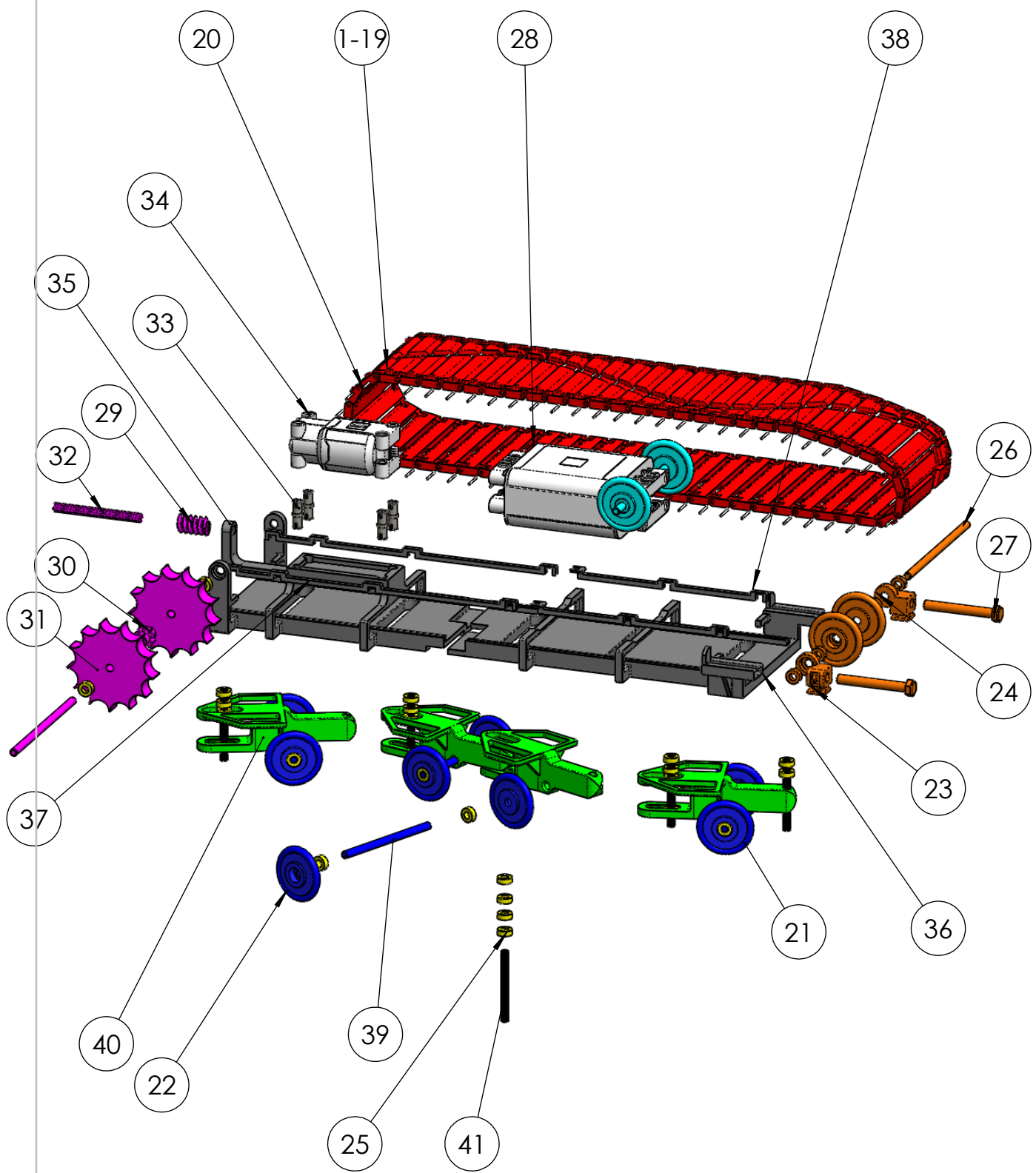
Figure F.3: Snake-like system of the CAD model.

F.2. SolidWorks Drawings

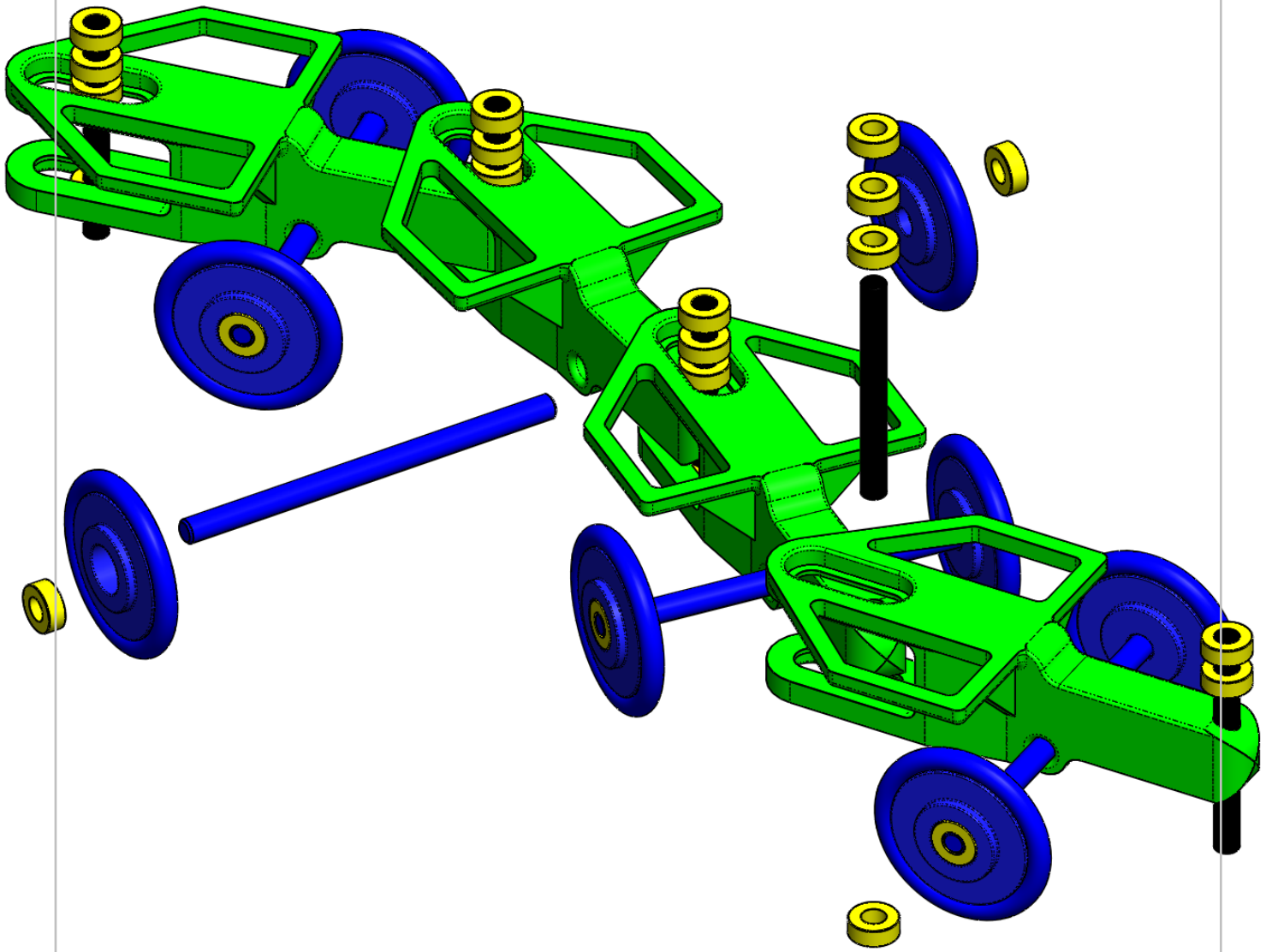
See next page.





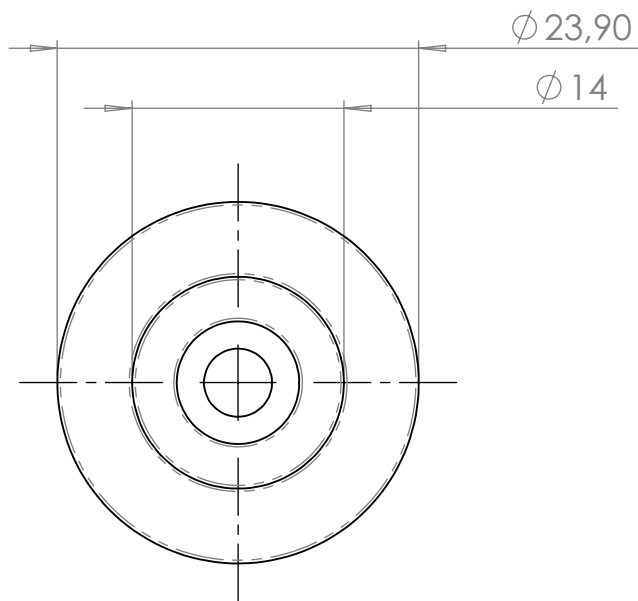
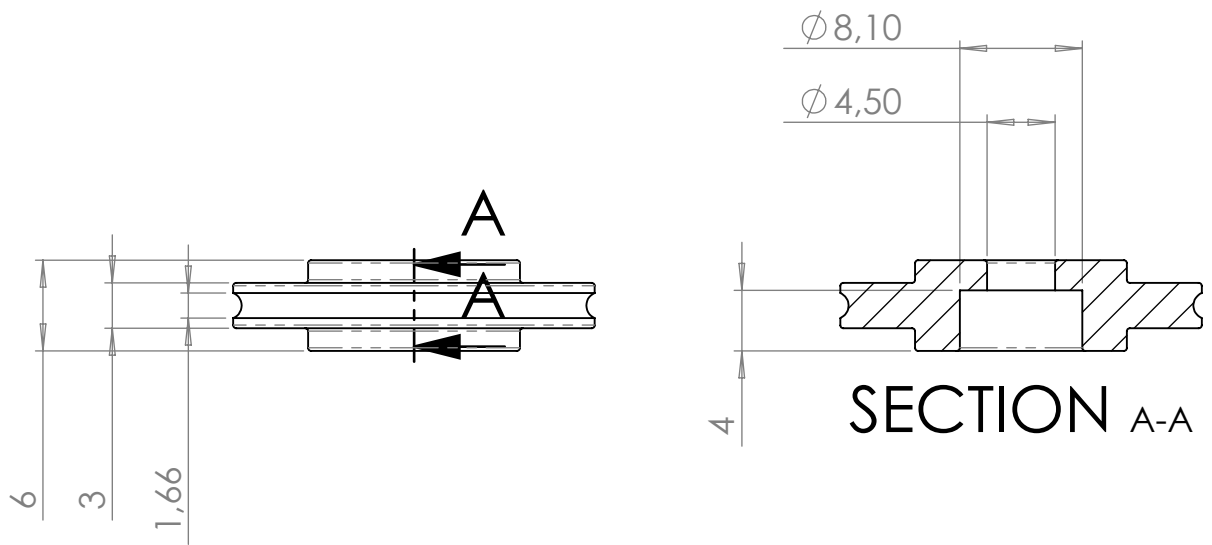
name				 units mm	
PRO02_0000_TotalAssembly				format	
TU Delft BioMechanical Engineering				A4	
scale	1:2	date	17-10-2019	weight	grams
author	Sander d'Hont, #4209893				
				drawing no. PRO02_0000	
				Total Assembly	



ITEM NO.	PART NUMBER	MATERIAL	BUY / MAKE	QTY.
1-19	PRO02_0402_BeltPart1	PLA	Make	3
2	PRO02_0403_BeltPart2	PLA	Make	3
3	PRO02_0406_BeltPart5	PLA	Make	3
4	PRO02_0404_BeltPart3	PLA	Make	3
5	PRO02_0405_BeltPart4	PLA	Make	3
6	PRO02_0407_BeltPart6	PLA	Make	3
7	PRO02_0408_BeltPart7	PLA	Make	3
8	PRO02_0409_BeltPart8	PLA	Make	3
9	PRO02_0410_BeltPart9	PLA	Make	3
10	PRO02_0411_BeltPart10	PLA	Make	3
11	PRO02_0412_BeltPart11	PLA	Make	3
12	PRO02_0413_BeltPart12	PLA	Make	3
13	PRO02_0414_BeltPart13	PLA	Make	3
14	PRO02_0415_BeltPart14	PLA	Make	3
15	PRO02_0416_BeltPart15	PLA	Make	3
16	PRO02_0417_BeltPart16	PLA	Make	3
17	PRO02_0418_BeltPart17	PLA	Make	3
18	PRO02_0419_BeltPart18	PLA	Make	3
19	PRO02_0420_BeltPart19	PLA	Make	3
20	PRO02_0401_PressPin	Stainless steel	Buy	114
21	PRO02_0102b_Tire	Rubber	Buy	12
22	PRO02_0102a_Wheelbase	PLA	Make	12
23	PRO02_0303_BeltPositionerLeft	PLA	Make	1
24	PRO02_0303_BeltPositionerRight	PLA	Make	1
25	PRO02_0105_BallBearing	Stainless steel	Buy	35
26	PRO02_0312_LongAxis_D4mm	Stainless steel	Buy	3
27	PRO02_0307_Bolt	Stainless steel	Buy	2
28	PRO02_0202_BatteryBoxLEGO	-	Buy	1
29	PRO02_0203_WormGearLEGO	PLA	Buy	1
30	PRO02_0204a_GearWheel	PLA	Make	1
31	PRO02_0204b_Propellingwheel	PLA	Make	2
32	PRO02_0205_Axis_shortLEGO	-	Buy	1
33	PRO02_0308_LegoPin	-	Buy	4
34	PRO02_0201_LargeMotorLEGO	-	Buy	1
35	PRO02_0301_MotorFrame	PLA	Make	2
36	PRO02_0302_GuideFrame	PLA	Make	2
37	PRO02_0304_BeltGuideA	PLA	Make	2
38	PRO02_0305_BeltGuideB	PLA	Make	2
39	PRO02_0101_Wheelaxis_L66mm_D4mm	Wood	Make	4
40	PRO02_0103_SegmentBase	PLA	Make	4
41	PRO02_0104_Pin	Wood	Buy	5



name PRO02_1000_SnakeSystem				 units mm	
				format A4	
scale	1:1	date	17-10-2019	weight	grams
author	Sander d'Hont, #4209893				drawing no. PRO02_1000
BioMechanical Engineering				subsystem Snake system	



name

PRO02_1002_Wheelbase



units mm

format

A4

drawing no.

PRO02_1002

TU Delft

BioMechanical Engineering

scale 2:1

date 17-10-2019

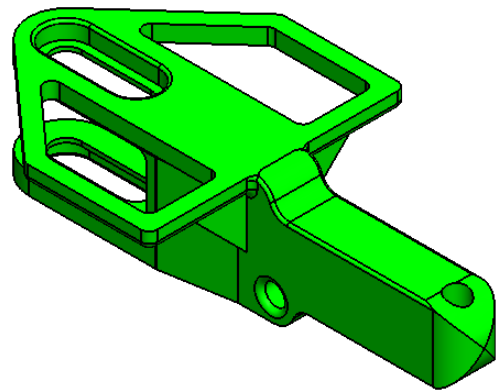
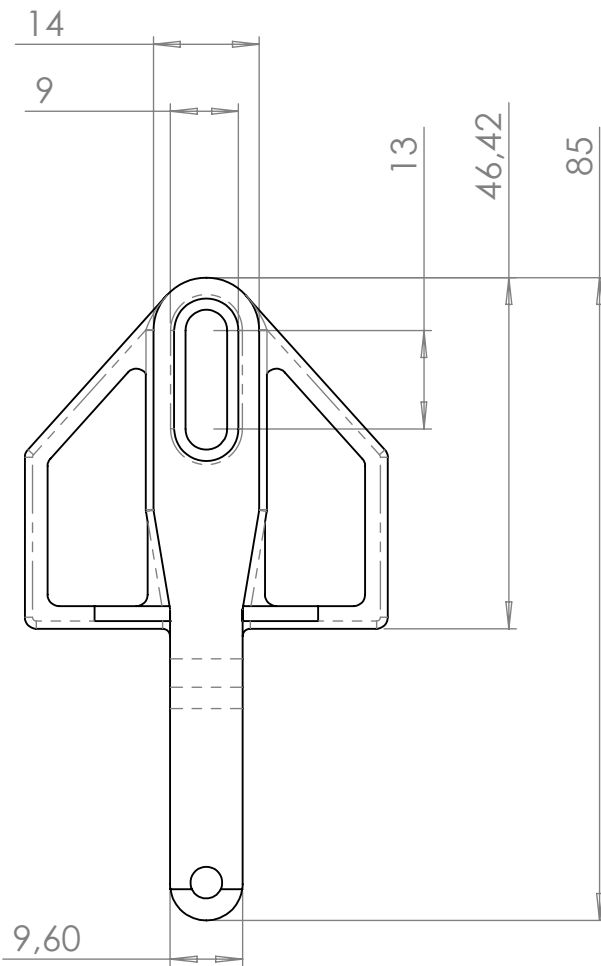
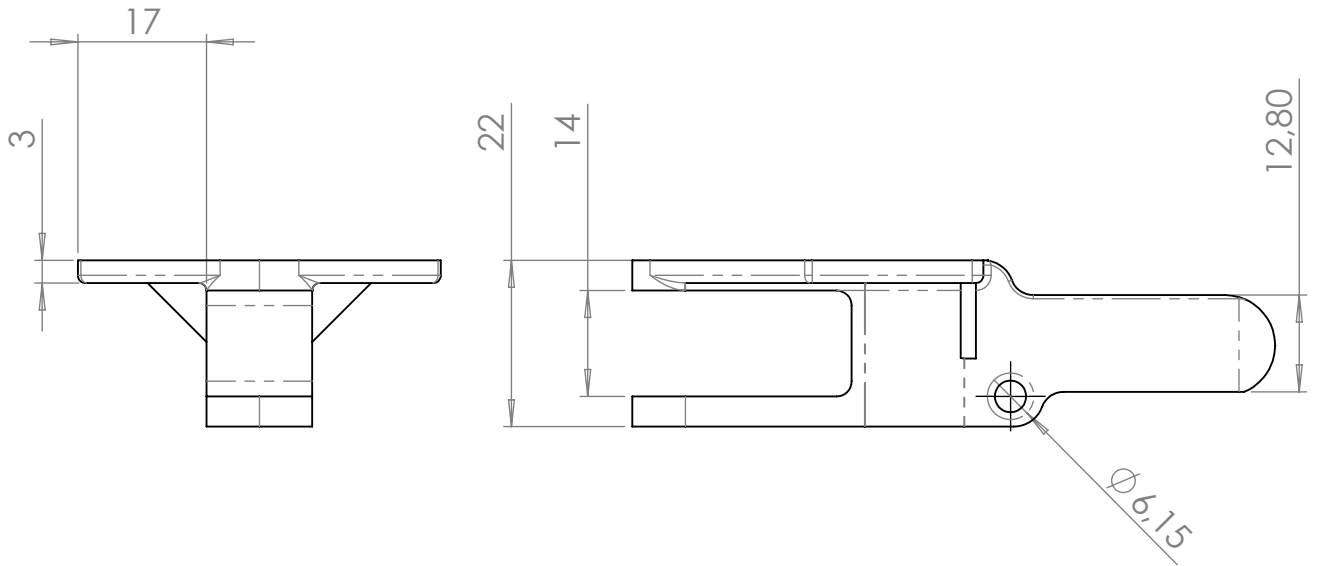
weight


grams

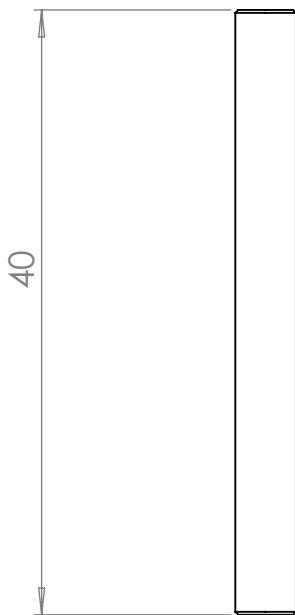
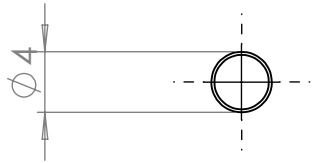
author Sander d'Hont, #4209893


subsystem

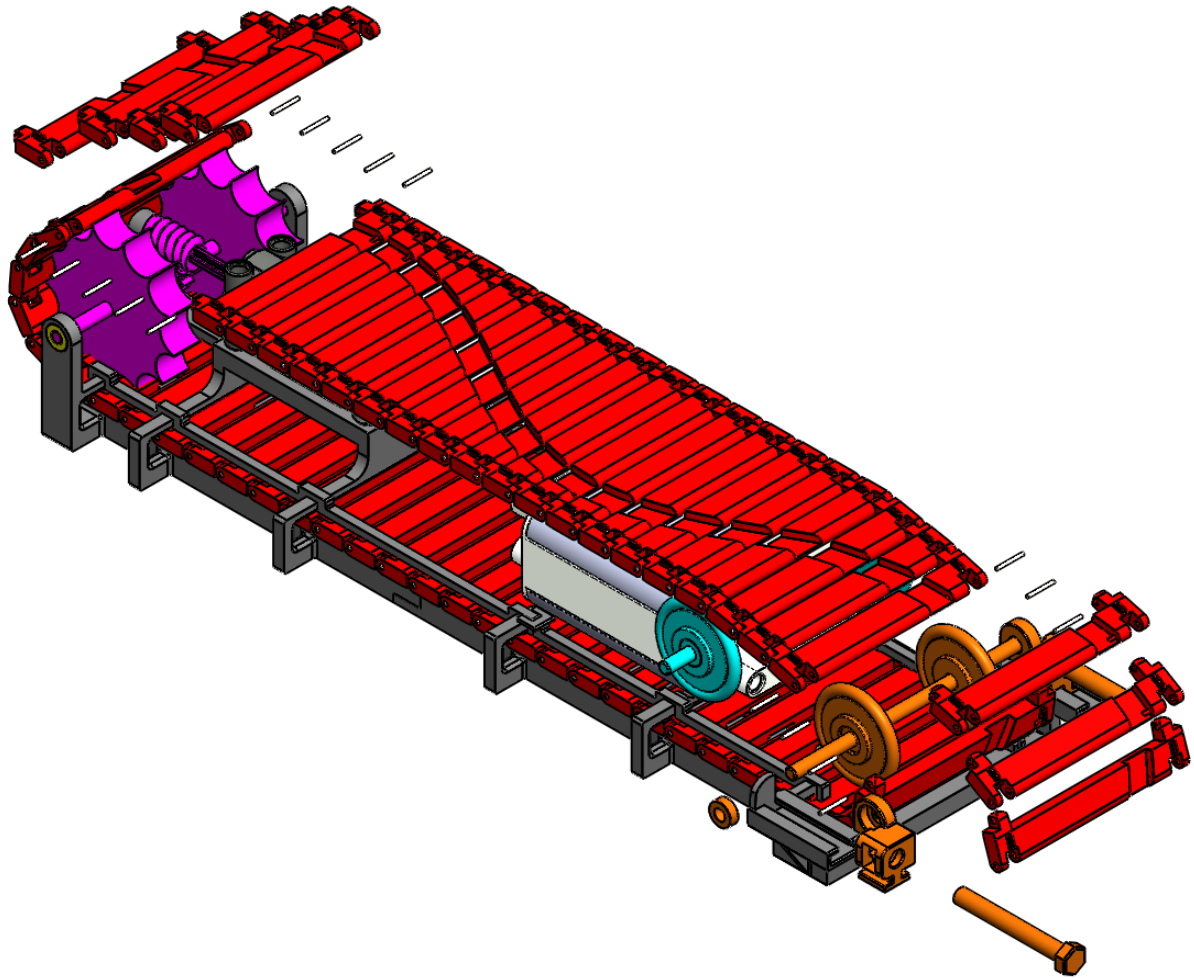
Snake-like system




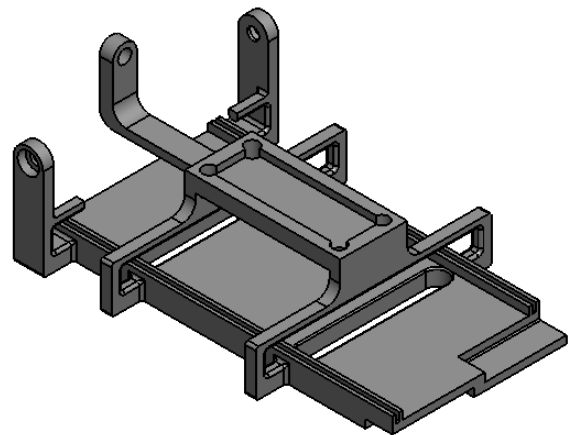
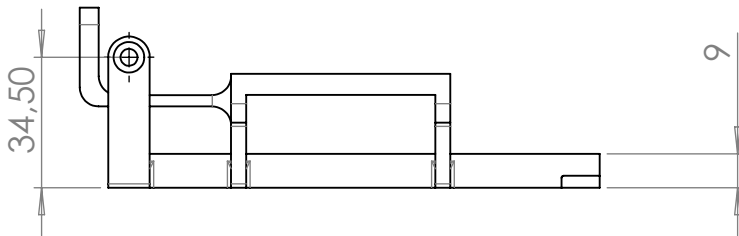
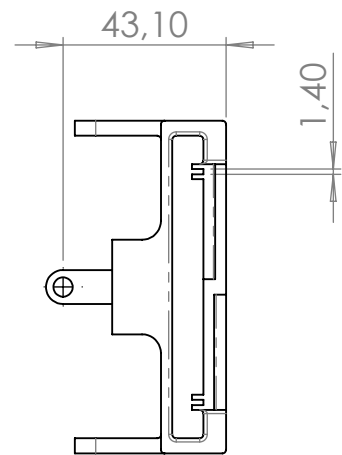
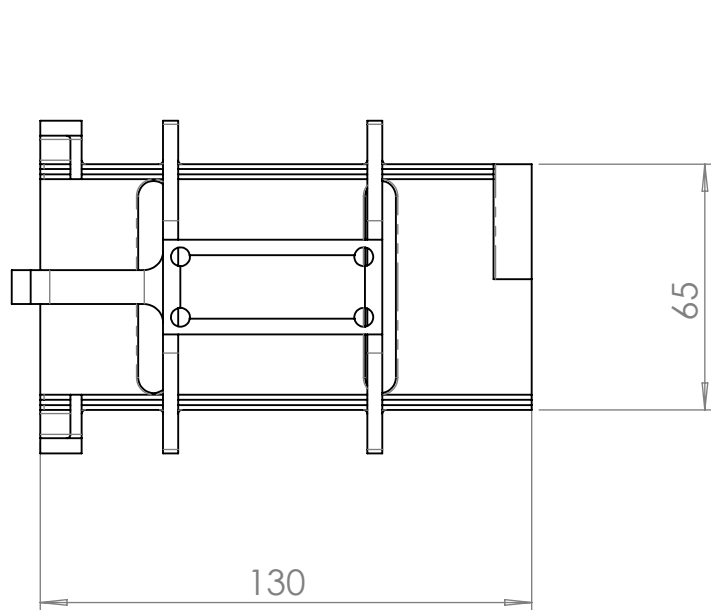
name					units	mm
PRO02_1003_SegmentBase					format	drawing no.
TU Delft BioMechanical Engineering	scale	1:1	date	17-10-2019	A4	PRO02_1003
	author	Sander d'Hont, #4209893				grams
						Snake-like system



name						units	mm
PRO02_1004_Pin				format		drawing no.	
TU Delft BioMechanical Engineering		scale	2:1	date	17-10-2019	A4	PRO02_1004
		author	Sander d'Hont, #4209893				grams



name		PRO02_2000_ShapeMemorySystem		 units mm	
format		A4		drawing no. PRO02_2000	
TU Delft BioMechanical Engineering	scale	1:2	date	17-10-2019	weight
	author	Sander d'Hont, #4209893			
				grams	subsystem Shape Memory



name

PRO02_2001_MotorFrame



units mm

format

A4

drawing no.

PRO02_2001

TU Delft
BioMechanical Engineering

scale 1:2

date 17-10-2019

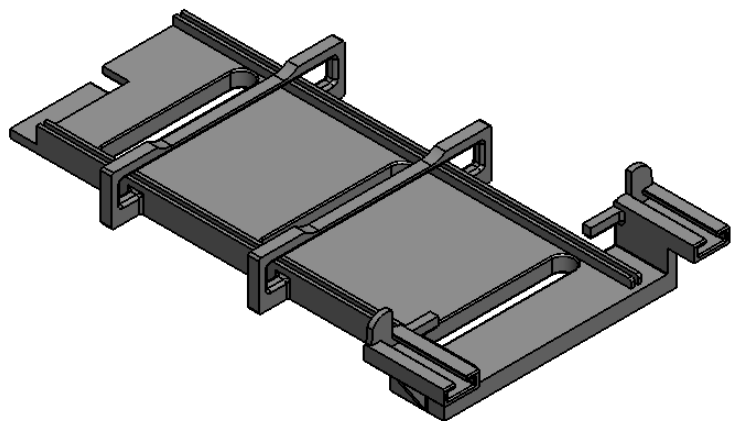
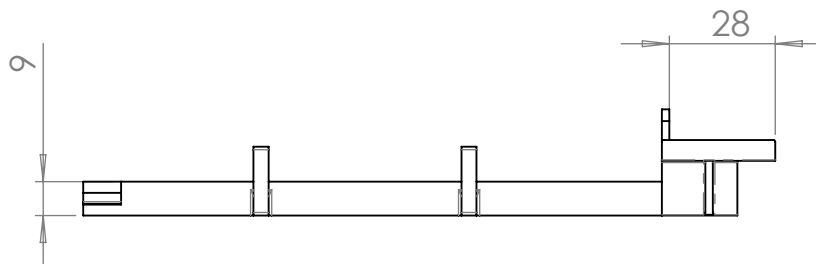
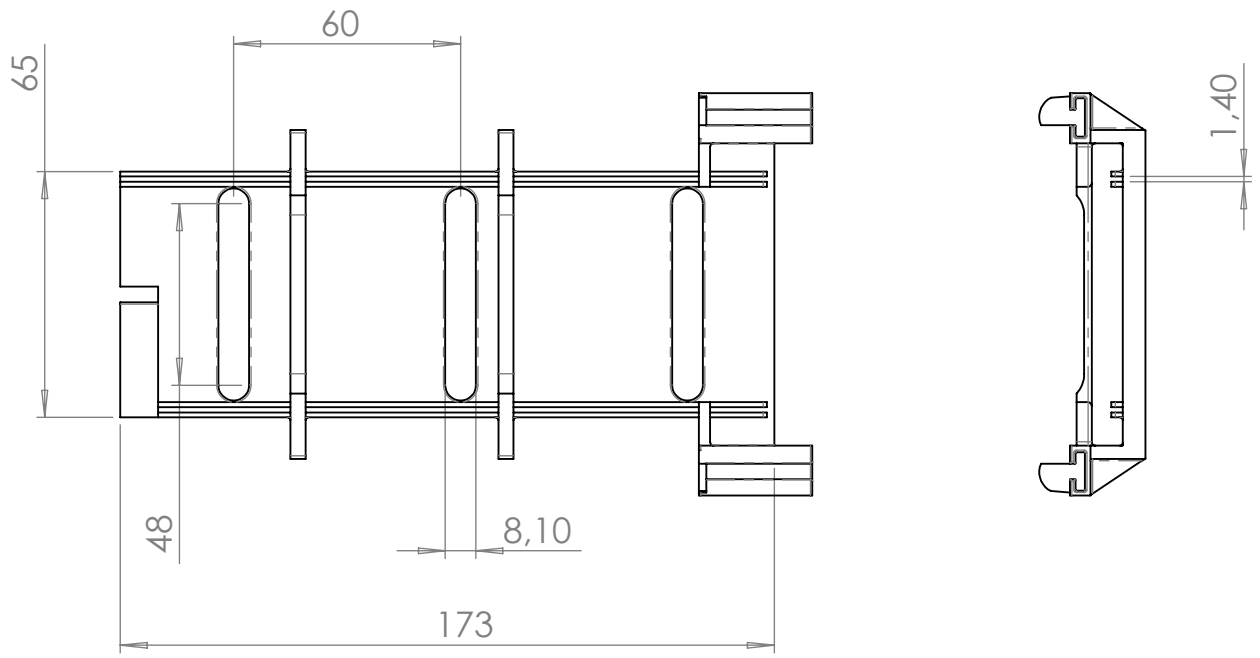
weight

grams

author Sander d'Hont, #4209893

subsystem

Shape memory



name
PRO02_2002_GuideFrame



units
 mm

format

drawing no.
PRO02_2002

TU Delft
 BioMechanical Engineering

scale
 1:2

date
 17-10-2019

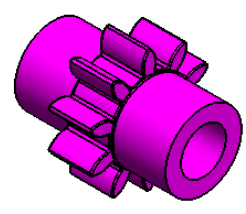
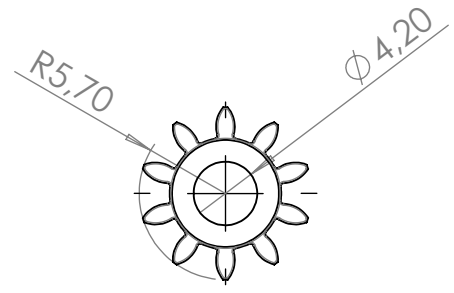
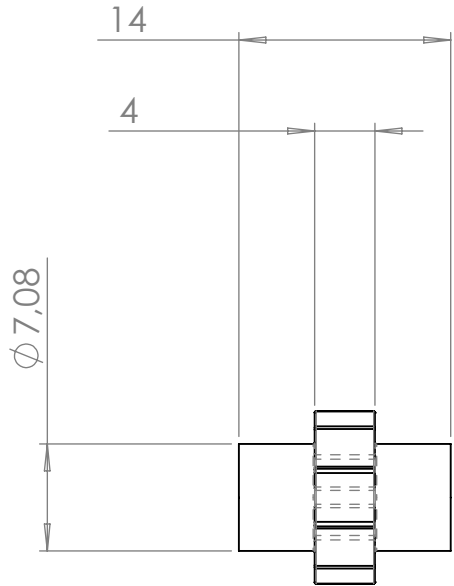
weight

grams

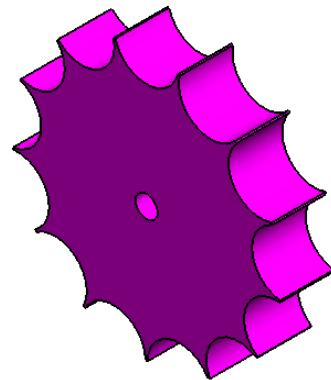
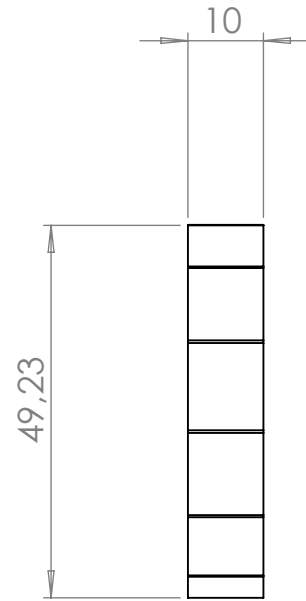
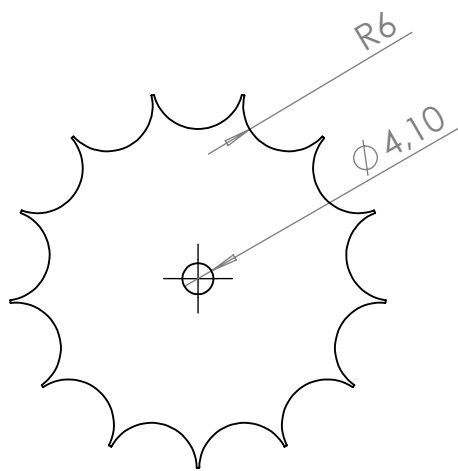
A4

author
 Sander d'Hont, #4209893

subsystem
 Shape memory



name						units	mm
PRO02_2003_GearWheel				format		drawing no.	
TU Delft BioMechanical Engineering		scale	2:1	date	17-10-2019	grams	A4 PRO02_2003
		author	Sander d'Hont, #4209893				



name

PRO02_2004_SprocketWheel



units mm

format

drawing no.

PRO02_2004

TU Delft
BioMechanical Engineering

scale 1:1

date 17-10-2019

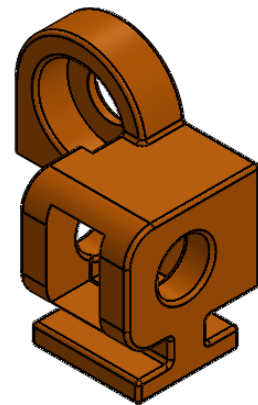
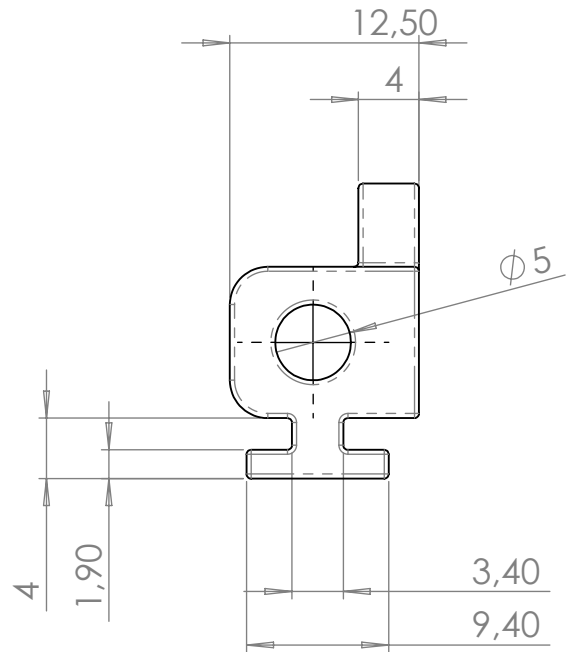
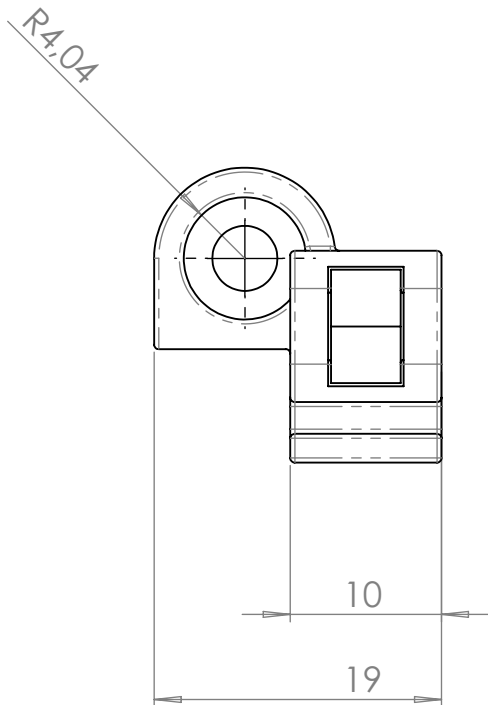
weight

grams

A4

author Sander d'Hont, #4209893

subsystem
Shape memory



name

PRO02_2005_BeltPositioner



units mm

format

drawing no.

PRO02_2005

TU Delft
BioMechanical Engineering

scale 2:1

date 17-10-2019

weight

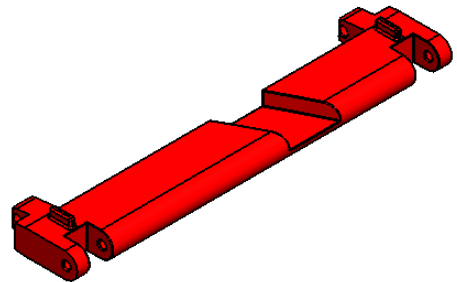
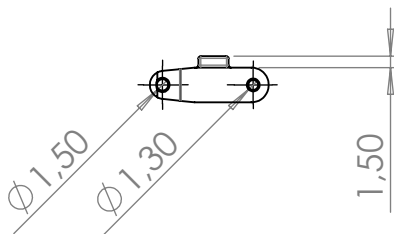
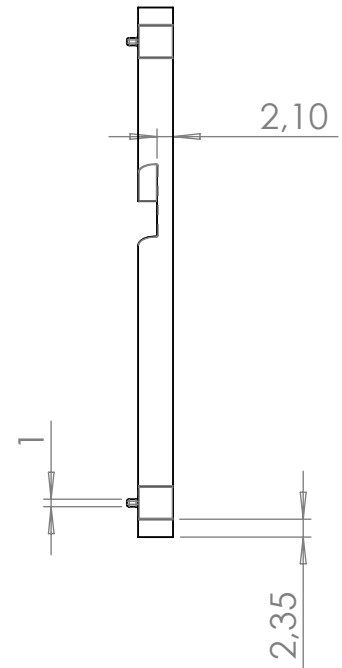
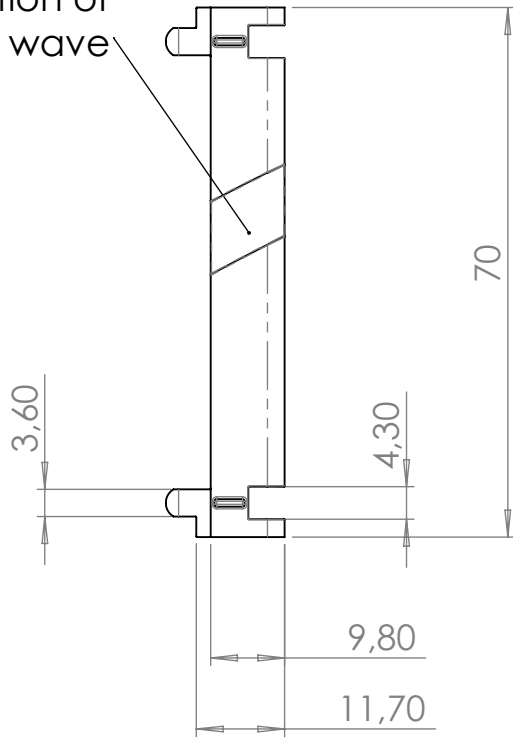
grams



A4

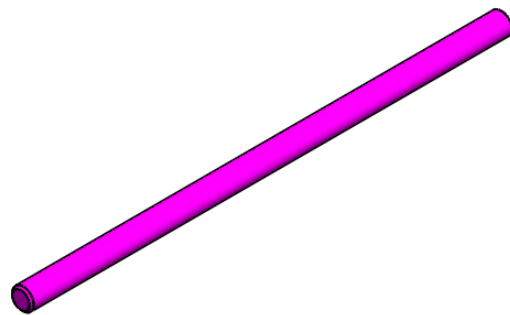
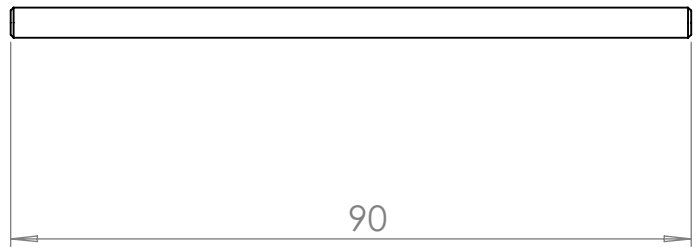
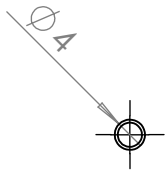
author Sander d'Hont, #4209893

subsystem
Shape memory

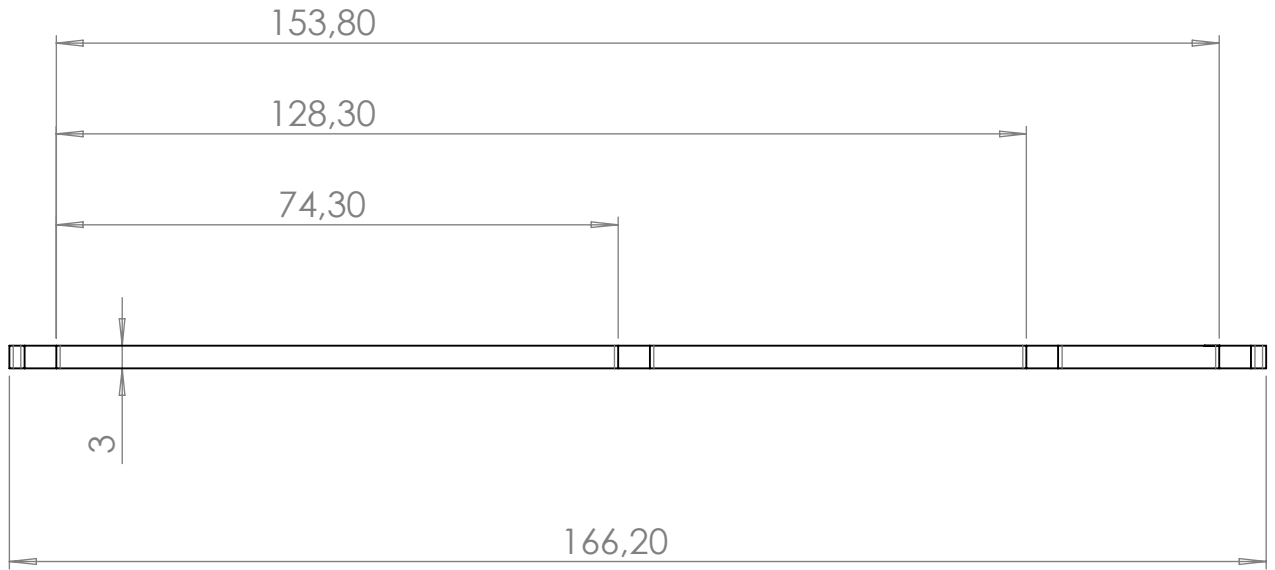
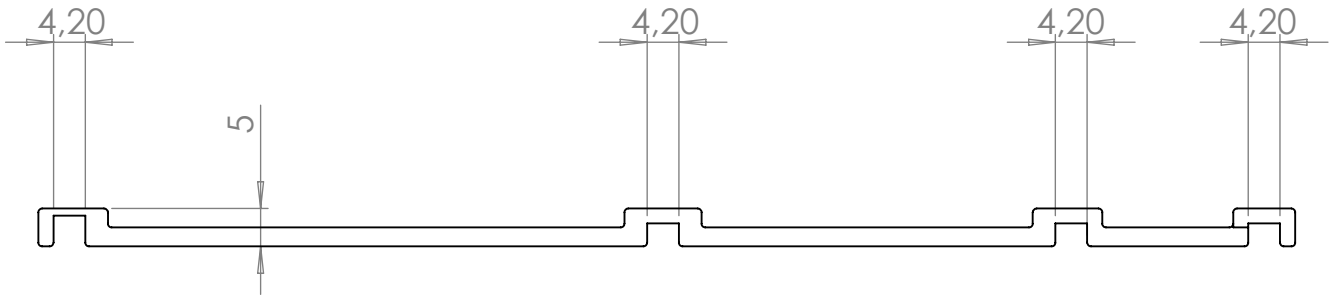
Fraction of sinus wave



name					units	mm
PRO02_2006_BeltPart					format	drawing no.
TU Delft BioMechanical Engineering	scale	1:1	date	grams		subsystem Shape memory
	author	Sander d'Hont, #4209893				



name						units	mm
PRO02_2007_LongAxis				format		drawing no.	
TU Delft		scale	1:1	date	17-10-2019	PRO02_2007	
BioMechanical Engineering		author	Sander d'Hont, #4209893			subsystem	
				weight	grams	Shape Memory	



name

PRO02_2008_BeltGuideA



units mm

format

A4

drawing no.

PRO02_2008

TU Delft
BioMechanical Engineering

scale 1:1

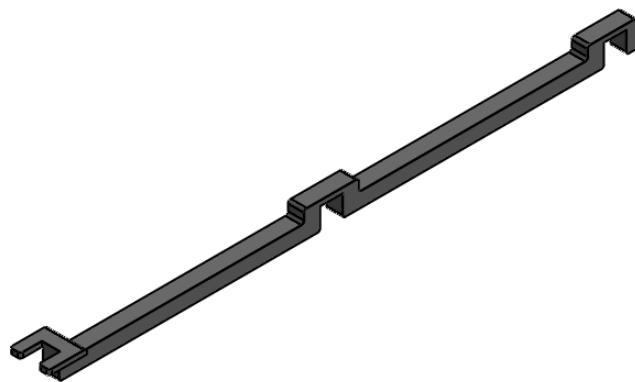
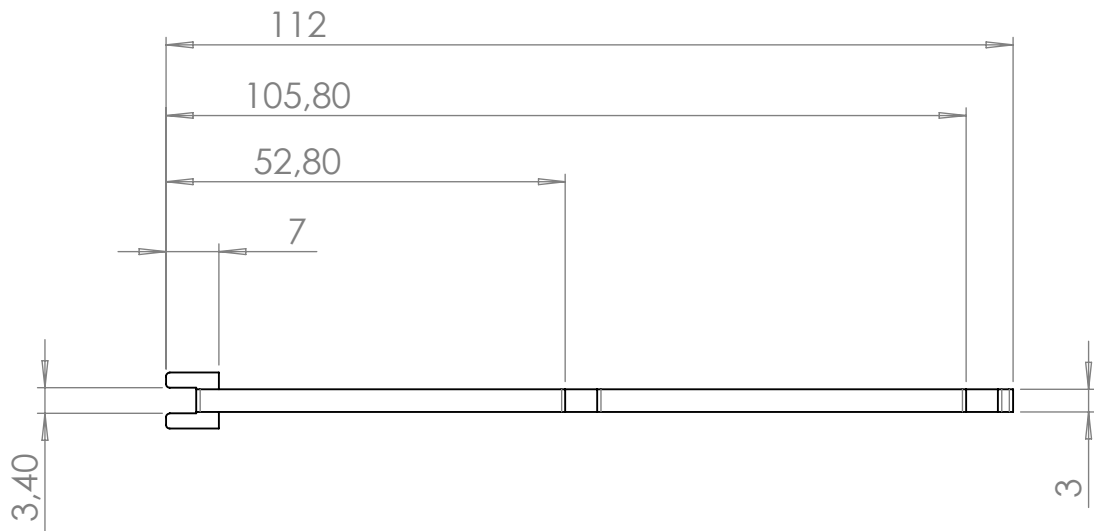
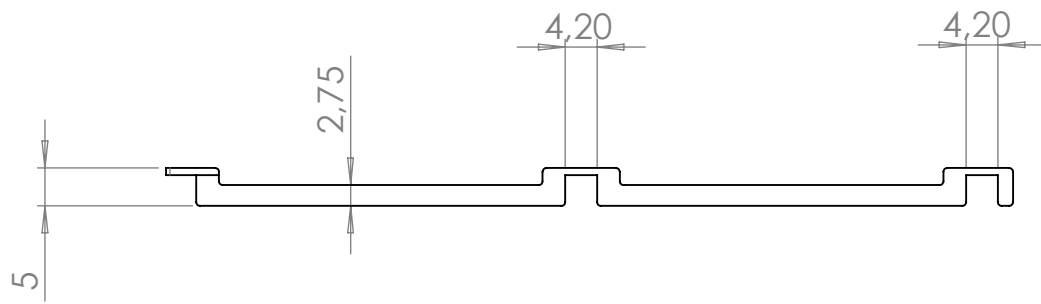
date 17-10-2019

weight

grams

author Sander d'Hont, #4209893

subsystem
Shape Memory



name

PRO02_2009_BeltGuideB



units mm

format

A4

drawing no.

PRO02_2008

TU Delft
BioMechanical Engineering

scale 1:1

date 17-10-2019

weight

grams

author Sander d'Hont, #4209893

subsystem
Shape Memory



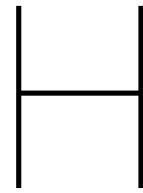
Model Parameters in Matlab

```
%% Parameters Simulink Model Simulation

% BMA0332 BME MSc – Thesis
%
% Sander d’Hont
% Studentnumber 4209893
% September 9th, 2019
%
% Has to be used in combination with the following files :
% Simulation_Sinusoidal_Wave_2D.m
% Simulink_Sinusoidal_Wave_3D.slx
%
% All parameters as dimensions, sinus parameters, path speed are
% described in this file so that the Simulink Model can be easily
% adapted to different situations and configurations. The file has
% to be ran prior to updating the Simulink Model.

%% Sinusoidal wave [cm]
filtertimeconstant = 0.05; % Filter Time Constant
fr_sphere_radius = 1.55; % Sphere Radius in Contact Force
fr_plane_length = 1000; % Plane Length in Contact Force
fr_plane_width = 1000; % Pane Width in Contact Force
fr_plane_height = 0.1; % Plane Height in Contact Force
fr_stiffness = 1e6; % Plane Stiffness in Contact Force
fr_damping = 1e5; % Plane Damping in Contact Force
fr_kinetic = 1e1; % Kinetic Friction Coefficient
fr_static = 1e1; % Static Friction Coefficient
A = 2; % Amplitude Sinusoidal Path
B = pi/15; % Frequenty Relation Sinusoidal Path
C = 0.005; % Shifting Distance Other Paths
d = 0.15; % Shifting Factor Other Paths
slot_length = 10; % Frame Slot Length
slot_space = 6; % Frame Slot Spacing
base_length = 5; % Segment Base Length
base_width = 1; % Segment Base Width
base_height = 1; % Segment Base Height
slider_length = 2.5; % Segment Slider Length
slider_width = 1.5; % Segment Slider Width
slider_height = 1.5; % Segment Slider Height
wheelaxis_length = 6.5; % Wheelaxis Length
wheelaxis_width = 0.2; % Wheelaxis Diameter
```

```
wheelaxis_height = 0.2;      % Wheelaxis Diameter
slot_block       = 0.2;      % Sliding Block Dimensions
wheel_diameter   = 3.1;      % Wheel Diameter
wheel_thickness  = 0.2;      % Wheel Thickness
path_speed       = 6;        % Relative Path Speed w.r.t. Frame
Time             = 60;       % Simulation Time
offset           = 350;      % x-Offset frame w.r.t. global world
offsetpath       = 350;      % x-Offset path w.r.t. frame
offsetheight     = wheel_diameter/2+0.02; % z-Offset frame w.r.t frame
wheelline_length = wheel_diameter-0.5; % Wheelline length
wheelline_thickness = wheel_thickness+0.05; % Wheelline thickness
```

Simulation Parameter: Wheel Axis Length

H.1. Assessed Situations

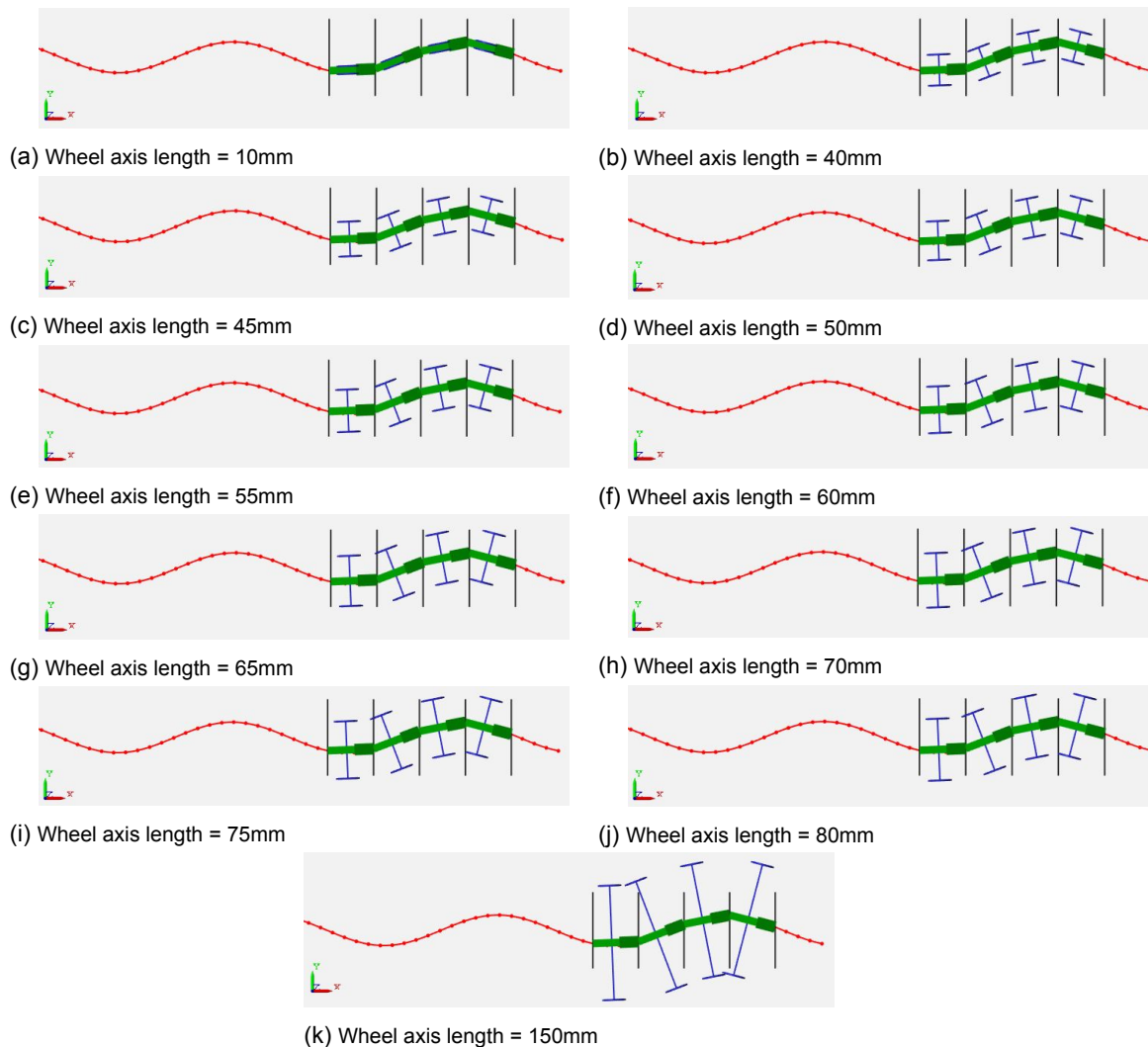


Figure H.1: Assessment of wheel axis length: All situations which were simulated for 20 seconds.

H.2. Assessment Results

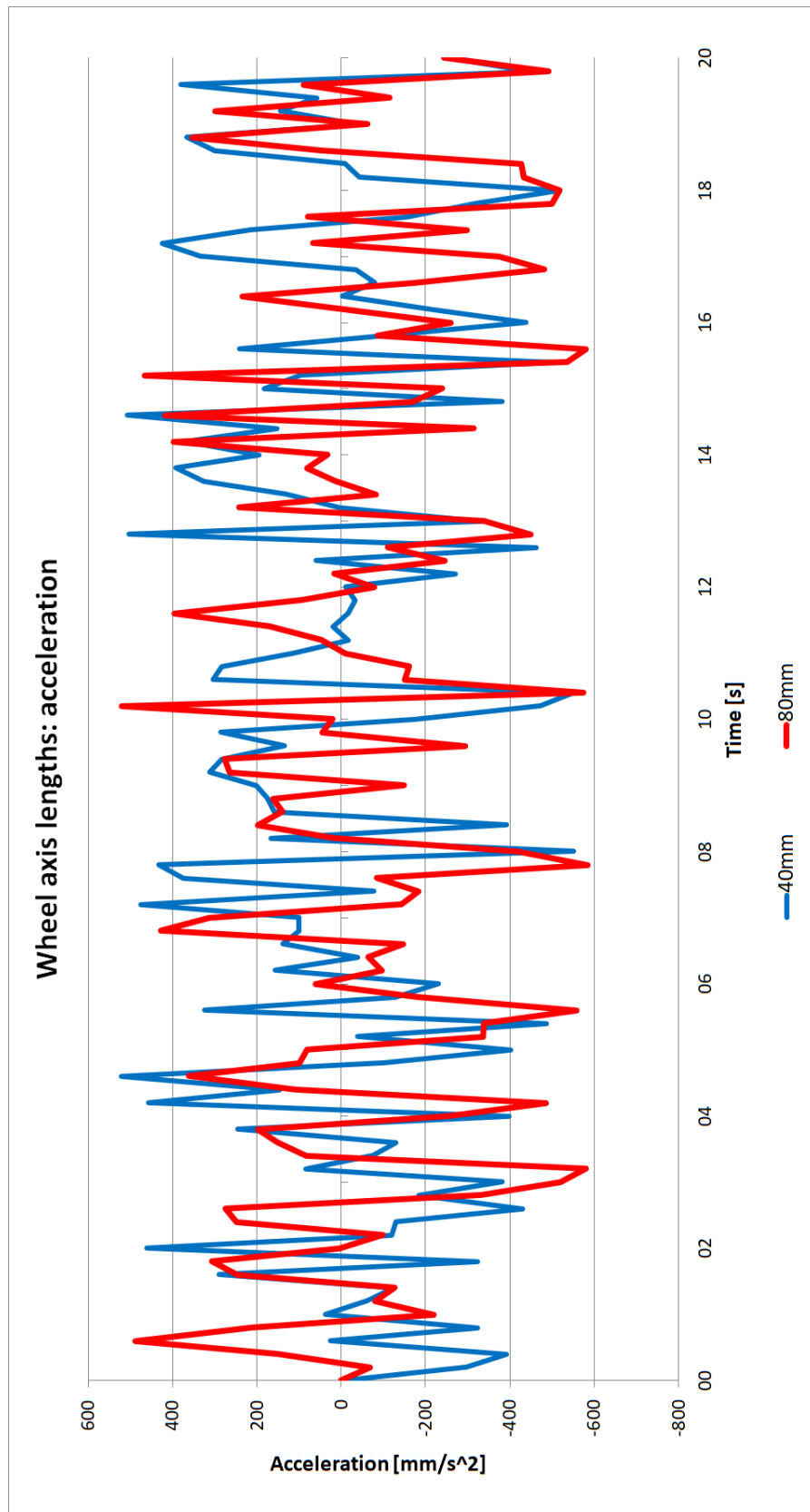


Figure H.2: Acceleration for configurations with different wheel axis lengths during the 20second simulation.

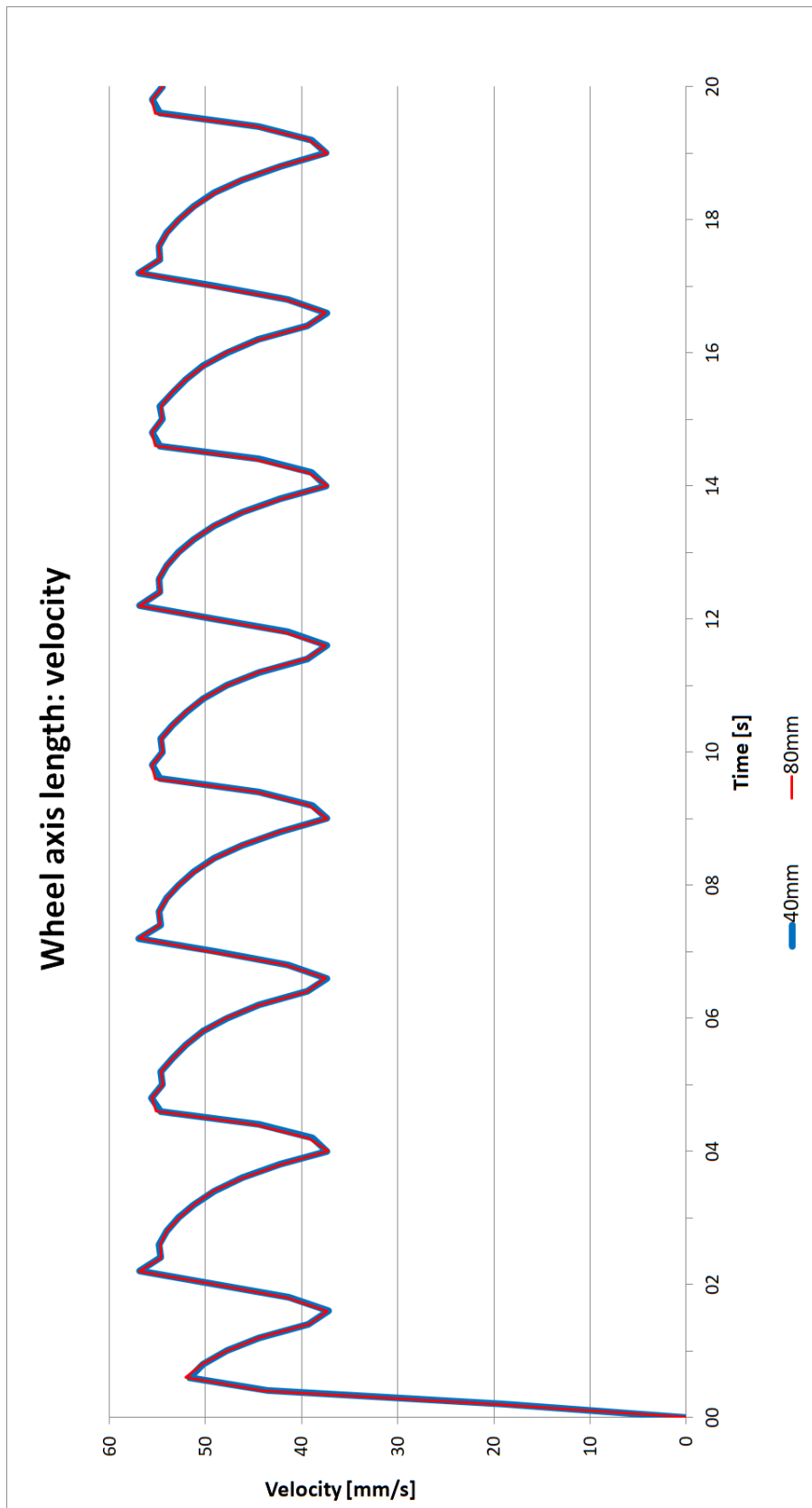


Figure H.3: Velocity for configurations with different wheel axis lengths during the 20second simulation.

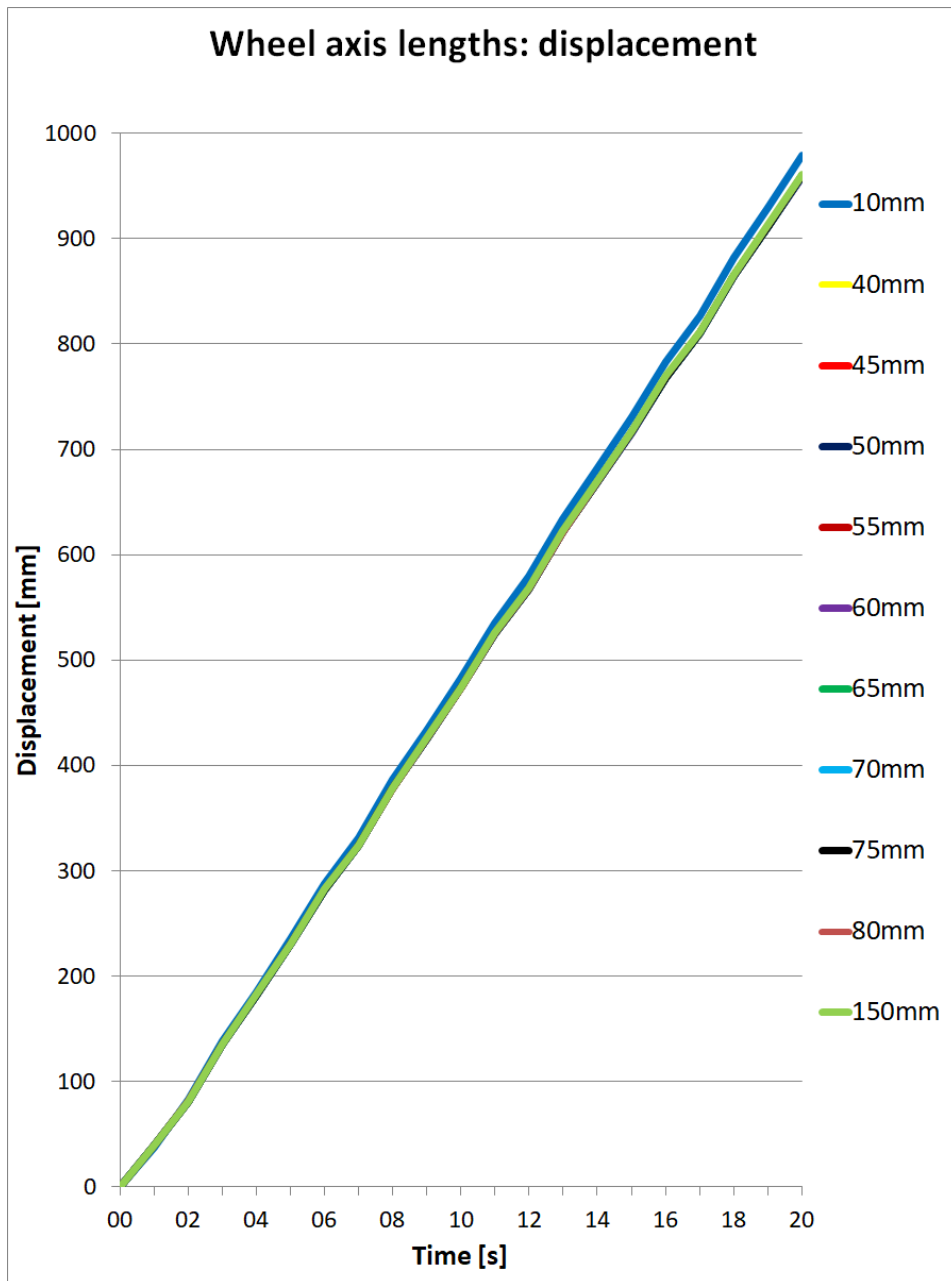


Figure H.4: Forward displacement for configurations with different wheel axis lengths during the 20second simulation.

Simulation Parameter: Sinus Amplitude

I.1. Assessed Situations

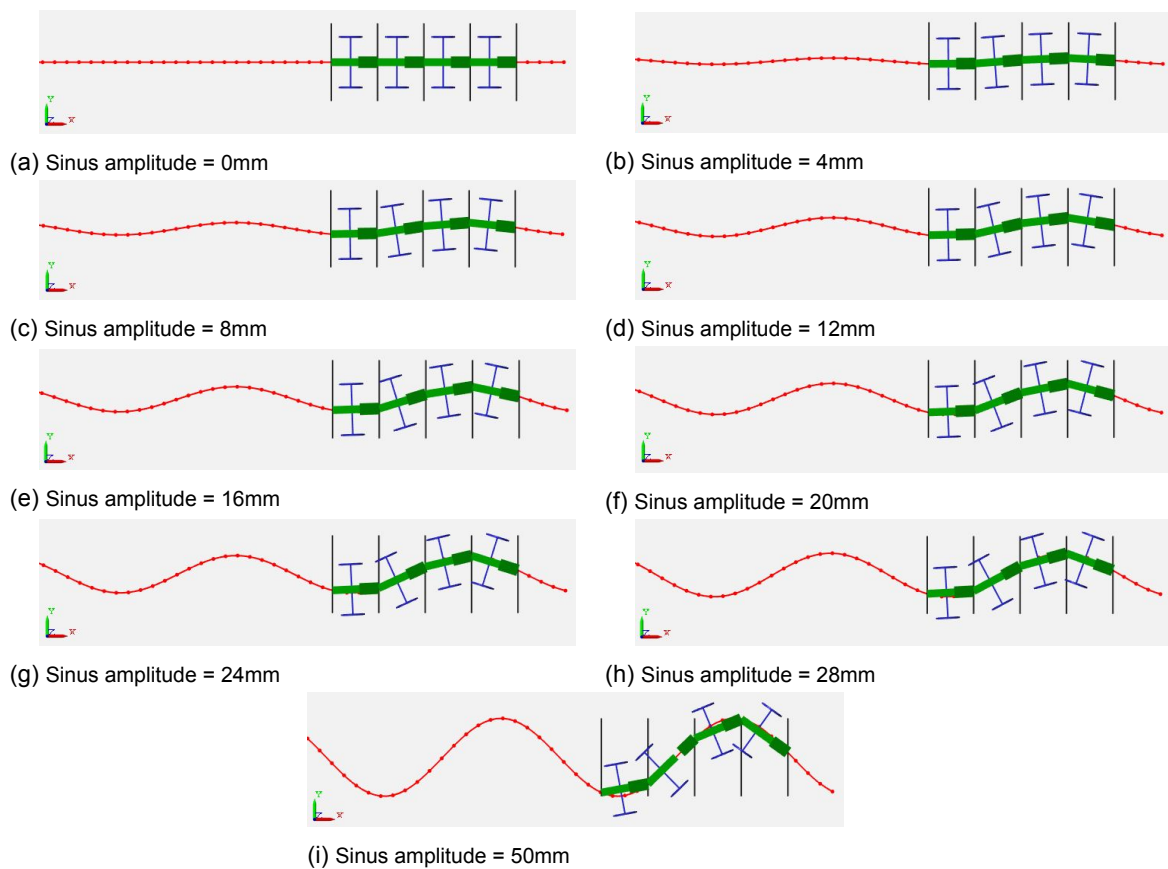


Figure I.1: Assessment of sinus amplitude: All situations which were simulated for 20 seconds.

I.2. Assessment Results

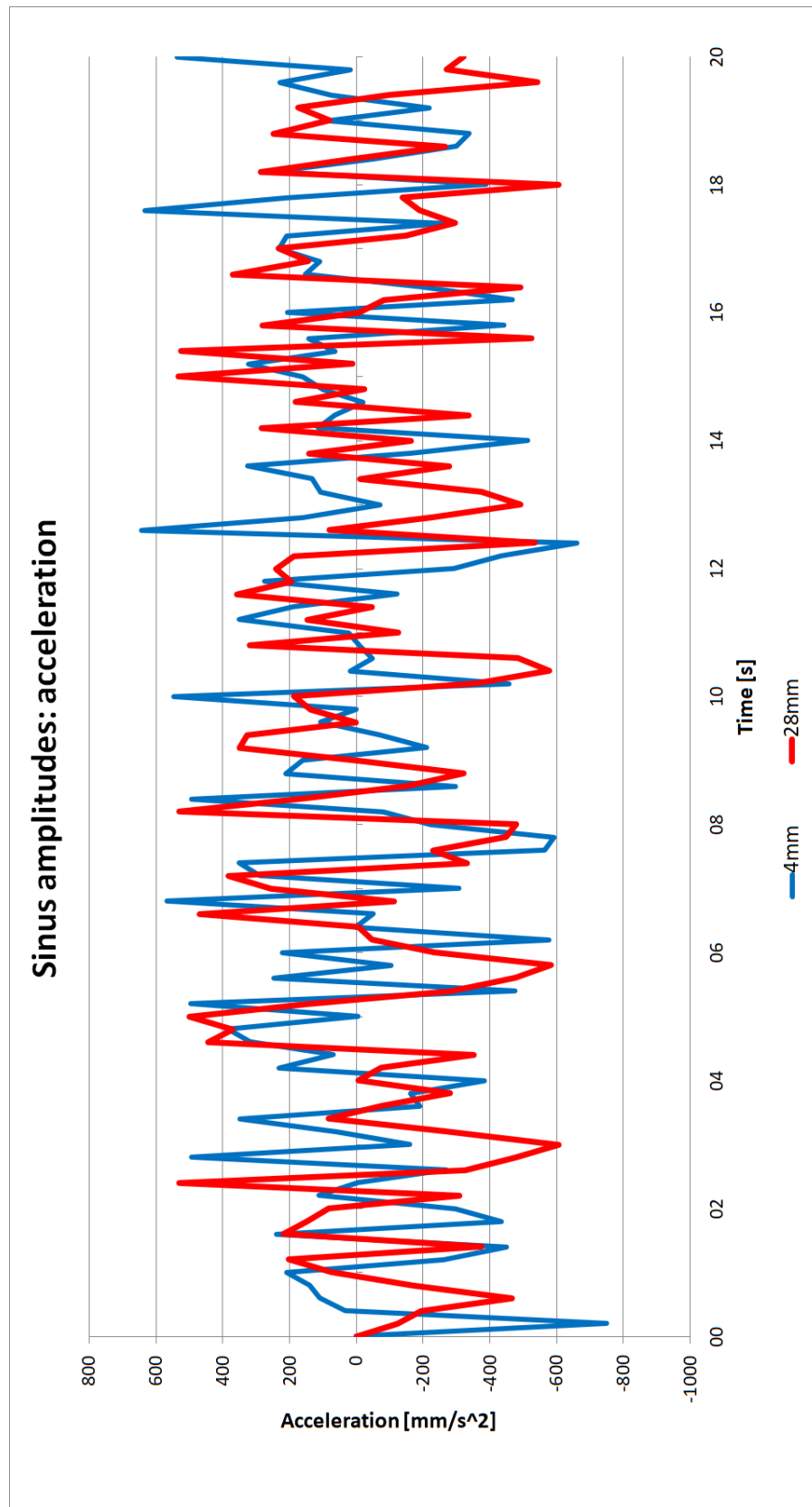


Figure I.2: Acceleration for configurations with different sinus amplitudes during the 20second simulation.

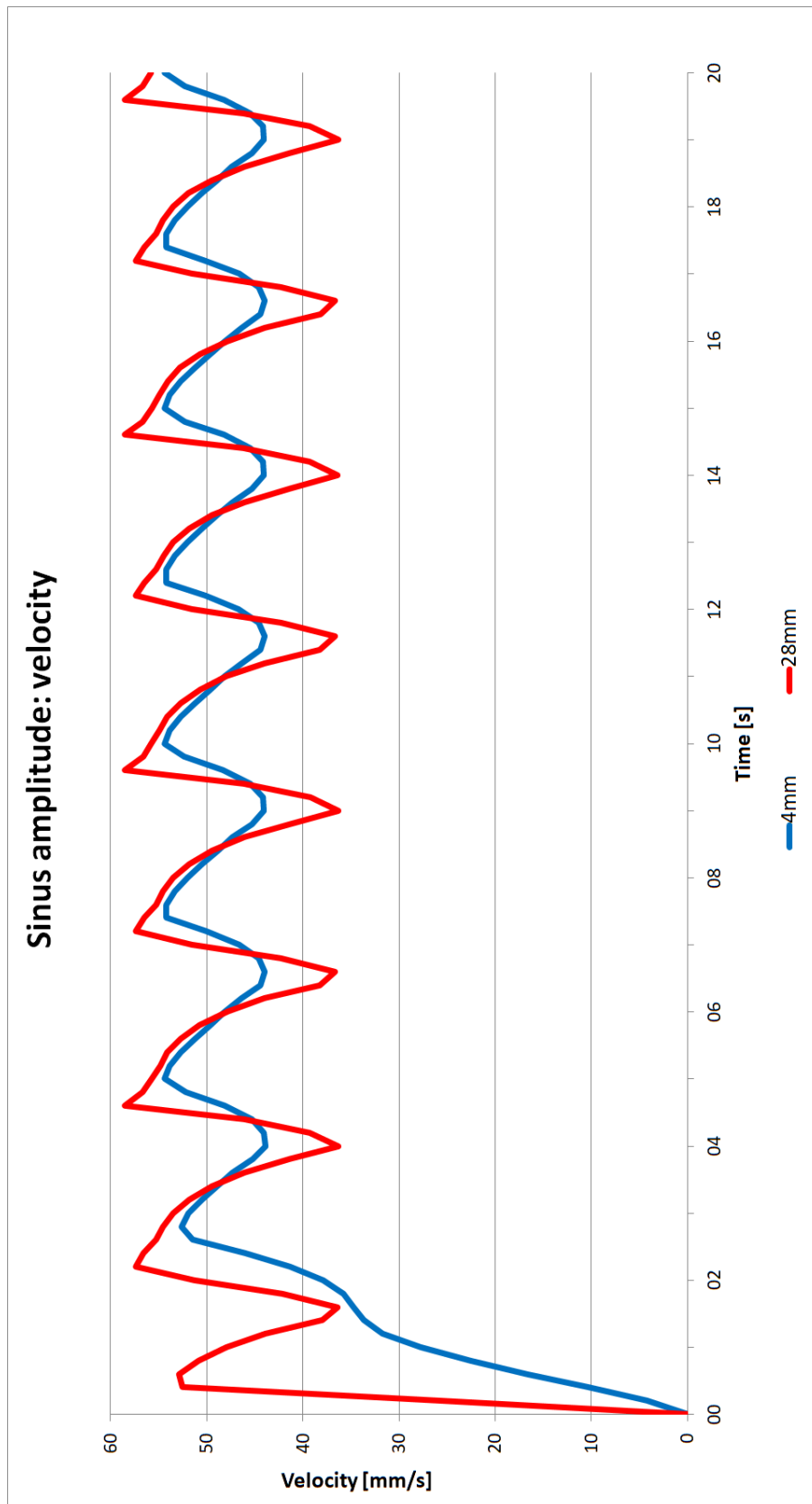


Figure I.3: Velocity for configurations with different sinus amplitudes during the 20second simulation.

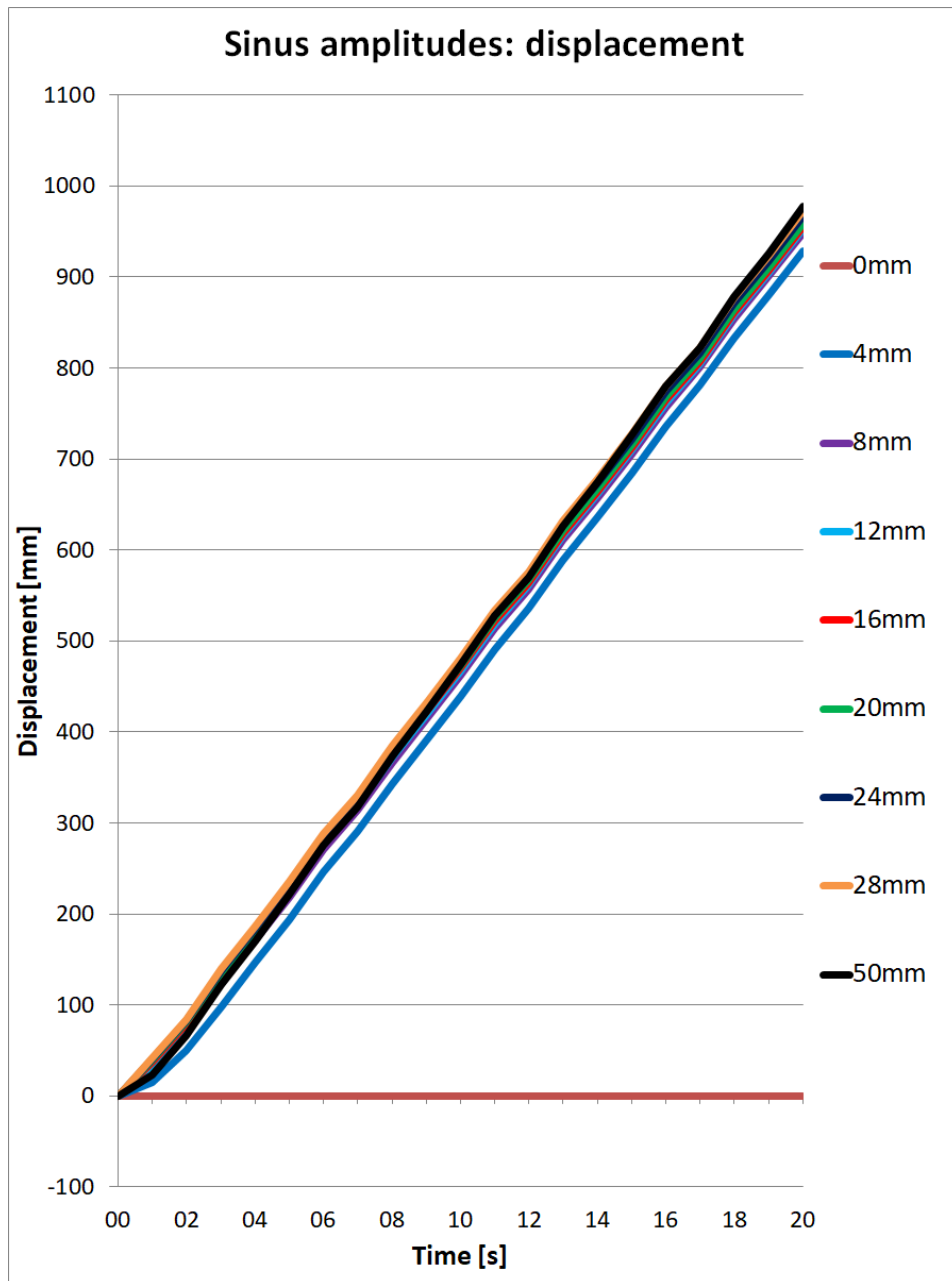


Figure I.4: Forward displacement for configurations with different sinus amplitudes during the 20second simulation.

Simulation Parameter: Sinus Frequency

J.1. Assessed Situations

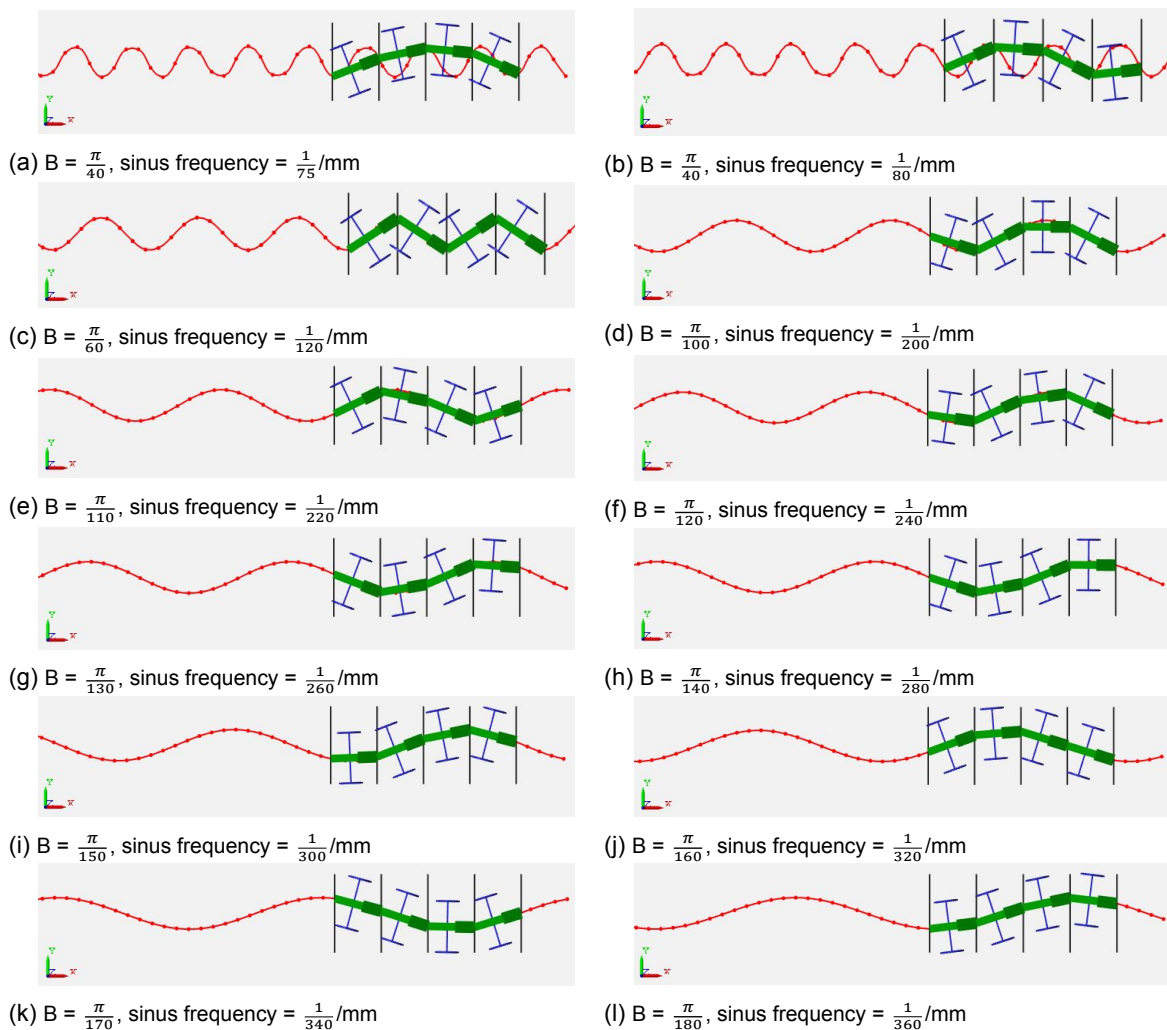


Figure J.1: Assessment of sinus frequency (1st half): All situations which were simulated for 20 seconds.

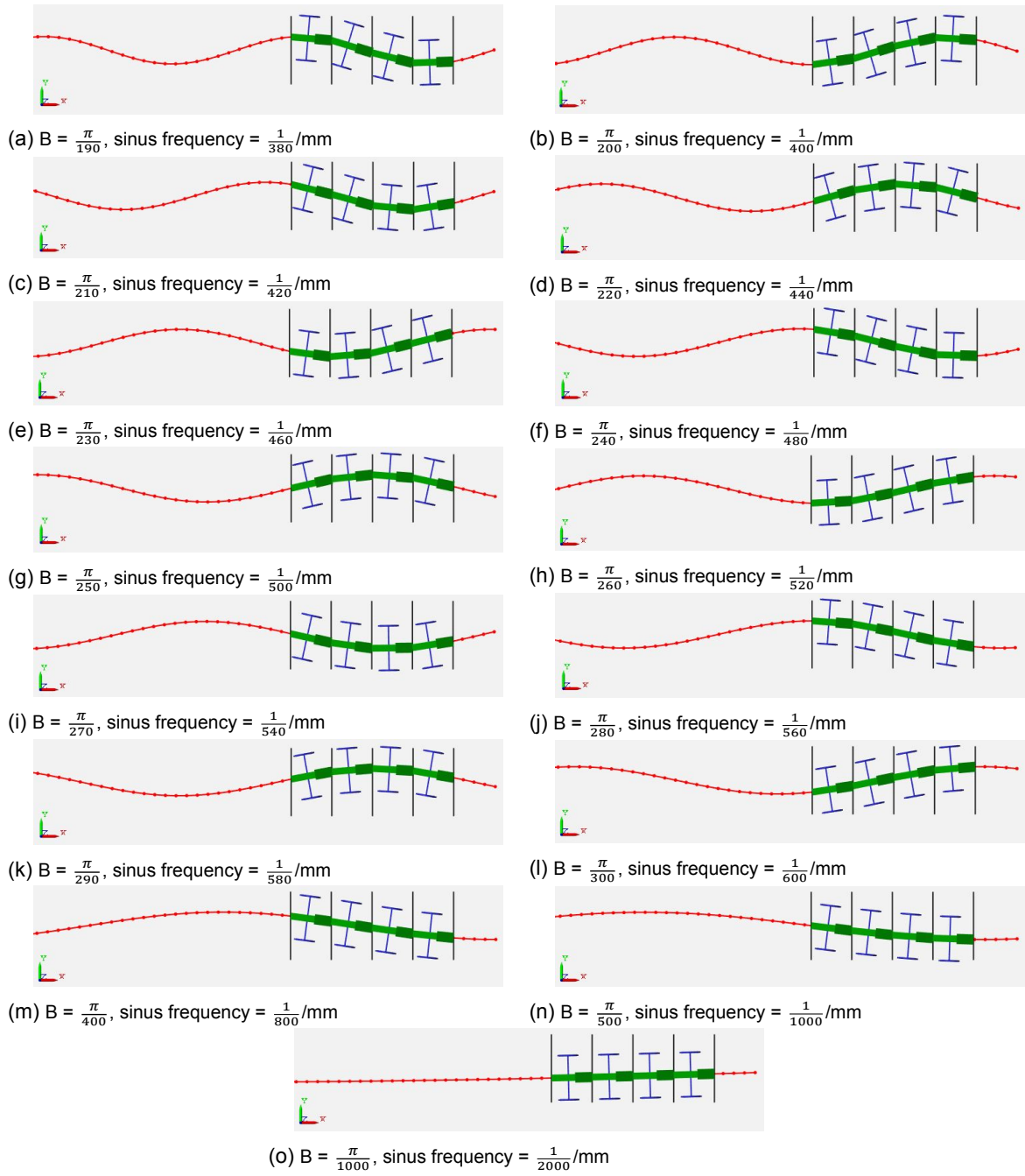


Figure J.2: Assessment of sinus frequency (2nd half): All situations which were simulated for 20 seconds.

J.2. Assessment Results

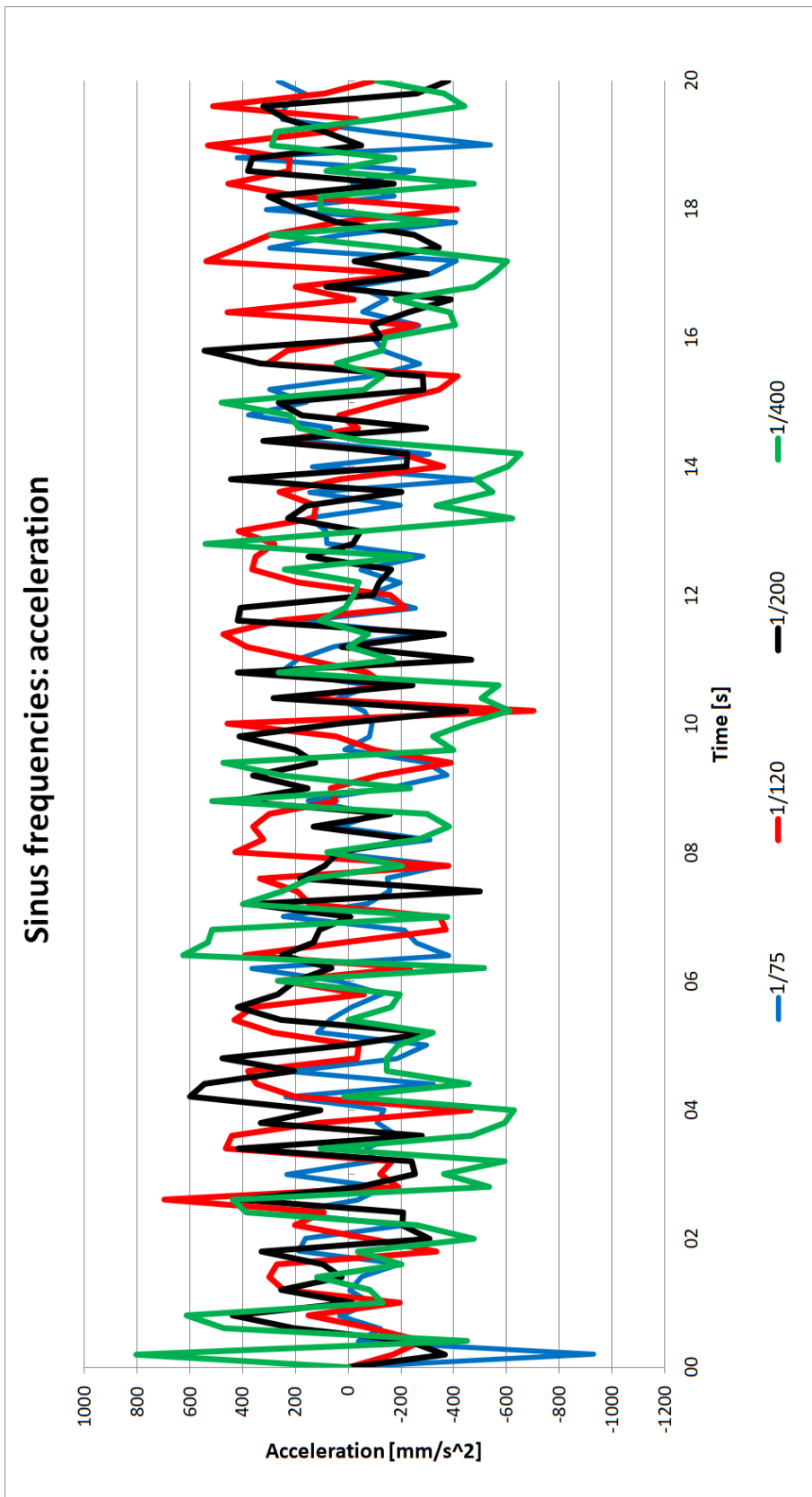


Figure J.3: Acceleration for configurations with different sinus frequencies during the 20second simulation.

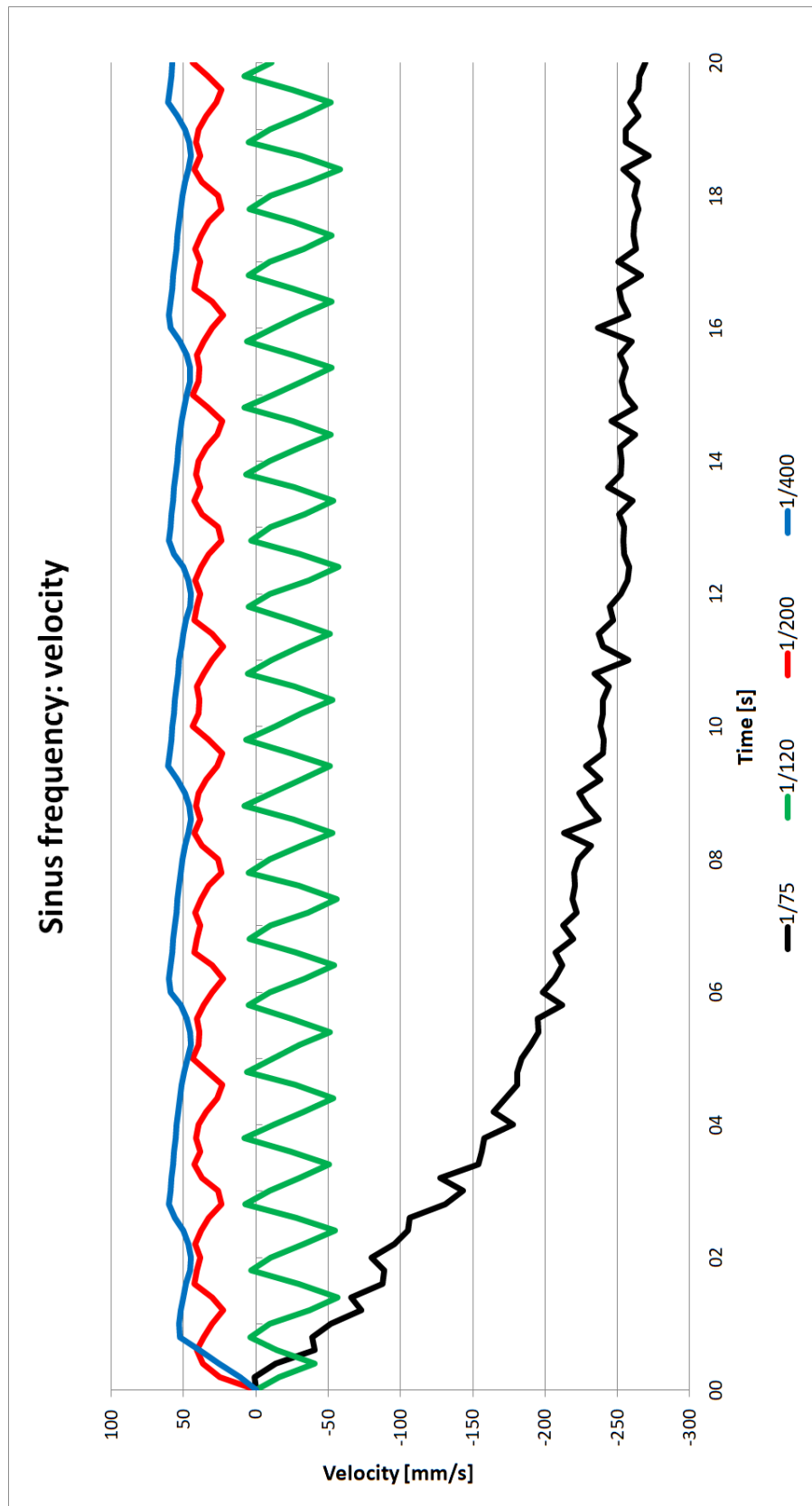


Figure J.4: Velocity for configurations with different sinus frequencies during the 20second simulation.

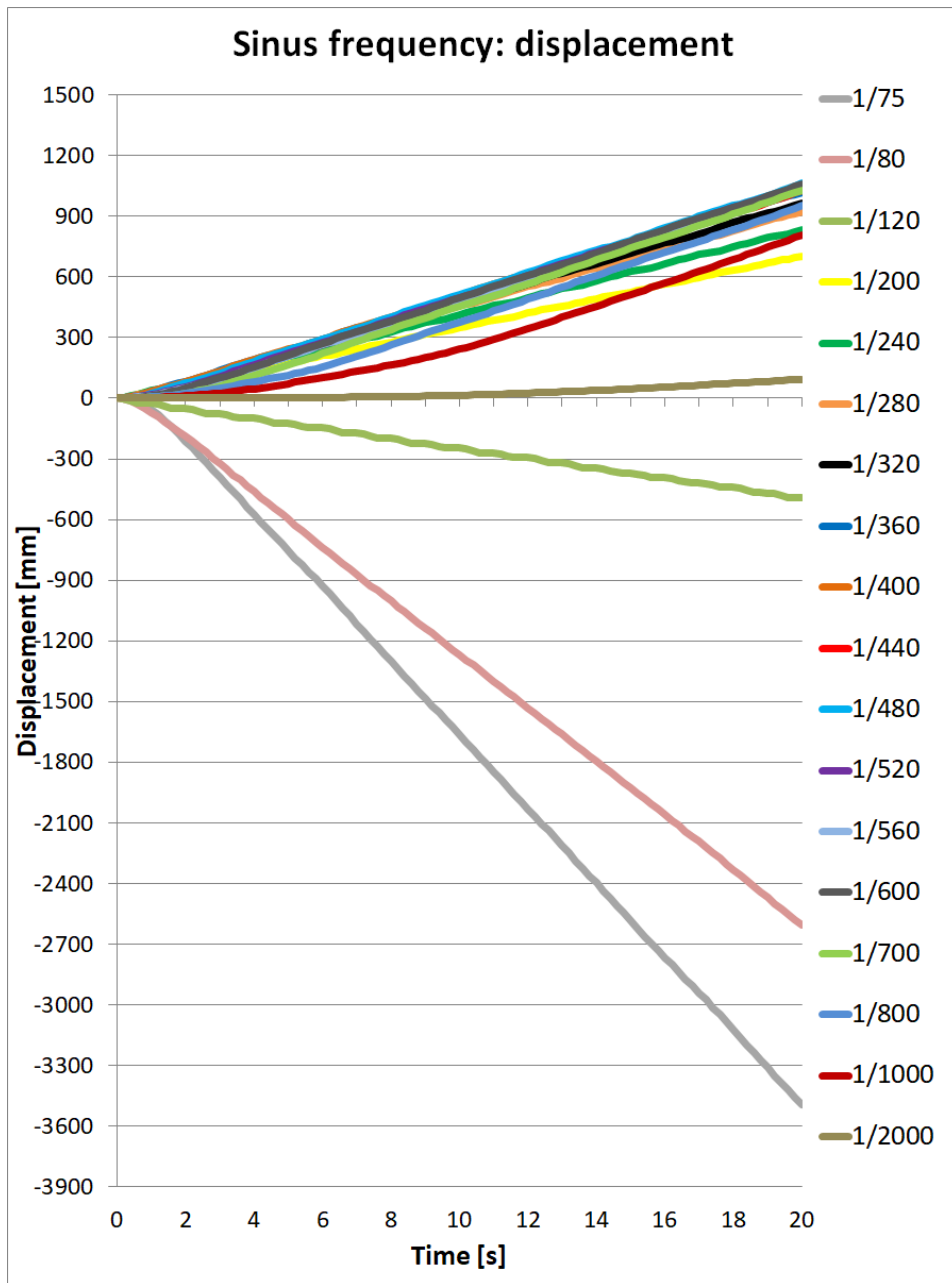


Figure J.5: Forward displacement for configurations with different sinus frequencies during the 20second simulation.